ANALYSIS OF AN EXISTING BUILDING FOR PROGRESSIVE COLLAPSE BY COLUMN REMOVAL

HONORS THESIS

Presented in Partial Fulfillment of the Requirement to Graduate with Honors Research Distinction from the Department of Civil, Environmental, and Geodetic Engineering at The Ohio State University

By

John M. Wade

The Ohio State University

2013

Undergraduate Honors Examination Committee:

Dr. Halil Sezen, Advisor

Dr. Abdollah Shafieezadeh, Committee Member

ABSTRACT

Progressive collapse, also called disproportionate collapse, is a structural engineering phenomenon defined as the failure of a building or other large structure with the sudden removal or failure of a major vertical load carrying component of the structure (such as a first floor column). Although numerous high-profile structures have failed due to progressive collapse (such as the World Trade Center Towers), and structural engineers have developed theories to account for progressive collapse in design, little experimental data exists to validate the theory. Large-scale structures can rarely, if ever, be test in a laboratory setting. The existing theory and design practices tend to produce overdesigned and expensive buildings, where more accurate or refined theory could economize design. This research involves analyzing models of progressive collapse scenarios and comparing the results of the model to experimental data from a recently demolished building on The Ohio State University Columbus Campus. In this experiment, the column of a steel frame building on the campus was removed with demolition equipment, and the response of nearby columns and beams was measured with strain gauges and displacement sensors. One perimeter frame of the building including the removed column was modeled in the structural analysis software SAP2000 and ASI Extreme Loading for Structures.

ACKNOWLEDGEMENTS

For helping me through this process, I would like to thank Professor Halil Sezen. His patience throughout the project has been greatly appreciated, and he is always eager to help. His guidance has laid the foundation of my knowledge in structural engineering. I would also like to thank Professor Abdollah Shafieezadeh for encouraging me and participating in my defense panel. I wholeheartedly thank Ebiji Akah for his collaboration on analyzing Haskett Hall. Akah's dedication, diligence, and aptitude enabled the success of the project. Additionally, thanks goes to Curtis Wood and Muhammad Shadab Lodhi, whose work with the experimentation of Haskett Hall made this project possible, and whose guidance was invaluable. Special thanks also goes to Loewendick Demolition Company for facilitating the experiment.

Many thanks go to Applied Science International for offering a license of their software for this research. This allowed the unique opportunity to work with an extremely sophisticated structural engineering program. The whole project was greatly enhanced by ASI's generosity. Thanks also goes to the College of Engineering for their funding, which allowed for this unique facet of my education.

Finally, I would like to thank all of my loving family members who have supported and encouraged me throughout this process.

VITA

August 20, 1990 ..... Born – Los Angeles, CA

May 6, 2013 .....Structural Engineering, URS Corp, Columbus, OH

December 15, 2013..... B.S. Civil Engineering, The Ohio State University

TABLE OF CONTENTS

LIST OF TABLES

LIST OF FIGURES

CHAPTER 1: INTRODUCTION

1.1 Overview

When local failure occurs in a structural element, the structure may be prone to spread the failure, jeopardizing the overall integrity. This phenomenon is referred to as progressive or disproportionate collapse. Formally stated, progressive collapse is "the spread of an initial local failure from element to element, eventually resulting in the collapse of an entire structure or a disproportionately large portion of it" (ASCE 7-05, 2005). Although numerous high-profile structures have failed due to progressive collapse (such as the World Trade Center Towers), and structural engineers have developed theories to account for progressive collapse in design, the phenomenon is not thoroughly understood.

Buildings are expected to be most susceptible to progressive collapse when the structural integrity of a column is compromised, since columns are the main supporting elements in buildings. The loss of a column increases the span length of connected beams and the load carried by adjacent beams. This effect is demonstrated in Figure 1.1.

1.2 Haskett Hall

This research presents the analysis of the potential for progressive collapse of an existing building on the campus of The Ohio State University (OSU). Haskett Hall was a building on the Columbus Campus of OSU that was built in 1925 and demolished in December 2011. With a significant portion of the architectural material remaining in the building, a column was removed at the ground level, and the response of the structure was measured. The experiment was conducted with the help of the demolition contractors.

1.3 Computer Modeling and Analysis

After the experiment, a portion of the structure around the removed column was modeled using two finite element computer programs (SAP2000 2011 and ASI Extreme Loading for Structures 2012). Properties of structural members were determined from the construction documents from 1925, pictures taken on the day of the experiment, and the American Institute of Steel Construction (AISC) Historic Sections Database (2013). Gravity loads acting on the structure during the experiment were determined from the weights of remaining materials in the building. An evaluation of the stiffness of the structure was also completed using the finite element model.

1.4 Previous Research

The research presented is part of a research program conducted by other researchers at OSU. In 2007, a progressive collapse analysis was performed on the Ohio Union Building in Columbus, Ohio, where steel columns were removed at the first floor (Song, 2010). Similarly, a progressive collapse analysis was performed on the steel building of the Bankers Life Casualty Company in Northbrook, Illinois (Giriunas, 2009). In each analysis, the building was tested for progressive collapse by removing columns and measuring the response. This data was then compared to a computer model of the frame.

The analysis of Haskett Hall continues work completed in theses by K. Giriunas (2009), B. Song (2010), S. Lodhi (2012), and E. Akah (2013), and a paper by C. Wood, all completed at OSU. Haskett Hall was analyzed in collaboration with Akah using experimental data collected by Akah and others. Akah (2013) calculated a portion of the loads and assisted in determining section properties used in the computer model.

1.5 Scope and Objectives

The purpose of this research was to assess the susceptibility of Haskett Hall (a finished building) to progressive collapse in a column removal scenario. To design buildings for progressive collapse, structural engineers require the ability to analyze the response of structures due to column loss. Thus the goals of this research are:

- Implement progressive collapse analysis methods
- Assess the capacity of Haskett Hall to resist progressive collapse
- Assess how loads are redistributed in a building after column loss
- Compare experimental and theoretical data
- Discuss the significance of the results related to structural design

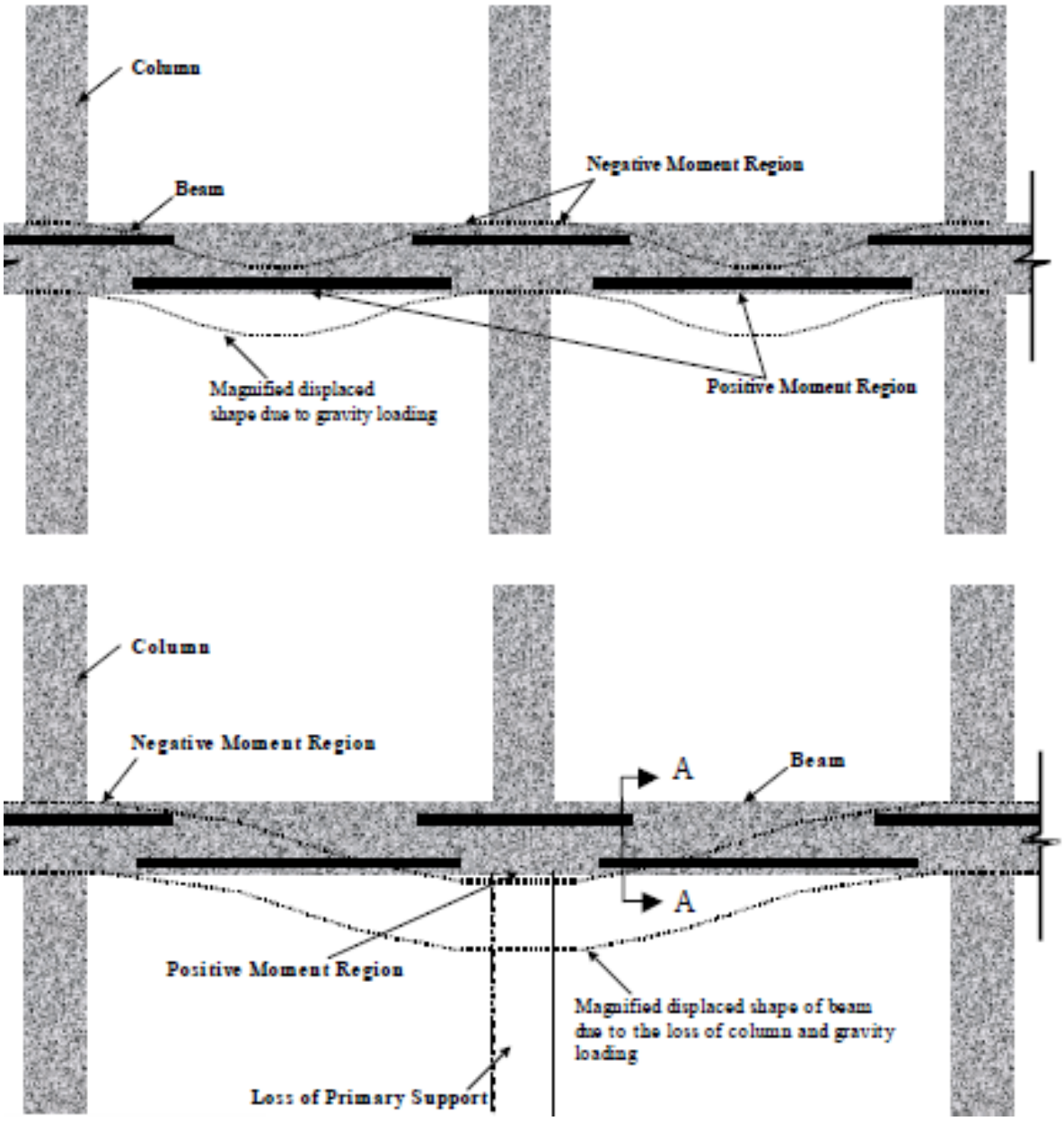

Figure 1.1: a) State of intact frame, b) state of frame after column removal (GSA 2003)

CHAPTER 2: HASKETT HALL DESCRIPTION

2.1 Introduction

In Chapter 2, a detailed description of the building used in the experiment is given. The building components and details discussed include the foundation, framing plan, floor layout, beams, columns, slabs, architectural façade, and roof. The qualitative state of the building plays a crucial role in the results of the experiment and the modeling process.

2.2 Haskett Hall

Haskett Hall was a steel frame building on The Ohio State University's Columbus Campus that was constructed in 1924 and demolished on December 19, 2011. The building contained four floors, no basement, and was used for classrooms, offices, and engineering laboratory testing. Originally named the Engineering Experiment Station, Haskett Hall was designed to house laboratories for research in concrete, metallurgy, beam mechanics, and atomic physics. These testing spaces led to several irregularities in the framing plan, such as a three-story material research laboratory on the entire the north end of the building. Construction documents that were used in this thesis are provided in Appendix A.

2.2.1 Framing Plan and Floor Layout

The framing plan for the exterior of Haskett Hall included seven columns running in the north-south direction and six columns in the east-west direction. There were a total of four floors, but no floors were continuous throughout the building due to expansive testing spaces. Figure 2.1 depicts the typical elevation view of the asymmetric framing plan in the north-south direction, while Figure 2.2 depicts the framing plan in the east-west direction. The floors in Haskett Hall were made of reinforced concrete slabs covered with linoleum and mastic. Most slabs in the building were either 7 in. thick and heavily reinforced, or 3 in. thick and supported by a reinforced concrete

joist pattern. Several thin slabs also contained steel I-beams encased in concrete for support, such as in Figure 2.3.

2.2.2 Foundation

The foundation of the building was shallow and contained no piles. Columns around the perimeter of the building were supported by a wall footing. Interior column footings were isolated and combined, where trapezoidal reinforcing mats were used. While Haskett Hall contained no basement, a shallow recess was constructed below-grade in the northwest corner to serve as a testing machine space, and this was supported by a mat foundation.

2.2.3 Exterior

An architectural façade, made of double-wythe brick, covered most of the exterior of Haskett Hall. The second floor, fourth floor, and roof exterior were also lined with architectural, masonic installations. Figures 2.3 and 2.34 depict the section view and the elevation view of the facade, respectively. The exterior of Haskett Hall also contained rectangular windows, arranged in rows for each floor, and seven doors for at-grade entrances.

2.2.4 Roof

The roof of Haskett Hall was composed of wooden tongue and groove decking supported by steel beams, trusses, and purlins. A composite surface of gravel and tar covered the decking and acted as the outermost roof layer. The roof was also sloped to allow rain water runoff to several rooftop drains, and several HVAC machines were housed on the roof.

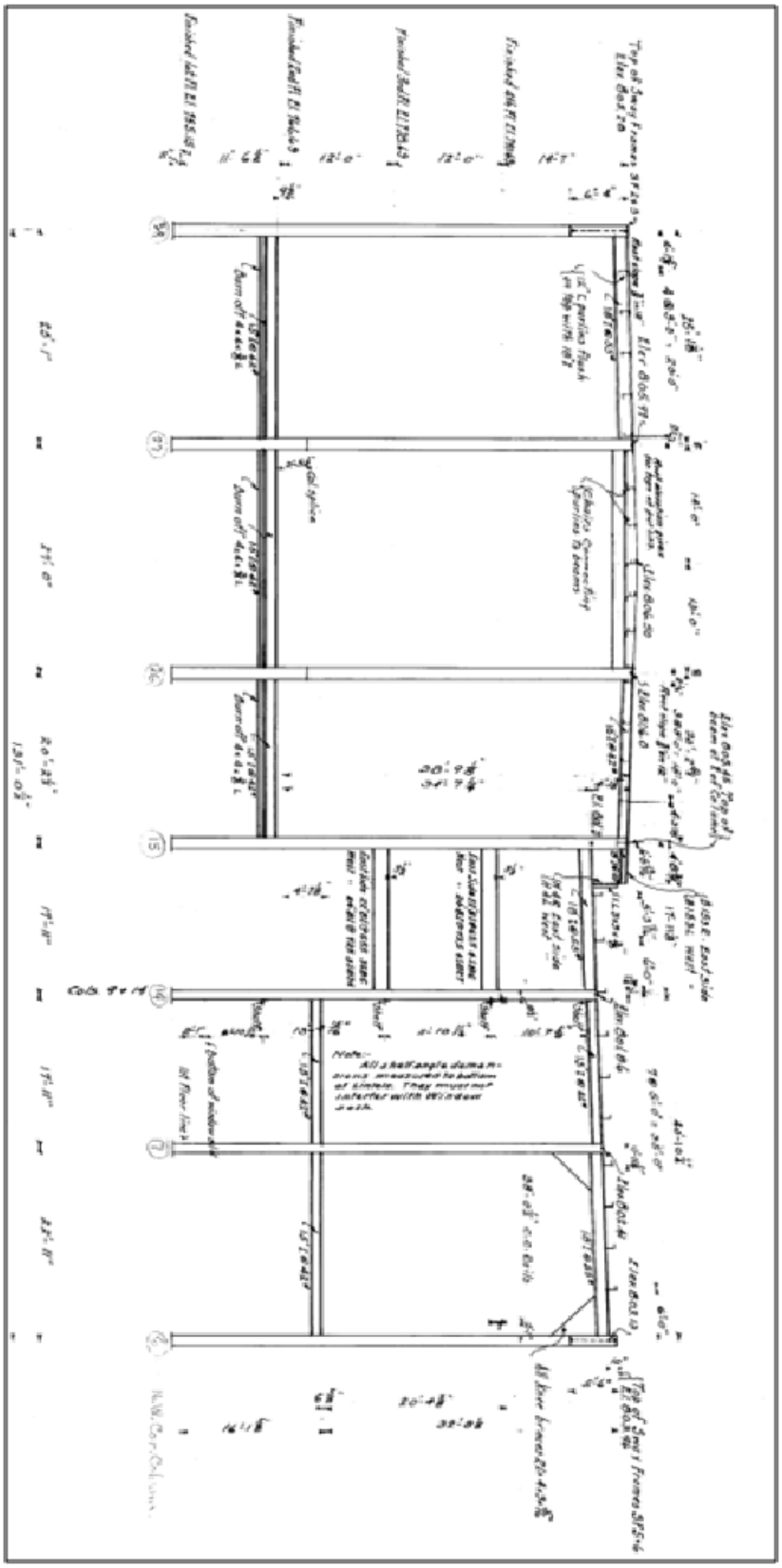

Figure 2.1: West exterior frame elevation view

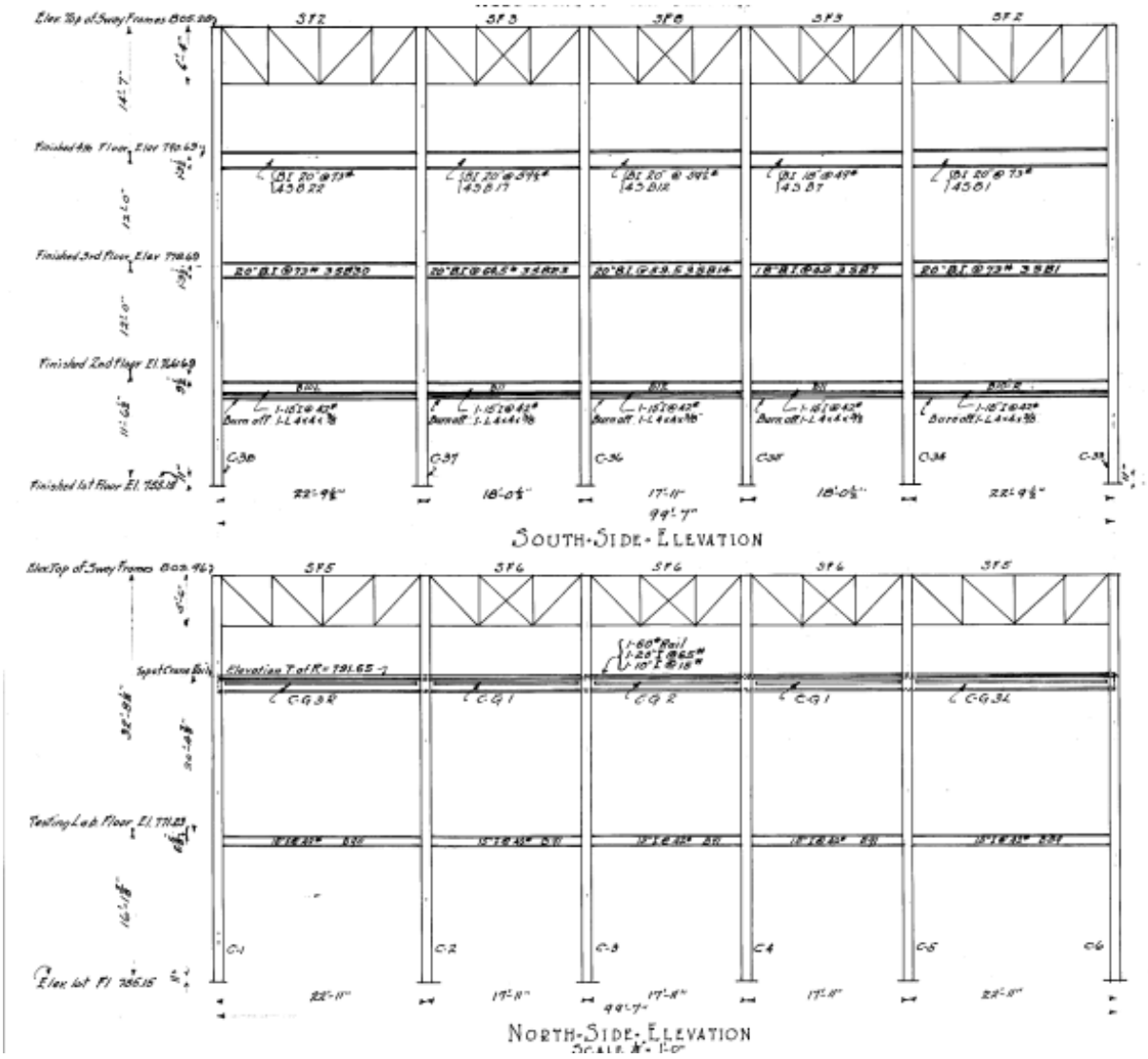

Figure 2.2: North and south exterior frame elevation views

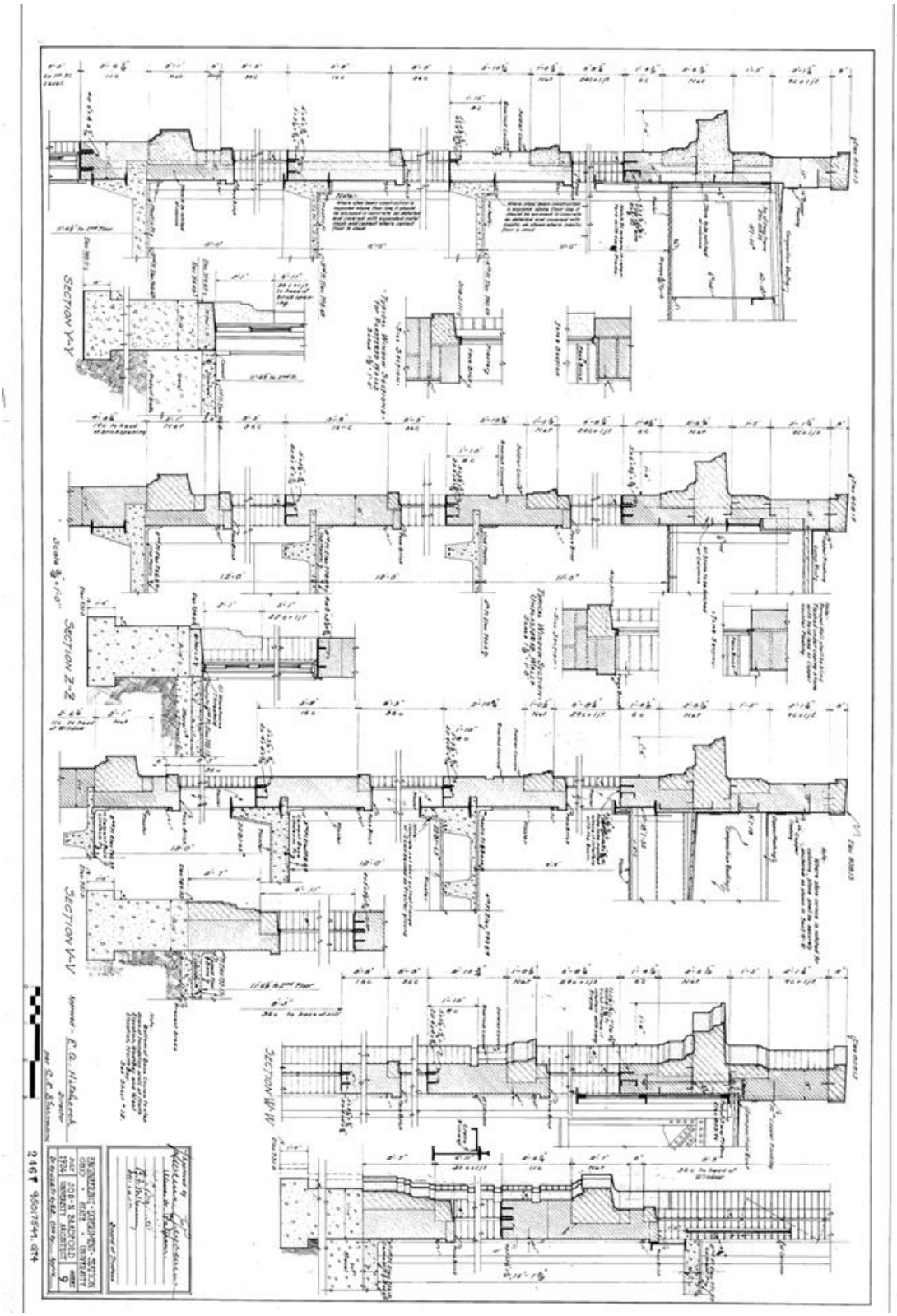

Figure 2.3: Section views of Test Frame

Figure 2.4: Architectural Views of Exterior of Building

CHAPTER 3: EXPERIMENT DESCRIPTION

3.1 Introduction

This chapter describes the instrumentation and experimentation conducted on the southwest frame of Haskett Hall. A description of the Test Frame and the selected column for removal is provided. The setup of test instruments, including strain gauges and displacement sensors, is also included. Measured strain data are tabulated and discussed, and the results of the experiment are analyzed.

3.2 Test Frame Instrumentation

The perimeter frame along the building's west side was designated the Test Frame (Figure 3.1), and the column just north of the southwest corner column was designated the Test Column (Figure 3.2). In Figure 3.2, the corner column is called "South Column", the far column is called the "North Column", and the interior column closest to the removed column is called "East Column." These columns were numbered 26, 28, and 38, respectively, in the construction drawings.

Loewendicks Demolition Company was contracted by OSU to perform the demolition. The company agreed to assist in the experiment by removing the architectural façade and performing the column removal. Architectural material on the ground level, including the brick façade and masonry units, in the bay just south of the Test Column and in the two bays just north of the Test Column was removed by Loewendicks in order to access the structural elements. During the column removal process, the strains and displacements of several structural elements were measured using strain gauges and displacement sensors.

3.2.1 Strain Measurements

The beams and columns surrounding the Test Column were instrumented with strain gauges to measure the change in strain during the experiment. A total of 16 strain gauges, numbered

Gauge 1 through Gauge 16, were used in the experiment. For a full description of the procedure for applying the strain gauges, refer to Akah (2013). The layout of strain gauges is shown in Figure 3.3 and is described below.

Seven strain gauges were installed on the North, East, and South Columns. All column strain gauges were installed to measure the change in longitudinal axial strain. First, a strain gauge was placed on each flange of the North Column at one third the story height (Gauge 1 and 2). The west side of the web of the East Column was also instrumented with a strain gauge at one half of the story height (Gauge 3). A total of four strain gauges were installed on the South column. Three gauges were placed at two thirds the story height on the south flange, the east web, and the north flange, and one gauge was placed one half the story height on the north flange (Gauge 4, 5, 6, and 7).

Nine strain gauges were placed on the three beams connected to the Test Column. Each gauge was installed on the bottom flange face of the beam within 2 in. of the beam's centerline. The strain gauges were installed perpendicular beam's longitudinal direction to measure the compressive or tensile stress developed from bending moment. The three beams spanned north, east, and south of the removed column, and each was designated as North, East, and South respectively. Gauges were installed on the beams in the order of East, South, and North.

The East beam was instrumented with a strain gauge at one half the distance between the East Column and the removed column (Gauge 8). Two gauges were also placed on the East beam at the connection to the removed column – one just north of the beams' centerline, and one just south (Gauge 9 and 10). The North beam's connection to the Test Column was also instrumented with strain gauges on the east and west sides of the beam's centerline (Gauge 11 and 12). Similarly, gauges were installed at the South beam connection to the Test Column, east and west of the beam

centerline (Gauge 13 and 14). A strain gauge was also placed on the South beam at one half the distance between the South Column and the removed column (Gauge 15). Similarly, a gauge was placed at one half the distance between the North Column and the removed column on the North beam (Gauge 16).

3.2.2 Displacement Measurements

Displacement sensors were also installed in the test area to measure the deflection of beams connected to the Test Column. The displacement sensors were Linear Variable Differential Transformers (LVDT), which use an electromagnetic couple to convert mechanical displacement into an electrical signal. LDTV's were instrumented to the North and South beams, offset from the connection to the Test Column (Figure 3.4), and oriented to solely measure vertical displacements. A third LDTV's was also positioned and oriented to measure horizontal displacements of the centroid of the North beam. To hold the LDTV's in place, wooden scaffolding was constructed by researchers Wood, Lodhi, and Savage, also seen in Figure 3.4.

3.3 Column Removal

Loewendick Demolition performed the column removal using a mechanical processor, a machine used to cut and rip structural steel members (Figure 3.5.a). The strain gauges and LDTV's were wired to a laptop on the site, and data were collected using a software package. During the column removal, all project personnel and researchers stood at a distance of approximately one hundred feet from the test site for safety.

The processor cut through the column over a period of approximately 90 seconds, making contact with the column a total of five times. The jaws of the processor also twisted and pulled the column out of plane during the column removal. Strain values were recorded every tenth of a second for all the strain gauges and LDTV's. When the column was completely cut through, the

frame did not experience progressive collapse, and researchers were able to photograph the cut state of the column (Figure 3.5.b). Finally, Loewendick continued with the demolition of the entire building.

3.4 Experimental Data and Analysis

Graphs of the experimental data versus the elapse time for each instrument are shown in Appendix B. All strain gauges measured zero strain at the beginning of the experiment, and all displacement sensors recorded zero displacement. Each period of contact between the processor and the column resulted in significant changes in the recorded strains and displacements. After the column was completely cut through, the strain and displacement graphs leveled out, indicating that gravity loads had permanently redistributed in the Test Frame.

3.4.1 Strain Data

The static strains, which are the strain readings at the end of the testing (at 360 seconds), are shown below in Table 3.1 and Table 3.2. These tables were originally compiled by Akah (2013). The experimental data in Table 3.1 and Table 3.2 below will be compared to the theoretical strain and displacement data from the model later in this thesis.

Table 3.1: Experimental strain data for columns

Gauge	Steel member	Location	Height on column	Change in strain ($x10^{-6}$ in./in.)
1	North Column	(S) Flange	3 ft-1 in.	-32
2	North Column	(N) Flange	3 ft-1 in.	-54
3	East Column	(W) Web	4 ft-7 in.	-31
4	South Column	(S) Flange	6 ft-2 in.	-7

5	South Column	(E) Web	6 ft-2i n.	-61
6	South Column	(N) Flange	6 ft-2 in.	-103
7	South Column	(N) Flange	4 ft-7 in.	-93

Table 3.2: Experimental strain data for beams

Gauge	**Steel member**	**Location on flange**	**Distance from column 27**	**Change in strain ($x10^{-6}$ in./in.)**
8	(E) Beam	Centered on N.A.	11 ft-4.75 in.	Not Available
9	(E) Beam	(S) of N.A.	At Test Column	26
10	(E) Beam	(N) of N.A.	At Test Column	-42
11	(N) Beam	(E) of N.A.	At Test Column	136
12	(N) Beam	(W) of N.A.	At Test Column	171
13	(S) Beam	(E) of N.A.	At Test Column	252
14	(S) Beam	(W) of N.A.	At Test Column	272
15	(S) Beam	Centered on N.A.	12 ft-9 in.	81
16	(N) Beam	Centered on N.A.	12 ft-9 in.	-10

All the final strains in columns were negative, indicating that the axial loads increased in each remaining column after the Test Column was removed. The highest change in compressive strain occurred in the South (corner) column, indicating that most of the gravity loads redistributed into the corner column. On beams, most strain gauges recorded positive values at the end of the experiment, demonstrating that positive moment had most likely developed. Gauge 8 failed to

record data during the experiment, and no analysis was performed using this instrument. Gauges 10 and 16 recorded negative final strain, which also seemed to be outlying results.

Strain gauges 4, 5, and 6 – each at six feet and two inches above the base of the South Column – each recorded significantly different strains. Gauge 4 was on the south flange of the column, and measured -7 x 10^{-6} in./in. Gauge 5 was on the web of the column, and measured -61 x 10^{-6} in./in. Gauge 6 was on the north flange of the column, and measured -103 x 10^{-6} in./in. The approximate strain diagram is shown in Figure 3.6, where the north flange experienced more compression and the south flange experienced more tension. This signifies that the column developed a significant amount of bending moment after column removal.

Spikes occurred in the graphs, likely a result of the twisting and pulling of the processors jaws (e.g. Figure 3.7). Following spikes, the strain data leveled out, coinciding with intermediate time periods when the processor temporarily withdrew from the Test Column. This intermediate strain data indicates that the forces in the intact structural elements approached equilibrium between processor contact periods, and that the load each member experienced from column removal increased as the cross-sectional area of the column decreased. The displacement sensor data illustrates a similar pattern between contact periods. As the column cross-section reduced, the frame was allowed to deflect downward above and around the removed column, and the gravity loads were redistributed away from the Test Column proportionally to the removed cross section.

Strain Gauges 9 and 10 were both on the East beam at the connection to the Test Column. These gauges' respective strains were expected to be comparable, but the final strains recorded had opposite sign values. The data for gauges 9 and 10 appears below as Figure 3.7. Examining this combined graph, 10's graph was revealed to have shifted down, but follows the slopes and

inflection points of 9's graph. This could indicate malfunction in either of the gauges or the twisting effect of the processor.

A number of intermediate strains appeared higher than the final recorded strains, including Gauge 4 in period 2, Gauge 14 in period 2, and Gauge 12 in period 3 and 4 (Figures B.4, B.6, and B.7). For Gauges' 12 and 14, this result could be explained by the pulling of the processor. The strains in 11 and 13 mirror the strains in 12 and 14; the gauges toward the outside of the frame (12 and 14) experienced more tension, while the gauges on the inside of the frame (Gauges 11 and 13) experienced more compression. The internal couple demonstrated by the strain varying over the cross-section indicates that the beams were bending about their weak axis. As the processor pulled the Test Column out-of-plane, moment developed in the beams about their weak axes to resist the lateral deflection. This result is illustrated in Figure 3.8.

3.4.2 Displacement Data

The displacement of the structure measured by the displacement sensors varied throughout the column removal process. After the 360th second, the displacements remained constant, and the final displacement of the structure after column removal was determined. The displacements measured are shown in Table 3.3.

Table 3.3: Experimental displacements

LVDT	Steel member	Orientation	Distance from column	Displacement (in.)
1	(N) Beam	Vertical	1 ft-6 in.	0.474
2	(S) Beam	Vertical	2 ft-4.75 in.	0.659

Figure 3.1: Haskett Hall in 1925, with the Test Frame location marked

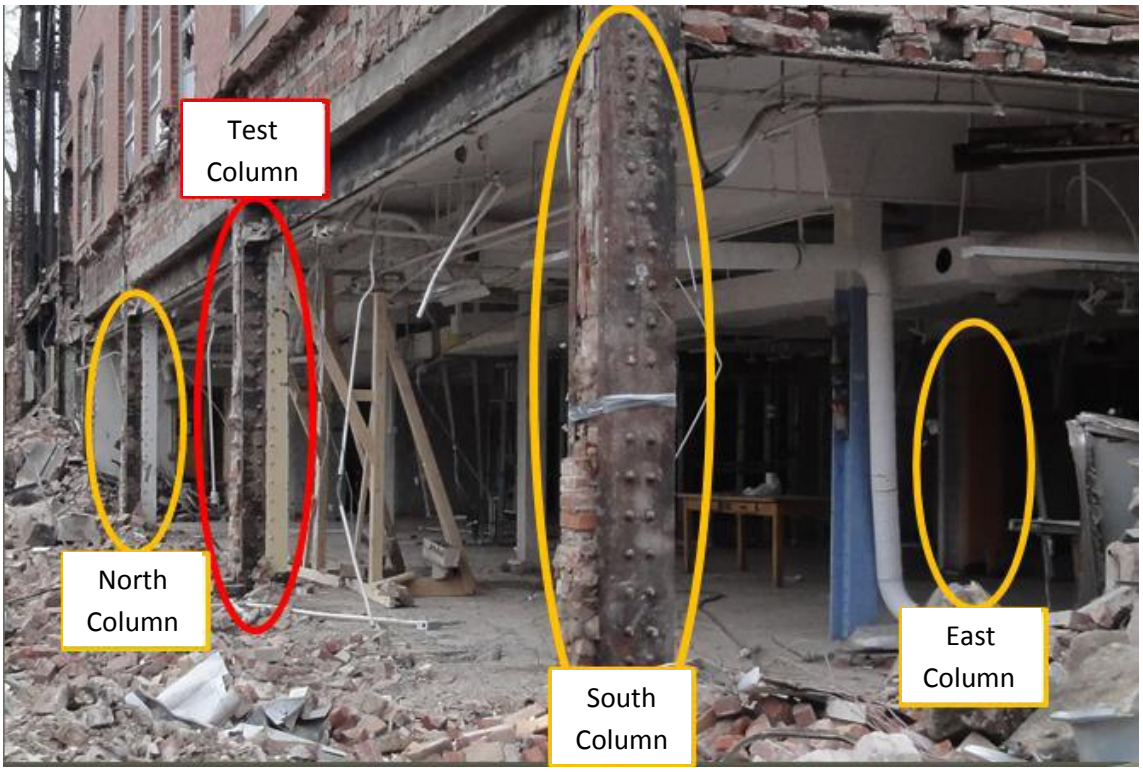

Figure 3.2: Test Column and Test Frame area

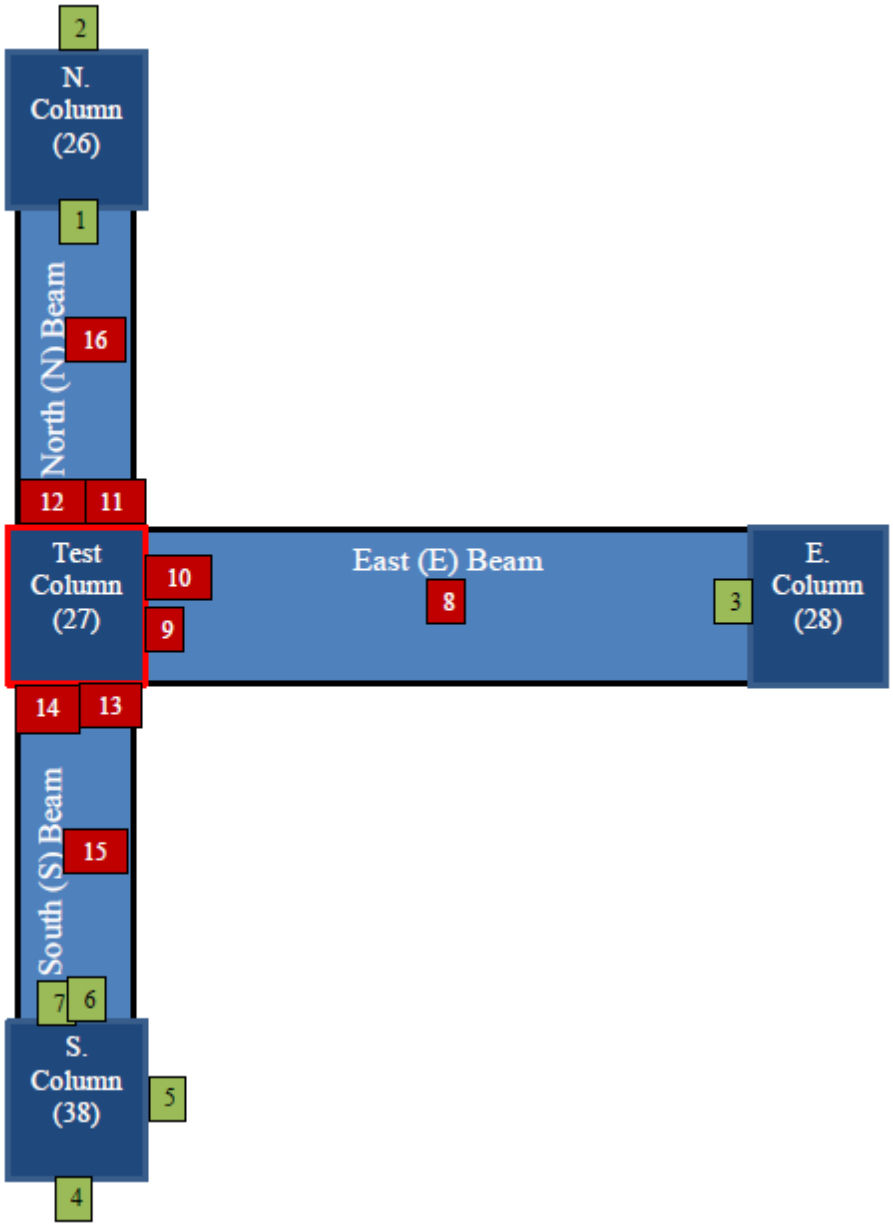

Figure 3.3: Layout of strain gauges (Gauges 1 through 7 are attached to columns; Gauges 8 through 16 are attached to beams)

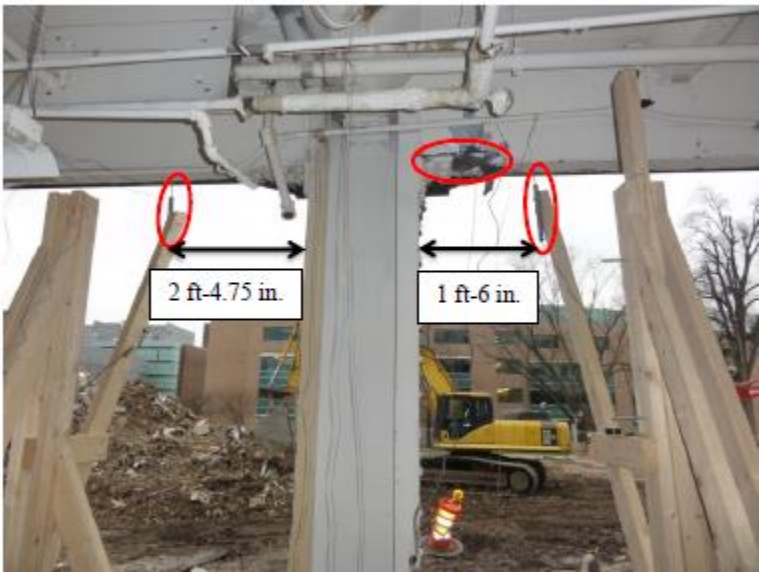

Figure 3.4: Position of displacement sensors and distance from removed column connection

Figure 3.5: (a) Processor removing column, and (b) column after removal

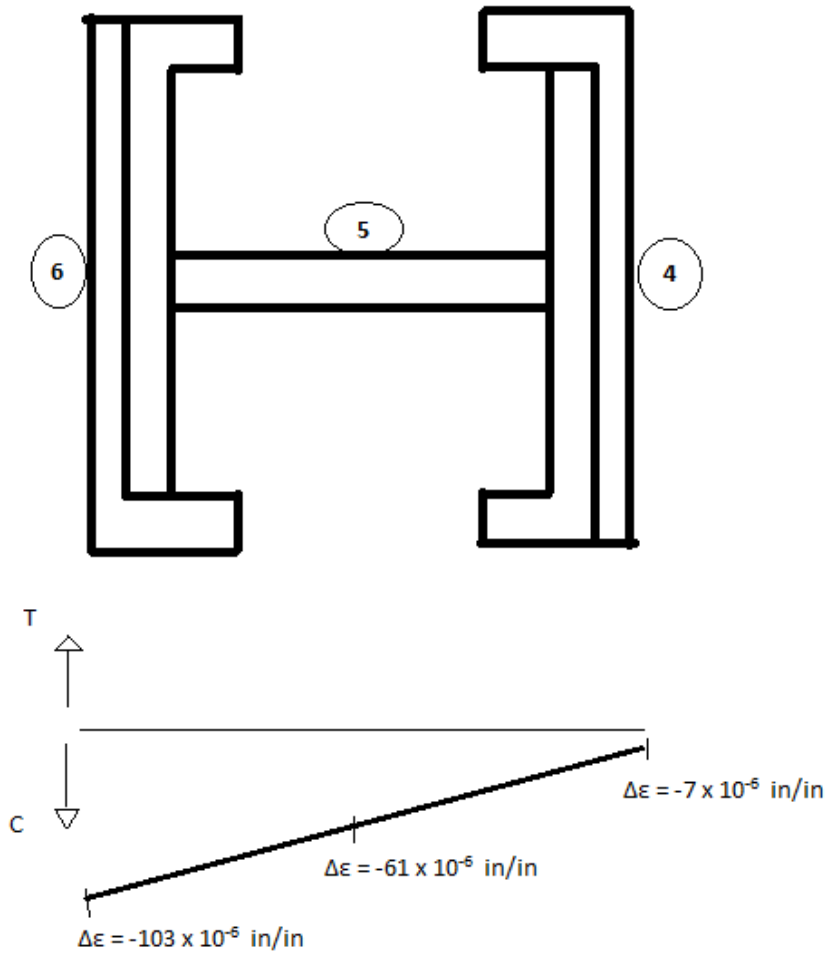

Figure 3.6: Approximate strain diagram across South Column at 6 ft – 2in. above the base

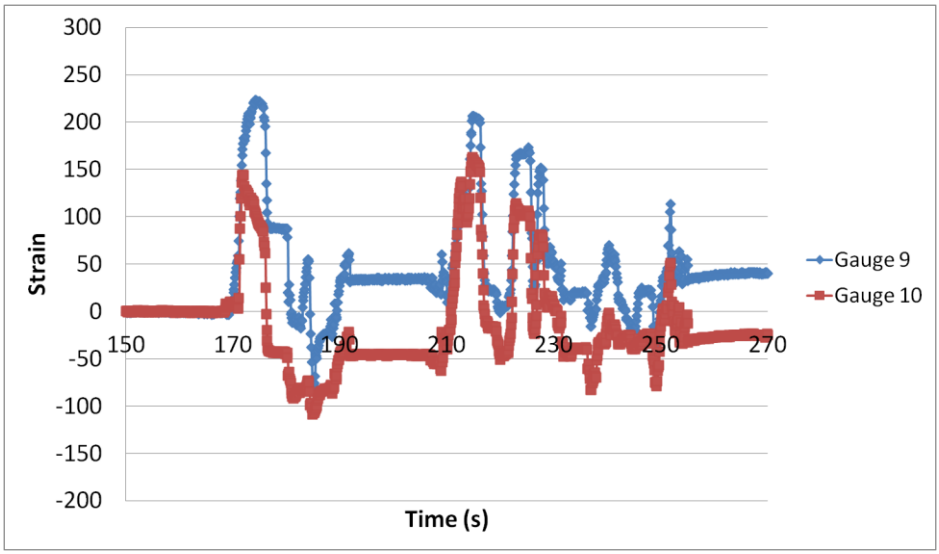

Figure 3.7: Strain vs. time for Gauges 9 and 10

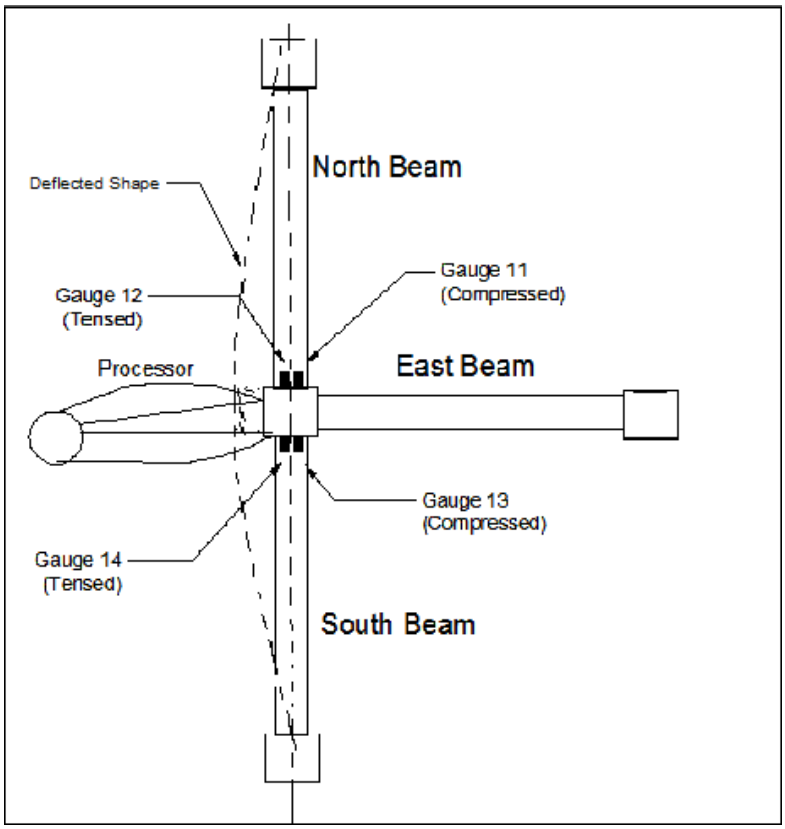

Figure 3.8: Out-of-plane bending of Test Frame from pulling of the processor

CHAPTER 4: FRAME DETAILS FOR MODELING

4.1 Introduction

This chapter provides the construction details of the experimental frame. The parameters used in modeling and their sources are explained. Dimensions and section properties for each beam and column are typically determined from the 1925 construction documents and photos taken on the day of the experiment. The methods used to determine loads for modeling are also given.

4.2 Framing

The geometry of the western perimeter frame of Haskett Hall was determined to perform the two-dimensional analysis. Bay widths, story heights, and geometric irregularities were determined from 1925 construction drawings. The columns numbered 6, 7, 14, 15, 26, 27, and 38 were included in the seven-bay frame (Figure 2.1). All construction drawings used in this investigation are included in Appendix A.

The beams were discontinuous throughout the west frame. The second story beams between column 6 and 7 (on the north end) were approximately 4.5 ft above the rest of the story to elevate the testing laboratory on this end of the building (Figure 2.1). No exterior beams were constructed on the third and fourth stories in the bays between column 15 and 38. Instead, a ribbed slab transferred floor loads to the girders inside the building (Figure 4.1).

4.3 Beam Details

The frame contained steel I-shaped beams, and concrete was cast around the steel beams mainly for fire protection (Figure 2.3). Beams were connected to columns by two clip angle sections and a bottom and top flange plate as shown in Figure 4.2. Construction drawings, such as in Figure 2.1, include the beam sizes; these sizes are listed below in Table 4.1. The AISC section dimension

symbols are used, which are shown in Figure 4.3. In this convention, A is the cross sectional area, d is the overall depth of the section, t_w is the thickness of the web, b_f is the width of the flange base, t_f is the thickness of the flanges, and I_x is the moment of inertia about the X-axis. Additionally, the beam sections are named with the convention *Shape depth* x *weight*. For example, B18x55 refers to a B section with an overall depth of 18 in. and weight of 55 lbs/ft

Table 4.1: Dimensions of beams in the Test Frame

Historic Member	A (in^2)	d (in)	t_w (in)	b_f (in)	t_f (in)	I_x (in^4)
B15x42	12.41	15.00	0.360	6.740	0.550	464.9
B18x55	16.19	18.12	0.390	7.532	0.630	889.9
B24x73.5	21.56	24.00	0.390	9.000	0.701	2095.7

The beam sizes provided in Figure 2.3 were used with the historic sections database of the *American Institute of Steel* Construction to determine the section properties listed above. Only the weight and depth of the sections were given in the drawing, and several sections in the historic database matched the values named in 2.3. Photographs taken of the framing on the day of the column removal were used to determine the final sections used in the analysis. This process is documented in Akah 2013.

4.4 Column Details

Haskett Hall's columns were built-up steel sections consisting of channel sections riveted to the top and bottom flange of a central I-section (Figure 4.2 and Figure 4.4). The two channel sections were oriented to bracket the center I-section. Bricks were laid in exterior channel sections, which increased fire protection (Figure 3.2).

Unfortunately, no column schedule was provided to the research group with the rest of the 1925 construction documents, and no drawings named any column sizes throughout the building. Thus, the column section dimensions had to be inferred from the scales in the provided floor plans and from photographs taken on the day of the experiment. Historically, architectural draftsmen have a reputation for providing accurately-scaled details, such as column depth and width, in construction documents.

First, dimensions for the I-sections and channel sections of each column were measured in the construction drawings and photographs. Next, I-sections were found in the historic sections list that fit the measurements well. Finally, assumptions were made about the channels bracketing the columns, and channel sections were chosen. These final section dimensions were used in the modeling process. A similar process for determining the column sections is provided in Akah 2013, and the same modeling parameters are used.

4.4.1 AutoCAD Analysis

Drawings were selected from the drawing set that clearly depicted the column sections and provided scale information. Most of these drawings were floor plans. Pictures that clearly show a dimension of a column section and a rivet head adjacent to the desired dimension were also found.

High precision was achieved in determining the column dimensions by scaling the drawings and photographs in AutoCAD. Using CAD software provided a benefit over measuring drawings by hand by providing consistent precision. Using a ruler, the measurement precision can vary each time a value is measured. Screenshots showing the dimensions in AutoCAD, as well as annotation of the measuring procedure, appear in Appendix C. A sample of this dimensioning is shown in Figure 4.5.

4.4.2 Scaling Methods for Drawings and Photos in AutoCAD

The architect of Haskett Hall included rulers at the bottom of each drawing indicating the scale or length used for an inch. A scale factor for each section was also given relating a fraction of an inch to 1 foot (e.g. 3/16 in.: 1 ft). The drawings were imported to AutoCAD and scaled using the SCALE function, where the scale factor was found using the ruler and scale factor given on each drawing.

The pictures were scaled using the fixed size of the rivet heads in the photographs. A rivet head was saved from the demolition, and its diameter was measured as 1.5 in. The diameter of the rivet heads in the pictures was measured, and a scale factor was found as 1.5 in. divided by the measured diameter of the rivet. The pictures were scaled in AutoCAD using the SCALE function and the factor described above. Figure 4.5 below shows an example of the scaling process.

The dimensions for the sections were then easily measured in AutoCAD. The measurements taken included the total base b (or depth of the channels), the depth of the I-beam section d_b, width of the I-beam flange b_b, thickness of the I-beam flange t_f, thickness of the I-beam web t_w, thickness of the channel web $t_{w\text{-}c}$, and width of the channel flange b_c. Table 4.2 below shows the measurements for all column dimensions. The measurements for individual drawings and photographs are provided in Appendix C.

Table 4.2: Section dimensions, average of drawing and photograph measurements (in inch units)

Column number	Base, b	WF depth, d_b	Flange base, b_b	Flange thickness, t_f	Web thickness, t_w
38	14.16	16.70	7.21	0.89	0.89
27	15.44	20.50	7.37	0.91	0.89
26	15.73	20.60	7.34	1.13	0.96
15 & 7	13.40	12.72	6.87	0.60	0.97
14	15.00	14.39	7.07	0.81	1.08
6	14.76	14.00	5.40	0.84	1.20

4.4.3 Limitations to Measurement Method

The accuracy of measuring the dimensions of the columns from drawings was limited by the accuracy in the architectural draftsman in the drawings. The column sections are very small compared to the total size of the drawings, so they were quite difficult to draw to a precise scale. Additionally, the drawings were initially hand-drawn and scanned electronically into a computer much later, and several sections appear to have been distorted by this process.

The accuracy of the picture analysis was limited by the perspective that the pictures were taken at. Many of the pictures had a skewed view of the columns, so that the actual dimensions had to be measured as a projected line. Also, few pictures showed the desired dimension and rivet head in the same plane. The scale factor for the rivet head became inaccurate when the desired dimension was further away from the rivet head.

4.4.4 Assumptions

A number of assumptions were imposed on the dimensions gathered in AutoCAD that further simplified the section selection process. For each column, the I-beam section inside the channels showed flange thickness increasing toward the web. This resembles the Standard Beam (S) shape. It was assumed that all sections were S shapes. The sections appeared relatively bulky in the pictures, so only sections with relatively high values for total cross-sectional area were considered. And finally, the foundation details in Figure A.6 shows that the width of the column footing for several sections was the same, so several sections were assumed to have been designed as the same. This is consistent with the columns section drawings on the plans. From this, column 14, 6, and the South Column were assumed to be the same section, the North and Test Columns were assumed to be the same section, and column 14 and 7 were assumed to be the same section. Finally, the thicknesses of the channels were hard to measure reliably, but their thickness appeared less than the thicknesses of the S-section's flanges. After S-sections were selected, channel thicknesses were selected as roughly half the thicknesses of S-section flange thicknesses. This value was uniformly assumed as 1/2 in.

4.4.5 Column Section Properties

The AutoCAD results were used in conjunction with the historic section spreadsheet to compile a list of section possibilities for each column. Each section in the Historic Sections database (AISC 2013) provides a Footnote that indicates the manufacturer and the year it was manufactured. Construction of the building started in 1924, but no Standard Beams provided in the database were manufactured in this year. It was assumed that the beams were manufactured in 1923, and sections were found in this year from a single manufacturer.

The results of the AutoCAD analysis (Section 4.4.1-4.4.2) confirmed the above assumptions, as did the Historic Sections list, as the dimension for each section within these categories converged relatively well. The values for each section vary from drawing to drawing, but stay within 10-15% of each other, showing good accuracy of this method of post-determining section dimensions.

Tables 4.3 through 4.5 provide properties of 15, 20, and 12 in. deep columns, respectively. In Tables 4.3 through 4.5, *A* represents the cross-sectional area, and I_X represents the moment of inertia about the strong (X) axis.

Table 4.3: Column section properties

Expected values (based on AutoCAD analysis)								
Column				*d (in)*		b_f *(in)*		
38				*15.68*		*7.55*		
14				*14.39*		*7.07*		
6				*14.46*		*6.96*		
27				*18.02*		*7.37*		
26				*19.36*		*7.38*		
15				*12.72*		*6.87*		
7				*11.68*		*6.24*		
Section used from Historic Sections								
	Type	Designation	A *(in^2)*	*d (in)*	t_w *(in)*	b_f *(in)*	t_f *(in)*	I_x *(in^4)*
38, 14, 6	S	S 15x81.3	23.91	15.00	0.826	6.400	1.034	795.5
26, 27	S	S 20x90	26.47	20.00	0.723	6.897	0.973	1569.0
7, 15	S	S 12x45	13.24	12.00	0.578	5.373	0.657	285.7

4.4.6 Channel Section Properties

After the dimensions for each I-beam section were determined, the dimensions for the bracketing channel sections were determined. The measurements for the base of the sections given above were used for the depth of the channel section, and a uniform thickness of 1/2 in. was assumed. Since no historic information was available for channel sections, the results of the

AutoCAD analysis were used to directly infer the dimensions of the channels. The results appear in Table 4.4 and will be used in modeling.

Table 4.4: Channel section dimensions (inches)

Column	Depth, d_c (in)	Web thickness, $t_{w\text{-}c}$ (in)	Flange width, b_c (in)	Flange thickness, $t_{f\text{-}c}$ (in)
7, 15	13.00	0.50	3.00	0.50
6, 14, 38	13.50	0.50	3.00	0.50
26, 27	15.50	0.50	4.00	0.50

4.5 Load Calculations

Weights were calculated for all elements that remained in the building at the time of demolition. These included the roof, brick façade around the outside of the building, windows, floor slabs, and some mechanical components throughout the building such as piping. Material weights are used to calculate dead loads in the computer model.

4.5.1 Floor Loads

The process of calculating floor slab loads on the second, third, and fourth stories is fully documented in Akah (2013) and will be summarized here. Both ribbed slabs and slabs with constant thickness were used in Haskett Hall. Each slab type required a different load calculation. The loads calculated by Akah appear in Appendix D.

Ribbed slabs consisted of a 3 in. thick slab supported by concrete joists spaced approximately 2 ft and 3 in. whose depth was 10 in. and base was approximately 5 in. These slabs transferred loads in one direction, parallel to the longitudinal direction of the joists. The joists were parallel to the plane of the Test Frame, so the weights of ribbed slabs resulted in point loads on columns in the Test Frame (Figure 4.1). The density of the reinforced concrete is assumed to be 150

pcf. An area load was calculated based on the volume of the slabs and joists, and the load on the column was calculated using tributary area.

Constant thickness slabs with an aspect ratio of 2:1 or greater were considered one-way and the loads they carried to beams were based on tributary width. Slabs with an aspect ratio less than 2:1 were considered two-way and carried trapezoidal and triangular loads to their supporting beams. The area of the slabs was divided according to their load contribution, and the thickness of the slabs was used to find the distributed loads.

4.5.2 Roof and Wall Loads

The roof and floor loads were determined using volume of material, material densities, and load transfer paths. Hand calculations for these loads appear in Appendix D. Figure 4.6 developed by Akah (2013) shows the calculated loads on the frame.

First, the volumes of the components given in the construction drawings were calculated. Next, densities for the construction materials were assumed to be typical values, since the construction documents did not specify material densities. The weights of components were then found by multiplying the density by the volume. Finally, the weights were transferred to structural elements. No live load existed in the building at the time of testing.

A plan view of the roof framing system is shown in Figure 4.7. The materials in the roof system included structural steel purlins, 2x4 wooden beams, wooden tongue and groove deck, and rooftop gravel. The depth of these materials per foot of wooden beams was calculated using the section provided in the construction drawings (Figure 4.8). The density of steel used was 490 pounds per cubic foot, and the density of wood used was 35 pounds per cubic foot. These materials were converted to an area load by multiplying the depth in the section by the density. The area load resulting from the purlins was calculated to be 22.2 psf. The unit weight of the gravel on the

roof was assumed as 5.5 psf and added to the weight of the other materials for a total roof area load of 27.7 psf. These weights were distributed to the frame by one-way load distribution using tributary areas, according to Figure 4.7.

The exterior wall sections were comprised of brick wall, limestone floor trim, and windows. After the wall section was partially demolished in the first story (removing the load-bearing capacity of the wall), the full weight of the façade was bearing on the beams and girders above. An average thickness of the wall was found to be 13 in. per foot of wall, including the width of limestone trims. The bricks in the façade were fully grouted, as indicated by photographs taken during the experiment and by the construction drawings. A density of 100 pounds per cubic foot was used for the bricks, and it was assumed that the density of the limestone trim would be comparable. The area of the windows was then calculated, and this value subtracted from the total area of the wall. Since there were no beams at the third and fourth floors, the weights of the walls were represented with point loads on the columns at these levels. For example, the area of brick the South and Test Columns at the fourth floor was found to be 120 square feet, and the load on the South Column (the corner column) was found to be 13.1 kips. There were steel beams at the second floor in the frame, and the weight of the bricks was represented with a line load along this beam. The total weight of the wall along this 72 ft section was found to be 64.3 kips, so the line load was found to be 0.889 kips per ft.

The dimensions of the windows were taken from the construction drawings, and volume of glass per window was calculated. The weight of each window was then calculated to be 100 lbs., and the weight of glass in each bay was distributed evenly throughout the bay to determine a line load on the beams. Since there were eight windows at the second floor, the line load representing the windows was found to be 0.012 kips per foot. At the third and fourth stories, the windows

were represented with point loads on columns. For example, one and a half windows were found to be supported by the South Column, so the point load here was calculated to be 150 lbs. at each floor.

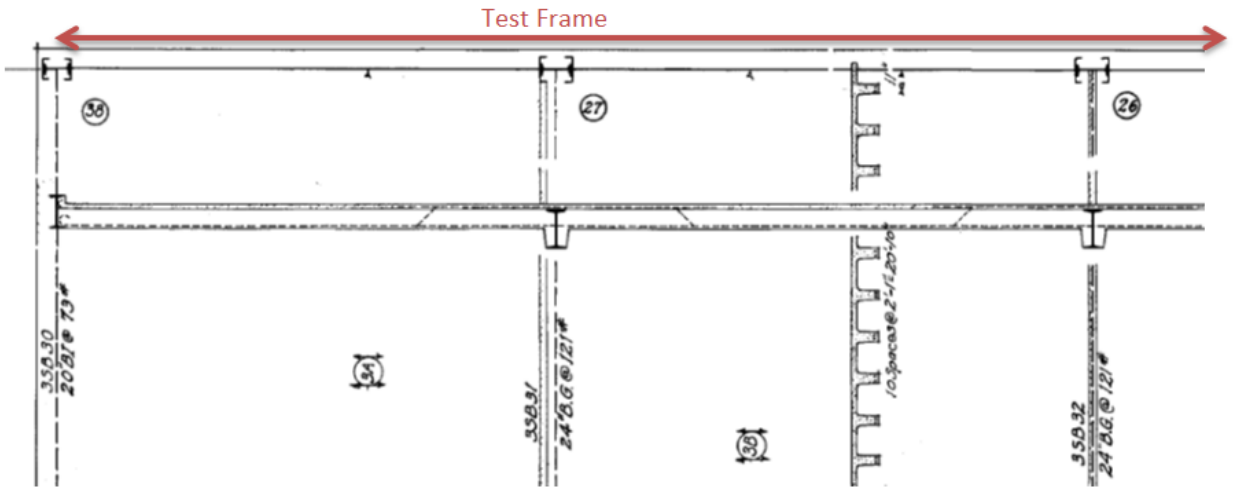

Figure 4.1: Ribbed slab section and Test Frame

Figure 4.2: Photograph of the beam-column connection, typical for all beams in the frame

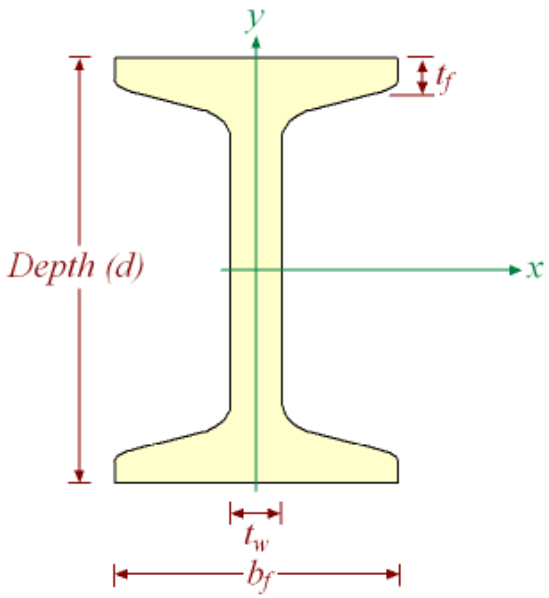

Figure 4.3: Typical steel section with dimensions (AISC 2013)

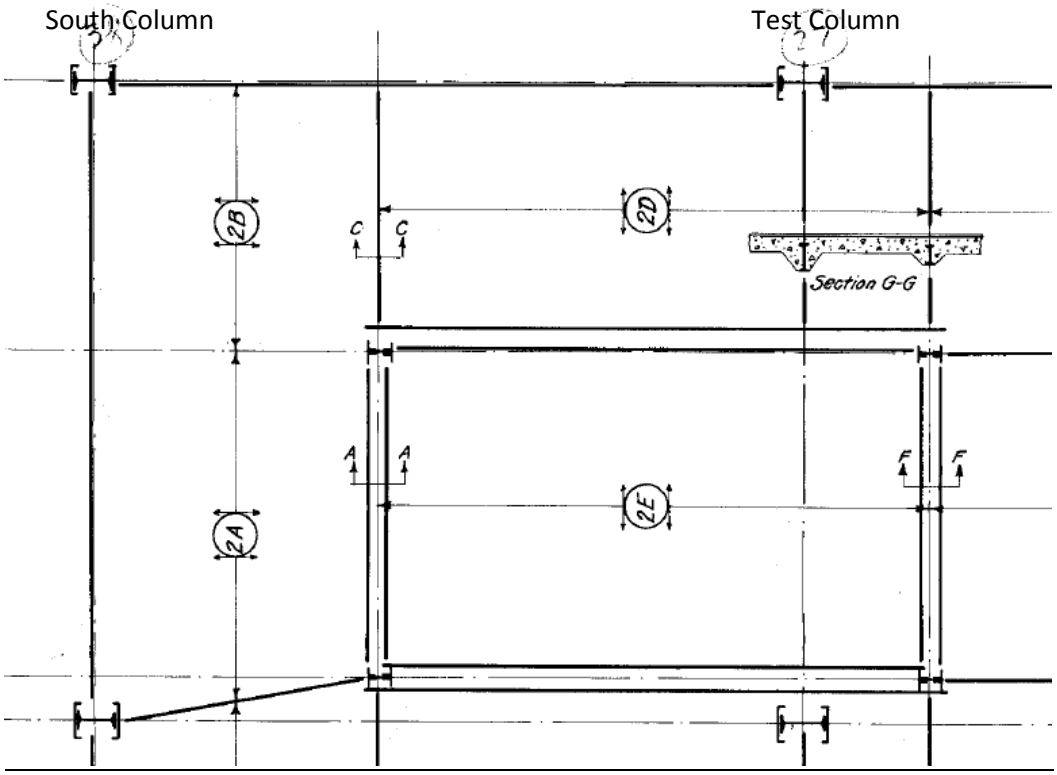

Figure 4.4: Plan view of second floor structural framing, showing column section geometry

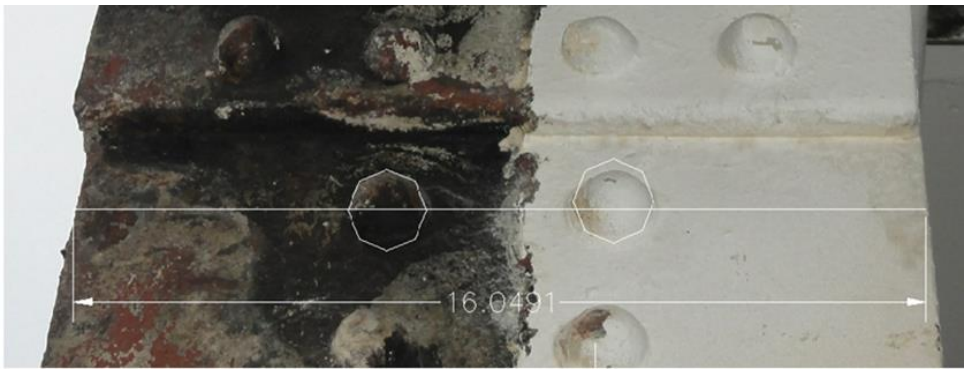

Figure 4.5: Sample of column section dimension measurement, where the channel depth is measured as 16 in.

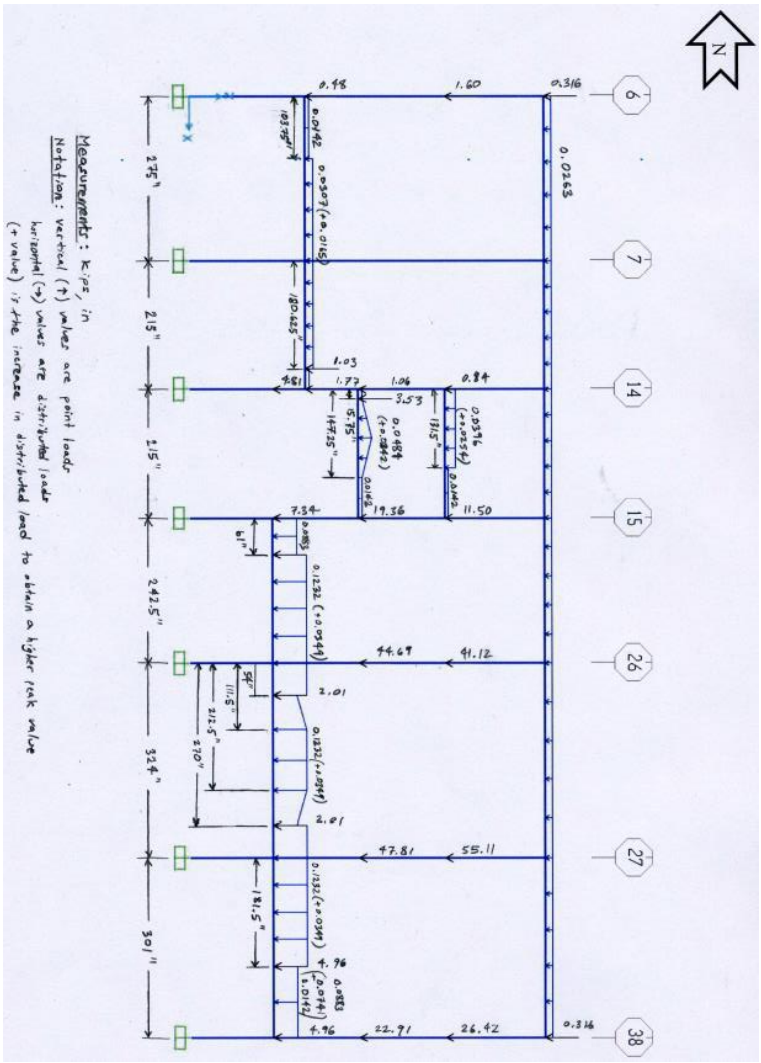

Figure 4.6: Results of load calculations, loads applied to the Test Frame (Akah 2013)

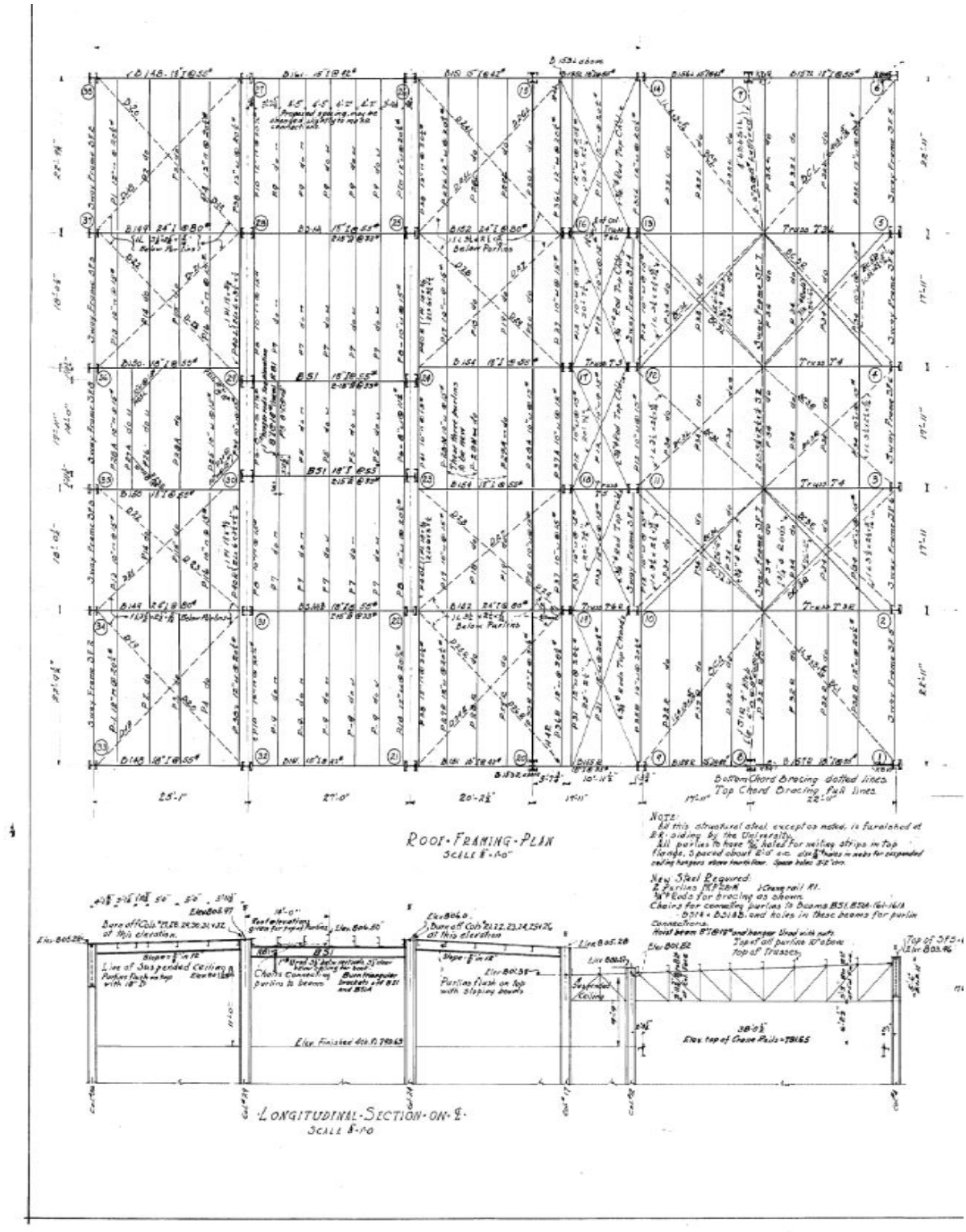

Figure 4.7: Roof construction details

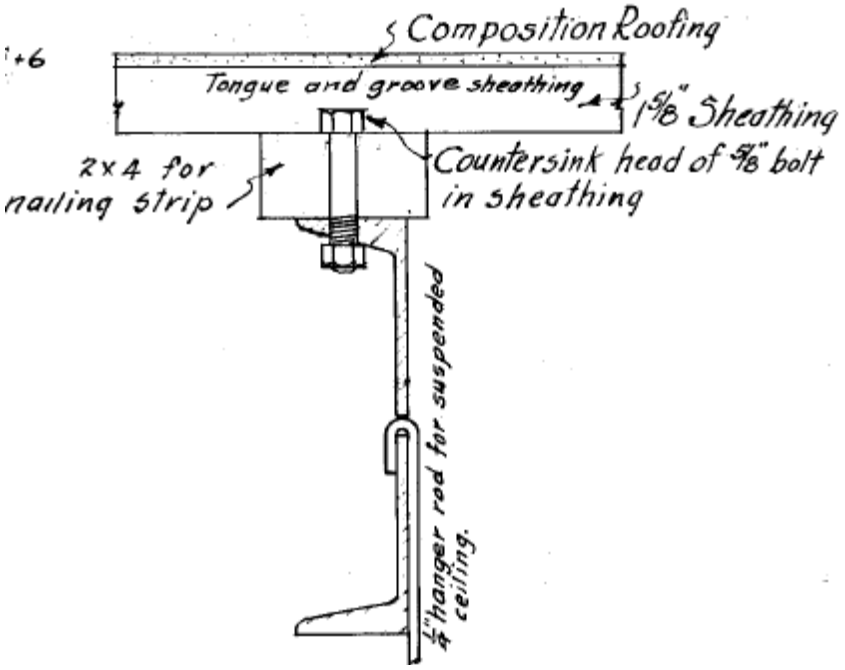

Figure 4.8: Section view of roof purlin

CHAPTER 5: CAPACITY MODELING PROCESS

5.1 Introduction

Chapter 5 provides the assumptions, parameters, and methods employed to create the initial computer models of Haskett Hall. The programs ELS (ASI 2013) and SAP2000 (CSI 2012) were used for modeling and analysis. The section properties and loads determined in the previous chapters are input to the program, and assumptions about loading characteristics and building response are discussed.

5.2 Goals

The initial computer model was created to analyze the susceptibility of the frame to progressive collapse after column removal. To achieve this goal, the calculated loads and section properties were input to the software. The column was removed in the model, and the resulting beam moments were compared to the capacities of the section. This model is called the Capacity Model. Figure 5.1 and Figure 5.2 show the final ELS and SAP2000 Capacity Models, respectively.

Linear static models were created in ELS and SAP2000. The models were static because, while the column removal was a dynamic process, the dynamic effects of the column processor are difficult to analyze and input to the softwares. Additionally, nonlinear models are significantly more difficult to create in SAP2000 than in ELS. Only the linear models are compared between the two programs.

5.3 Assumptions

The models used finite element theory to solve for equilibrium in structural elements as loads were applied. All non-structural material (including infill walls) was assumed to contribute no load carrying capacity. In the model, the frame extended along the ground in the X direction and upward in the Z direction (Figure 5.1 and 5.2). The frame existed in one plane in the Y-direction.

Rotation about the X and Z axes and translation in the Y axis was restrained in the model to ensure that the problem remained two-dimensional. The base of each column was assumed to be fixed (Figure E.5 and Figure E.15).

All beams in the frame were encased in concrete for fireproofing, as can be seen in Figure 5.3. This concrete was assumed to have cracked, contributing no capacity to the section. However, the concrete slab above the steel beam shown in Figure 5.3 was assumed to contribute to the structural capacity of the section. T-sections composed of steel I-beams and reinforced concrete were modeled in the frame.

A linear static analysis of the frame model was performed, neglecting the nonlinear behavior of structural elements and dynamic load effects. This allowed for very simple analysis of load redistribution after the frame reached static equilibrium in the experiment. The susceptibility of the building to progressive collapse was then determined using the Demand Capacity Ratio (DCR) according to the General Services Administration (GSA 2003). The DCR is calculated using Equation 5.1:

$$DCR = \frac{Q_{UD}}{Q_{CE}} \qquad \text{Eq. 5.1}$$

In Equation 5.1, Q_{UD} is the acting load effect on the structural element in question, and Q_{CE} is the expected un-factored nominal capacity of the element. In this analysis, Q_{UD} is determined from GSA (2013) Equation 4.1:

$$Q_{UD} = 2(DL + 0.25LL) \qquad \text{Eq. 5.2}$$

where *DL* is the load effect from dead loads, and *LL* is the load effect from live loads. Since no live load was assumed to be acting on the frame, only dead load contributed to Q_{UD} calculation.

To analyze the frame's susceptibility to progressive collapse with *DCR*, only the moment capacity of the section is considered. The shear capacity beams and columns and the capacity of

connections is not considered. Thus, Q_{CE} is the plastic moment of beams (M_P), and is calculated using Equation 5.3:

$$M_p = F_y Z_x \qquad \text{Eq. 5.3}$$

Where F_y is the yield stress of the steel section, and Z_x is the plastic section modulus. The plastic section modulus was obtained from the section properties in SAP2000, and the values are shown in Figures E.17 through E.20. The typical yield stress for steel at the time that Haskett Hall was constructed (1925) was assumed to be 36,000 psi. The plastic moment M_P was calculated for the North and South beams and found to be 9601 kip-in. and 9273 kip-in., respectively.

Although ASI ELS offers very sophisticated meshing capabilities, beams and columns were only segmented into elements along their longitudinal section. Thus, beams and columns were modeled as finite line elements. This allowed all plane sections to remain plane, following elastic beam theory. Results of this analysis were compared to the SAP2000 results.

5.4 Model Components

The information used to create the model included the length and orientation of beams and columns, the dead loads on the structure from the weight of remaining material, structural material properties, connection details between structural elements, section properties of beams and columns, and the finite element mesh. The length, position, and orientation of structural elements in the model was obtained from the construction documents, and appear in Figure 2.1 Dead loads on the structure were determined in Section 4.5, and the results appear in Figure 4.6. Screenshots of the information that was input to ELS and most of the information input to SAP2000 appear in Figure E.3, Figure E.4, and Figure E.14. The section properties used were identical to those used by Akah (2013), and screenshots of these properties in SAP2000 are shown in Figure E.6 through E.12 and Figure E.17 through Figure E.20

5.4.1 Material Properties

The concrete ultimate compressive strength in the slabs and beams was specified in the plans as 4000 pounds per square inch (psi). The concrete was transformed to steel, as documented below, so no concrete properties were given to the program. The yield stress of steel was considered to be 36,000 psi, which was the typical yield stress of steel that was fabricated in 1925. The modulus of elasticity of concrete was assumed to be 3.65×10^6 psi, and the modulus of elasticity of steel was assumed to be 29×10^6 psi. Steel material properties were given directly to the softwares, as shown in Figure E.1 and Figure E.13.

5.4.2 Connections and Loads

The connections in the frame were given as moment connections to the program. To achieve moment connections in ELS, steel elements are extended into the members that support them. In SAP2000, elements are connected at a single point in the model space, while in ELS, elements are connected at a number of points (Figure E.2 and E.21). By default, the connection in ELS will have more rigidity, since the connection size includes the depth of the connecting beam. To achieve this effect in SAP2000, rigid end offsets are used. The rigid end in SAP2000 was assumed to be the full depth of the connecting column section equal to 21 in., and this section property is show in Figure E.16.

5.4.3 Composite Section Properties

The process of determining the section properties for the steel, I-shaped beams and columns is described in Section 4.3 and 4.4. These sections were input to ASI ELS directly, as the program allows the user to provide section dimensions. Figure 5.3 shows the extent of the concrete around the second story beams in the frame, making the section composite steel and concrete. The concrete in the web section was assumed to have cracked in bending, and the

effective composite section is shown in Figure 5.6. Since the steel beam and concrete slab form a T-beam section, the effective width of concrete contributing to bending capacity was found using the American Concrete Institute (ACI) equation (ACI 318, 2008):

$$b_{eff} \leq \begin{Bmatrix} \frac{1}{4} span\ length \\ -b_w + 16h_f \\ beam\ spacing \end{Bmatrix} \qquad \text{Eq. 5.1}$$

In this equation, b_{eff} is the effective top flange width, *span length* is the distance from the center of the supports at each end of the beam, b_w is the base of the web of the section (taken as the base of the steel flange), h_f is the height of the effective flange (taken as the thickness of the concrete slab), and *beam spacing* is the center to center distance between the beam and the adjacent parallel beam. The least effective flange width is found with the first equation, using one fourth the span length.

The composite sections were transformed to pure steel when input in the model. A scale factor for the transformation was found using Equation 5.2:

$$n = E_c/E_s \qquad \text{Eq. 5.2}$$

where E_c is the modulus of elasticity of concrete (equal to 3645 ksi for concrete of compressive strength $f_c' = 4000\ psi$), and E_s is the modulus of elasticity of steel (equal to 29,000 ksi). The scale factor *n* was found to be 0.126, and the effective flange width of the transformed steel material was adjusted accordingly to model accurate stiffness of the section. The results of this analysis and the values used are shown below in Table 5.1, and the pure steel transformed section is shown in Figure 5.5. The values for b_{eff} found using *I* were used in the model, and these values are shown in bold.

Table 5.1: Effective section properties of composite second story beams (Akah, 2013)

Beam between Columns (#, #)	Span Length (in.)	Concrete b_{eff} (in.)	Steel b_{eff} using n (in.)	Steel b_{eff} using I (in.)
15, 26	242.5	60.63	7.62	**5.50**
26, 27 (North Beam)	324.0	81.00	10.18	**7.30**
27, 38 (South Beam)	301.0	75.25	9.46	**8.00**

When calculating the *DCR* of the section, the plastic section modulus was calculated from the transformed section. This neglects the crushing of concrete as a possible failure mode. However, the *DCR* obtained from this assumption gives a sense of the building's susceptibility to progressive collapse.

5.4.4 Element Mesh

Finite element theory represents real-world phenomena as a series of elements of finite size. In structural analysis, beams and columns are generally divided into a number of elements along their length. The mesh of finite structural elements refers to the size of the elements, or how many finite elements represent one real object.

The mesh in SAP2000 was handled by the solver, which automatically chooses the best mesh size for the given program. No changes were made to the default, automatic meshing capabilities in SAP2000.

In ELS, the mesh was defined by how many elements to use in the cross section of the members and how many to use along the members' length. To save on analysis time, beams and columns were meshed with one element in the cross section. Beams close to the removed column were meshed with 90 elements along the length, and columns were meshed with 80 elements along the length. Figure 5.7 shows the mesh in ELS close to the removed column. To save on

computation time, columns and beams outside of Figure 5.7 were meshed with between 10 and 40 elements.

Additionally in ELS, the elements are connected with springs, as shown in Figure 5.8. This is the key characteristic of the applied element method (AEM), where springs connect elements. This allows for more direct modeling of structural analysis problems. In the ELS Model 1, five springs were attached to each flange and web in beams. 25 springs connected the transformed concrete at the top of composite beams. In the columns, five springs connected the flanges, webs, channel webs and channel sections.

5.5 Data Collection and Analysis

To compare the experimental data to the predicted response, the changes in strains and displacements due to column removal had to be simulated in the model. To obtain the theoretical data, two models were constructed, named Model 1 and Model 2. The Test Column was intact in Model 1 but was deleted in Model 2. The strains and displacements of each point where data was collected in the experiment was recorded in each model. The predicted strains and displacements were found by subtracting the data for Model 2 from Model 1. This is consistent with the linear static procedure.

In both softwares, reading the stress was more convenient than reading the strain. The stress was recorded and later used to calculate the strain. Figure 5.9 shows how the stress was read in SAP2000, while Figure 5.10 shows how the stress was read in ELS.

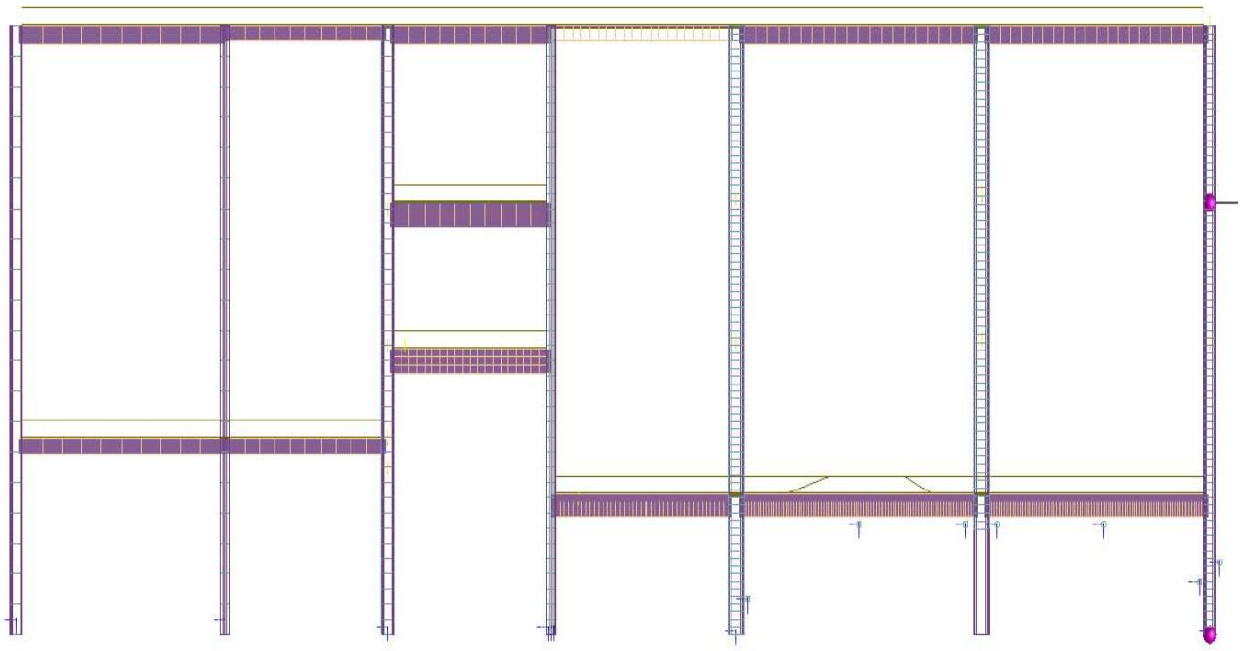

Figure 5.1: ASI ELS model of Test Frame, column removed

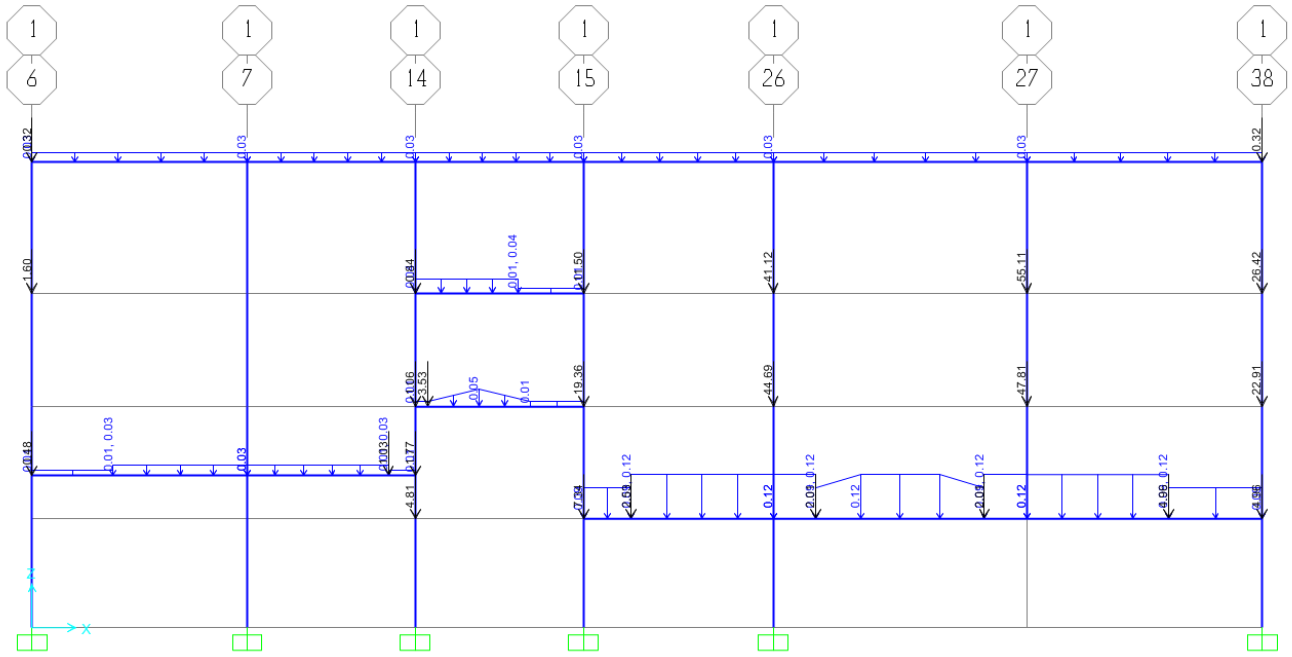

Figure 5.2 SAP2000 model of Test Frame, column removed

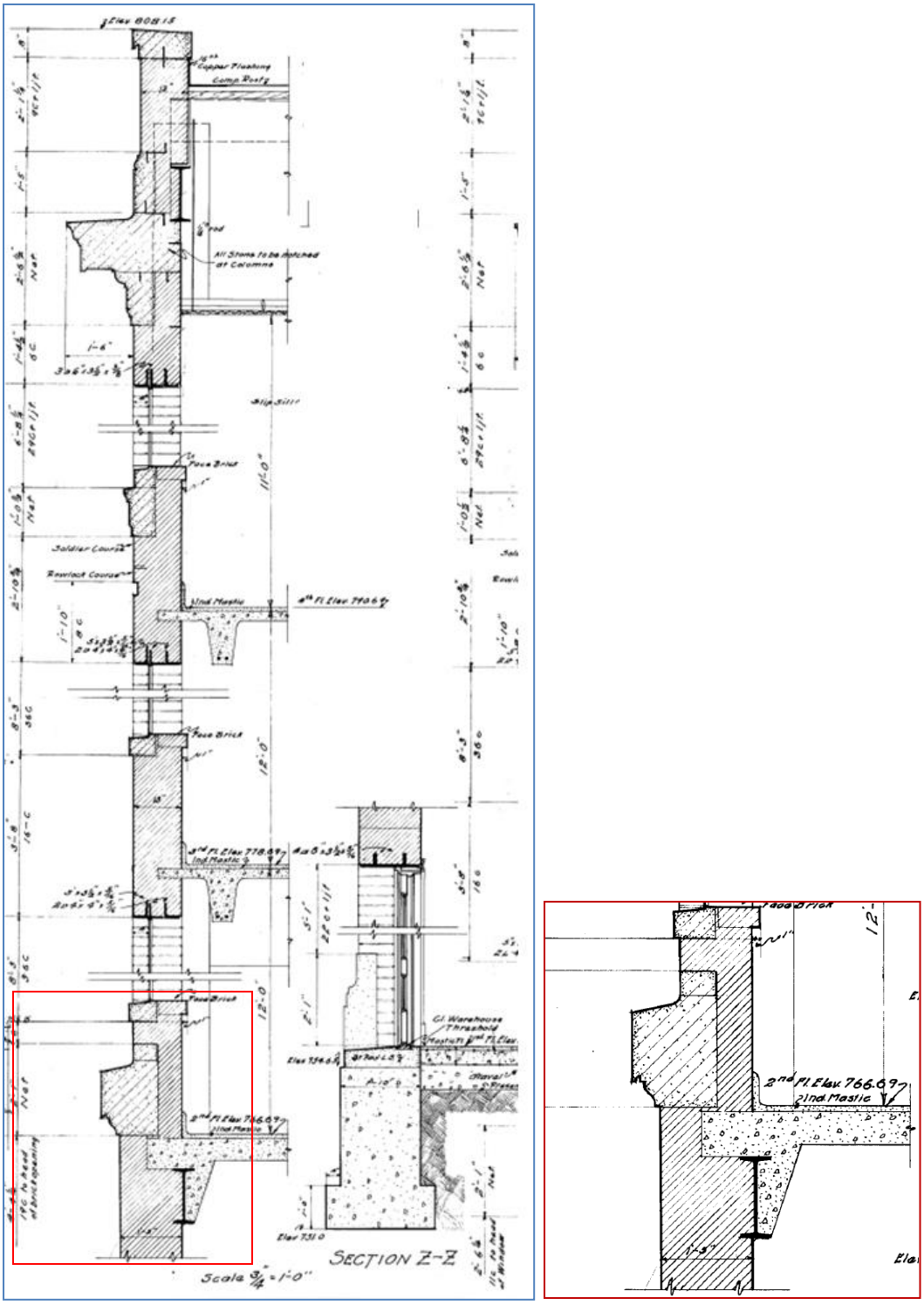

Figure 5.3: a) Wall section for test frame, and b) second story beam encased in concrete

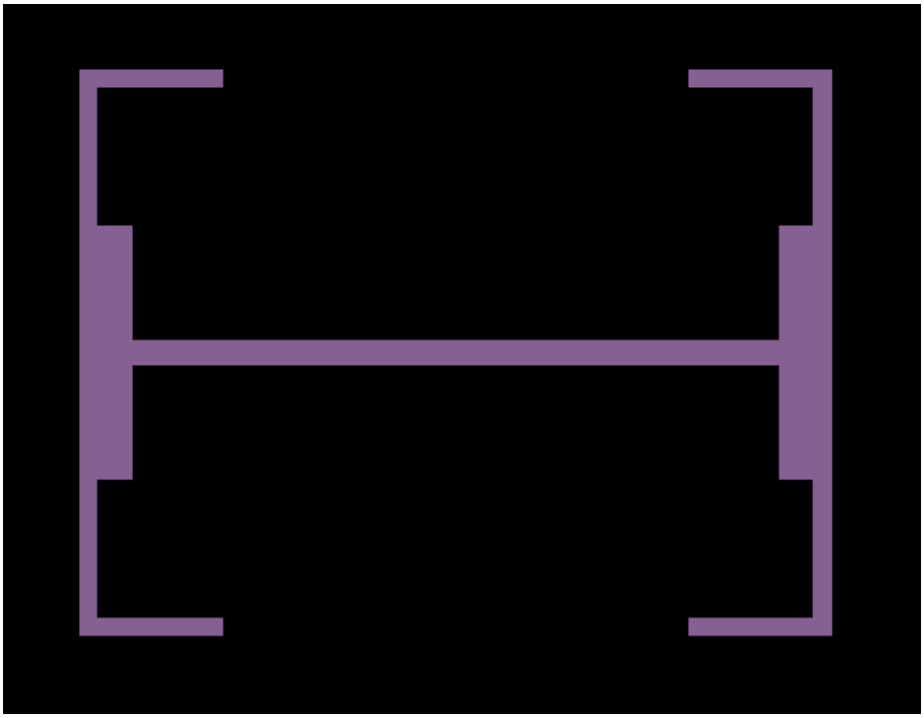

Figure 5.4: Build-up Column 26

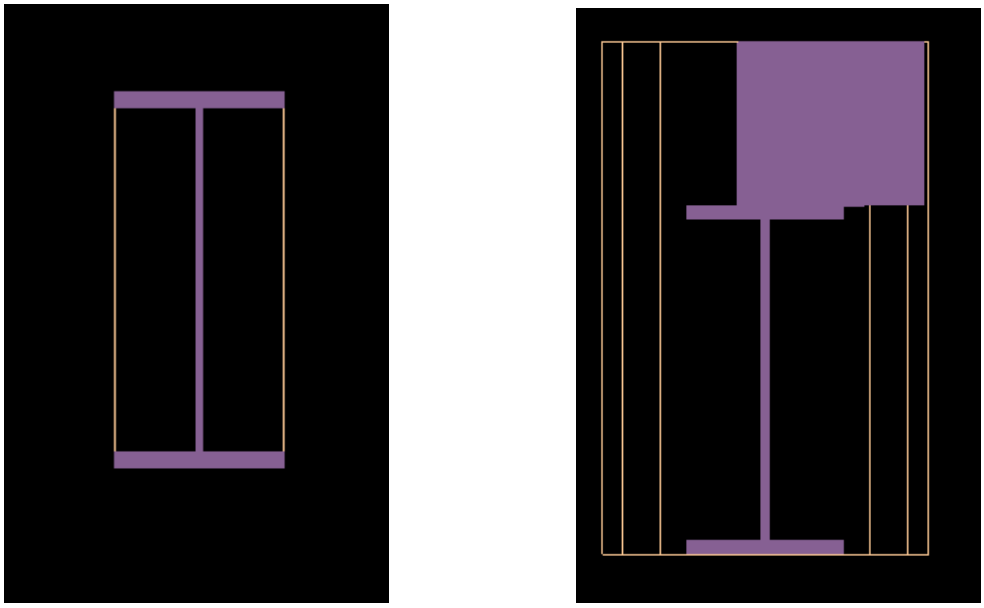

a) b)

Figure 5.5: a) Bare steel 15 in. beam, b) Transformed steel second story beam

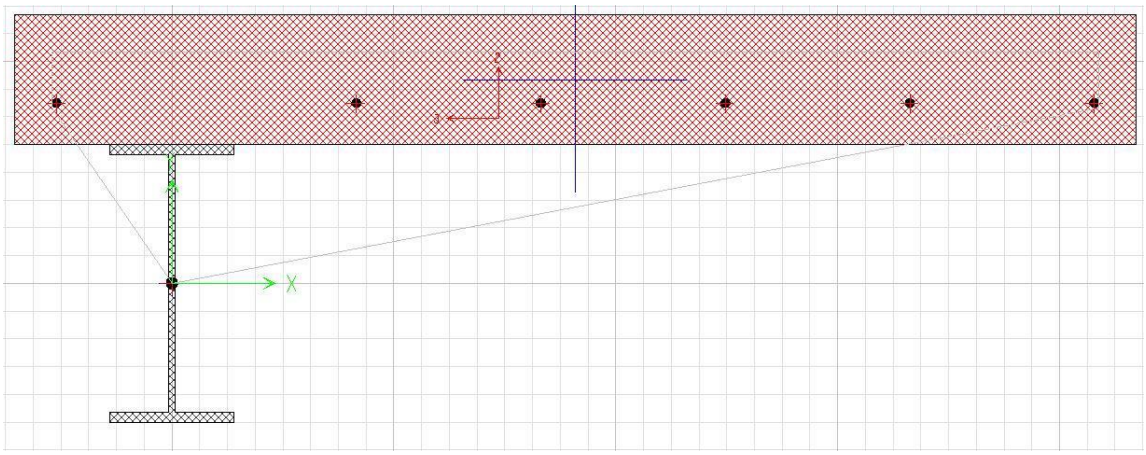

Figure 5.6: Composite beam sections (Akah 2013)

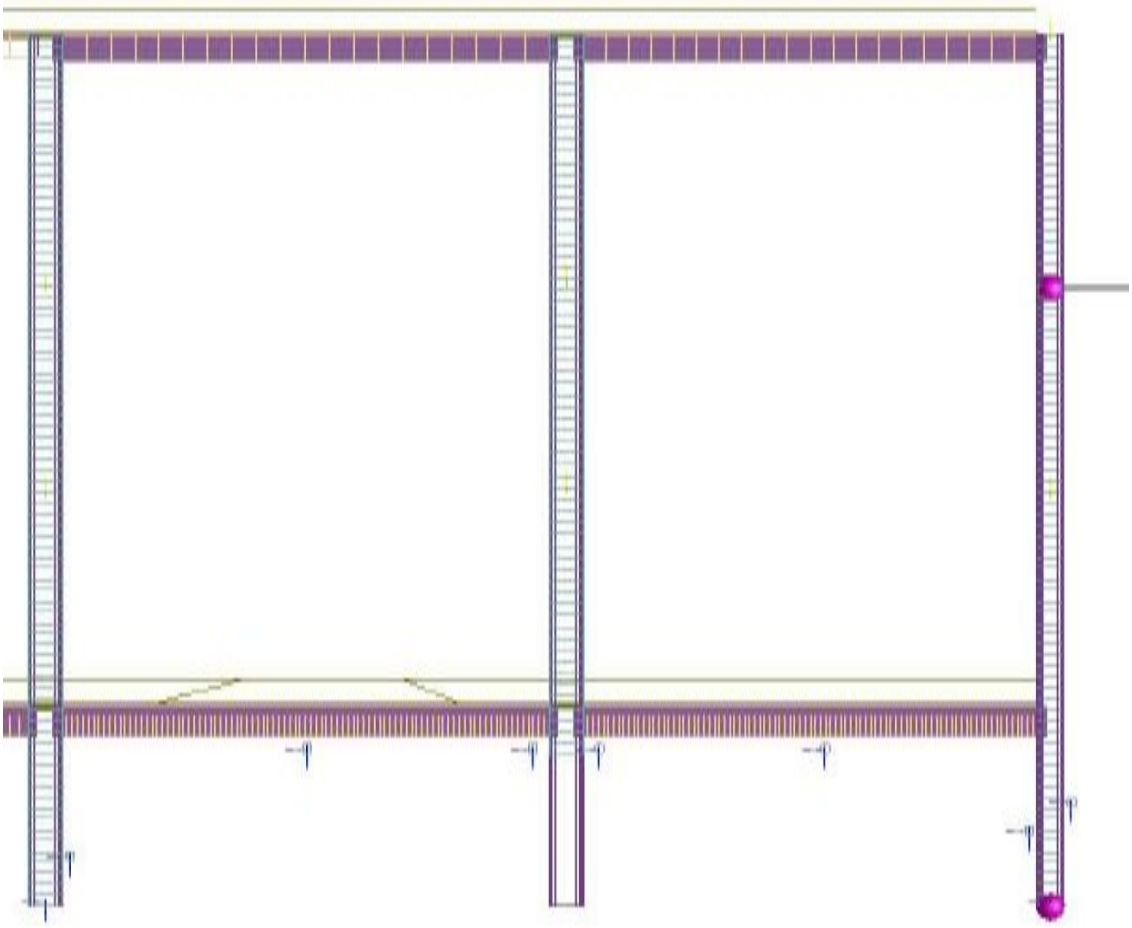

Figure 5.7: ELS mesh close to the removed column

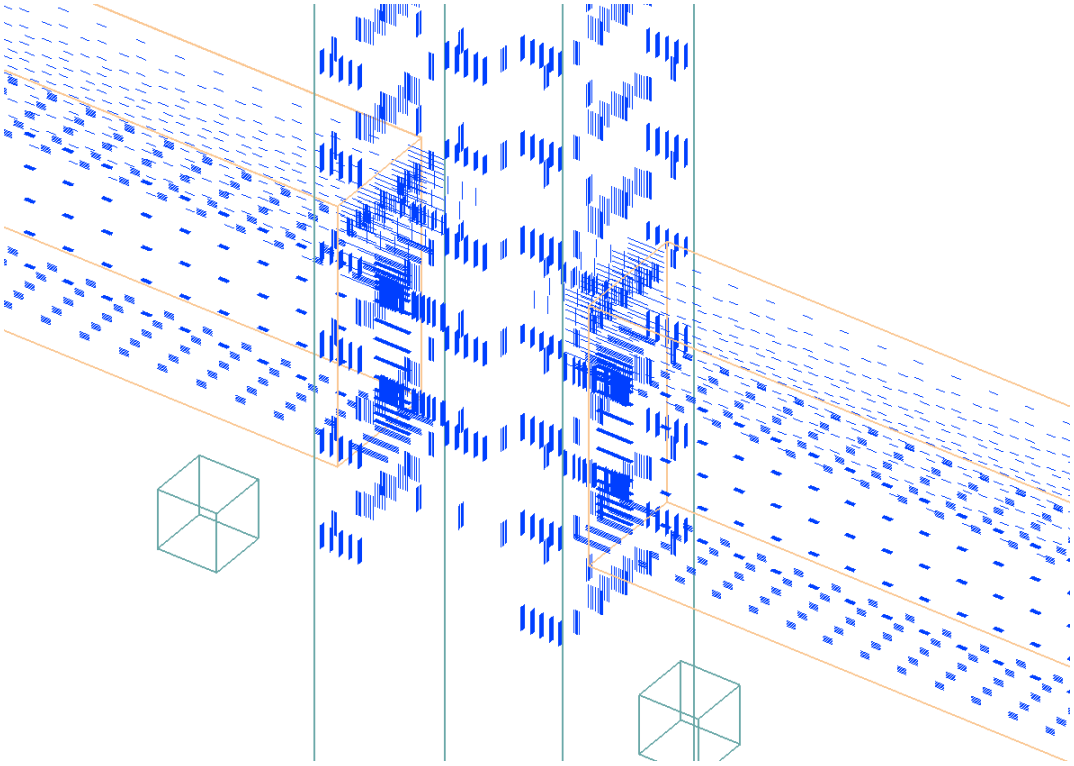

Figure 5.8: Connecting springs between elements in ELS

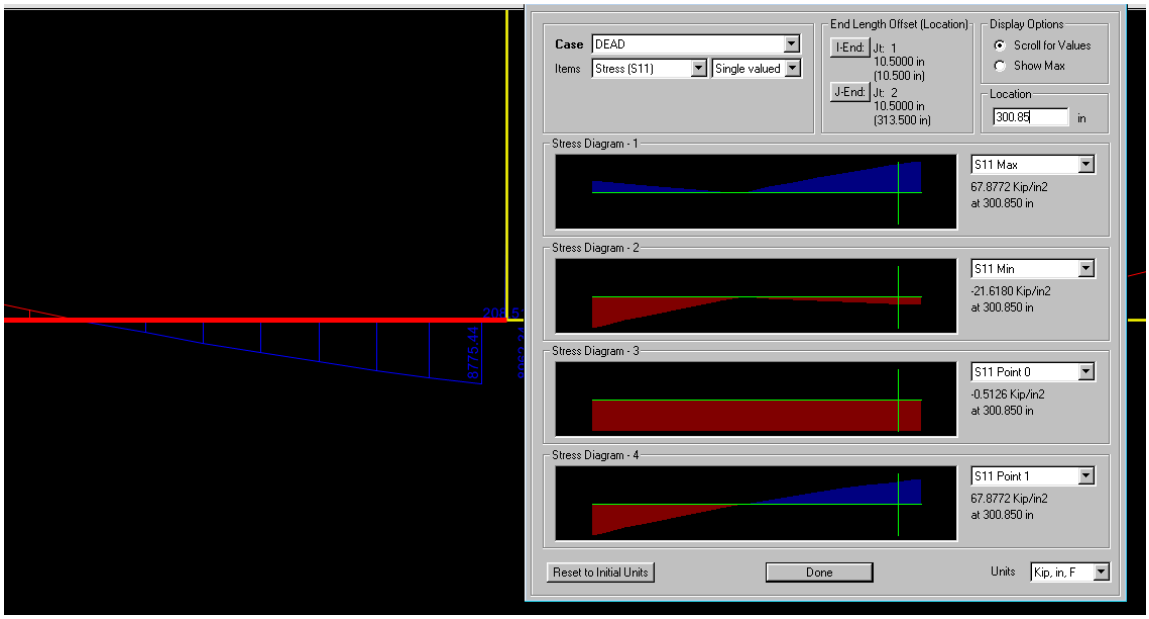

Figure 5.9: Obtaining strain value for Gauge 11 in SAP2000

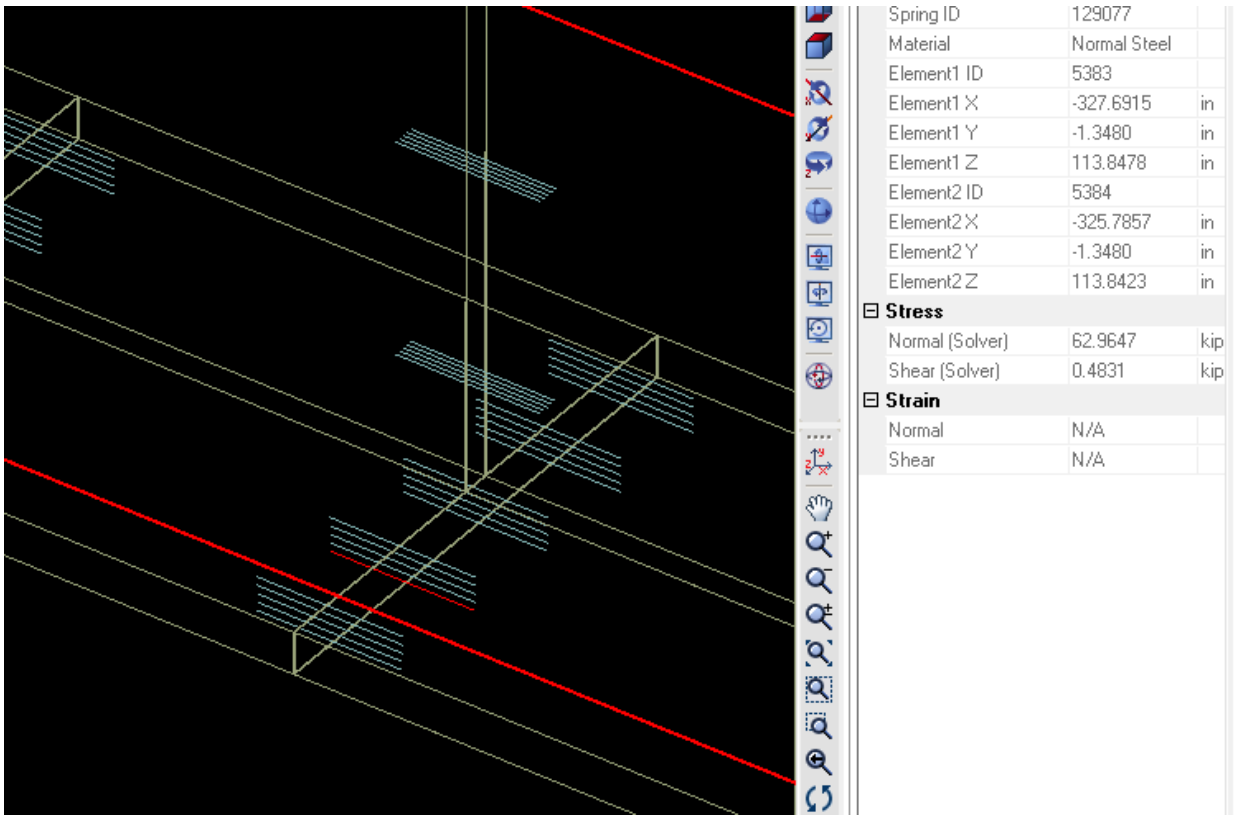

Figure 5.10: Obtaining Strain Value for Gauge 11 in ELS

CHAPTER 6: ANALYSIS AND COMPARISON OF EXPERIMENTAL AND PREDICTED STRAIN DATA

6.1 Introduction

In Chapter 6, the calculated response of the models is reported. The strain data is obtained from two separate models and compared to the experimental strain. Additionally, the demand-to-capacity ratio of the frame members is calculated, and the susceptibility of the frame to progressive collapse is evaluated. Two models – named Model 1 and 2 – were used for this analysis. Model 1 was created with the parameters determined in previous chapters, and Model 2 was created by deleting the removed column.

6.2 Model 1 Frame Response

The displaced shape of the frame in Model 1 for SAP2000 (2011) and ELS (2013) are shown in Figures 6.1 and 6.2, respectively. The frame generally compressed under the applied loads, several columns (such as 38 and 15) were bent in double curvature, and beams became bent in the positive direction (concave upwards). The frame tended to drift south toward the Test Column area, most likely because of the lack of beams at the third and fourth stories in this area and frame members being pulled toward the region where the column was removed.

The moment diagrams for the North and South Beams and Columns in Model 1 in both softwares are shown in Figure 6.3. The moment at the midspan of the North Beam (on the left in the figure) was found to be 573 kip-in. and 606 kip-in. in SAP2000 and ELS, respectively. The difference in moments is likely caused by differences in relative stiffnesses of joints between the two programs. ELS models joints by connecting the elements at multiple points, whereas the elements in SAP2000 are only connected rigidly at single points (Figures E.2, Figure E.21).

The axial forces in columns around the Test Column were obtained in both programs for Model 1. Figure 6.4 shows the axial forces at the base in North, Test, and South Columns to be 149,

172, and 86 kips, respectively, for SAP2000. In ELS, the forces in the columns were 149, 169, and 80.1 kips. These values show high agreement between the two programs.

6.3 Model 2 Frame Responses

After the results of Model 1 were obtained, Model 2 was created in SAP2000 and ELS by deleting the Test Column in Model 1. The displaced structure of Model 2 for both softwares appears in Figures 6.5 and Figure 6.6. The frame displaced massively (3.78 in.) at the location of the removed column, where the point loads on the removed column were transferred to connecting beams. The North and South Column were in double curvature, indicating bending moments in these members.

The moment diagrams for the North and South Beams and Columns in Model 2 in both softwares are shown in Figure 6.7. The moment at the connection to the removed columns in the North beam is 8775 k-in. and 8584 kip-in. in SAP2000 and ELS, respectively. This shows a relatively good level of agreement between the two softwares for linear elastic analysis.

The axial force in the North and South Columns were 238 kips and 175 kips, respectively, in SAP2000. In ELS, the axial forces for the North and South Columns were found to be 238 kips and 171 kips, respectively. This result shows very good agreement between the two programs in determining load redistribution with linear elastic analysis. These results also indicate that much of the load in the Test Column was redistributed to the North and South Colum due to column removal.

6.4 Strain and Moment Data Results

Reading strain in both softwares was relatively difficult, so instead the stress was recorded at critical locations. The elastic strain was determined from the stress using Equation 6.1:

$$\varepsilon = \frac{\sigma}{E} \qquad \text{Eq. 6.1}$$

where ε is the calculated strain, σ is the recorded stress, and E is the modulus of elasticity of the material (29,000 ksi for structural steel). These calculations are tabulated in Appendix F. The strain gauges recorded change in strain as the column was removed, so the change in strain needed to be calculated between the two models. The strain in Model 2 was subtracted from Model 1, and the results were compared to the change in strain measured in the experiment. These results are tabulated in Table 6.1 for columns and Table 6.2 for beams.

Table 6.1: Measured and calculated strains in columns

Gauge	Column, Location	Experiment $\Delta\varepsilon$ (x 10^6)	SAP2000 $\Delta\varepsilon$ (x 10^6)	SAP2000 difference (%)	ELS $\Delta\varepsilon$ (x 10^6)	ELS difference (%)
1	North, (S) flange	-32	-29.7	7.33	-19.9	37.9
2	North, (N) flange	-54	-95.9	77.55	-165.3	206.2
4	South, (S) flange	-7	236.6	3479.3	144.9	2169.6
5	South, (E) web	-61	-72.4	18.7	-69.7	14.2
6	South, (N) flange	-103	-381.7	270.6	-373.5	262.6
7	South, (N) flange	-93	-210.7	126.6	-217.2	133.6

For SAP2000, the lowest percent difference between the software and the experiment in a column was 18.7 % in the South Column in the center of the flange, and the highest was 3480 % in the South Column on the flange outside the frame (on the far right in Figure 6.7). For ELS, the percent difference in the same locations was 14.2 % and 2170 %, respectively. This demonstrates that, in general, the experimental data agreed more with the data collected in ELS, likely due to the extra stiffness of joints in ELS. The strain in the middle of the web is related to the axial force in the column in linear elastic beam theory. Thus, the low percent difference between the software and

the experiment at this point indicates that the axial force added to this column from column removal is relatively accurate. However, the strain at the column flanges is related to the bending moment in the columns as well as the axial force. Given the high percent difference in the flanges, the bending moment added to the South Column by removal of the Test Column is likely too high. Another possibility is that the foundations of the columns acted more semi-pinned, allowing less bending moment close to the base of the columns than develops in the model with fully-fixed bases. And finally, the moment diagram is shown for the South Column in Figure 6.7. The inflection point of the moment is shown where the diagram crosses the member itself (approximately 30 % above the base of the column), indicating where the moment in the section is zero. The inflection point of the moment diagram may be inaccurate in the model.

The percent difference between SAP2000 and the experiment for in Gauge 1 and 2 on the North Column was 7.33 and 77.6, respectively, while the values in ELS were 37.9 and 206. This indicates similar trends as those observed in the South Column. The response of the column in terms of axial force, bending moment, and inflection point is similar as for the South Column. The average strains in the North Column are less than those in the South Column for both the experiment and the model. This might be because the South Column is at the corner of the building where the structure ends. The North Column is surrounded and supported by more structural material than the South Column, so more load has to be transferred to the South Column.

Table 6.2: Strain results for beams

Gauge	Frame beam	Experiment $\Delta\varepsilon$ (x 10^6)	SAP2000 $\Delta\varepsilon$ (x 10^6)	SAP2000 difference (%)	ELS $\Delta\varepsilon$ (x 10^6)	ELS difference (%)
11	(N) Beam	136	2603.8	1814.6	2440.9	1694.7

12	(N) Beam	171	2603.8	1422.7	2440.9	1327.4
13	(S) Beam	252	2693.4	968.8	2510.5	896.2
14	(S) Beam	272	2693.4	890.2	2510.5	823.0
15	(S) Beam	81	34.1	57.8	-28.8	135.6
16	(N) Beam	-10	62.2	720.7	56.9	669.0

The average percent difference between experimental and calculated strains in beams was approximately 1300, indicating that the loads included in the Capacity Model were unrealistically high in representing the experiment. Additionally, the stiffness of the model did not take into account the structure outside the two-dimensional frame. Including three-dimensional effects could have decreased the percent difference in this analysis. Strain in the South beam was higher than in the North beam in both the experiment and the model. Unlike columns, the percent difference between the model and the experiment for beams in ELS was generally much lower than SAP2000.

Compared to strains measured in other gauges on beams, the measured strain values were relatively low in Gauges 15 and 16 (which are located on the bottom flanges of the South and North Columns, respectively, 12 ft 9 in. from the face of the Test Column). The strain is related to the moment in beams, so these gauges were likely placed close to inflection points in the moment diagram. Figure 6.7 shows that the inflection points were close to the locations of Gauges 15 and 16 in the models as well, indicating that the models were close to realistic. However, the experimental error in Gauge 16 was 721 and 669 (Table 6.2) for the two softwares, indicating limited agreement between the inflection point from the models and experiment. The experimental error for gauge 15 on the South beam was 57.8 and 136 for SAP2000 and ELS,

respectively (Table 6.2), demonstrating the only location for beams where SAP2000 produced closer results to the experiment.

6.5 Calculations of Demand-Capacity Ratios

The capacity of the North and South Beams and Columns was calculated using Equation 5.3 and compared to the maximum moments in these members calculated from the computer models. This analysis is demonstrated in Table 6.3.

Table 6.3: Beam capacity calculations

Beam	Mp (k-in.)	Software	Maximum moment (k-in.)	Location	Calculated DCR
North Beam	9601.2	SAP2000	10,350	(N) Column Connection	2.16
		ELS	9511	(N) Column Connection	1.98
South Beam	9273.6	SAP2000	9015	(S) Column Connection	1.94
		ELS	8631	(S) Column Connection	1.86

According to GSA (2003), a beam exceeding a *DCR* value of 2 is considered to fail, and the structure is susceptible to progressive collapse. One beam in the SAP2000 model exceeded a *DCR* of 2, and the model predicts that this structure is likely to collapse. Additionally, all of the beams are close to exceeding a *DCR* of 2, indicating that the beams were exceeding the steel yield stress in at least one portion of their cross-section.

Several simplifications in the model could have a significant affect on the DCR. Transverse beams (perpendicular to the frame) are not considered in the two-dimensional analysis, and these members would likely add to the capacity. The slabs in the experiment likely epxerienced two-dimensional bending, which would not be captured by the composite beams bending only about the y-axis. Additionally, the structural stiffness of brick and masonry in the walls was not

considered. And finally, connections in the model between the beams and coumns and the column foundations may be very unrealistic.

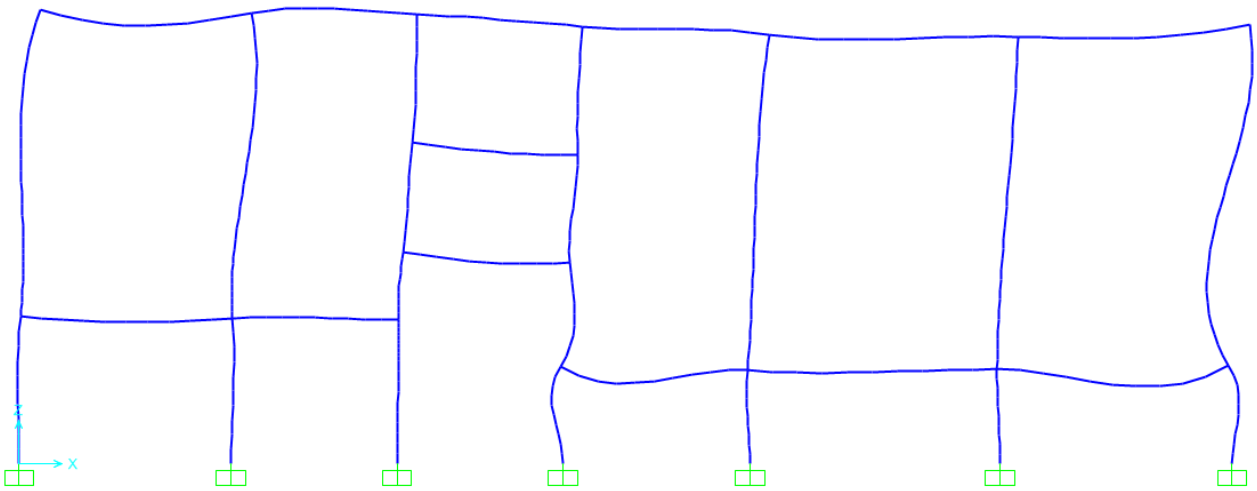

Figure 6.1: Displaced shape of Model 1 in SAP2000

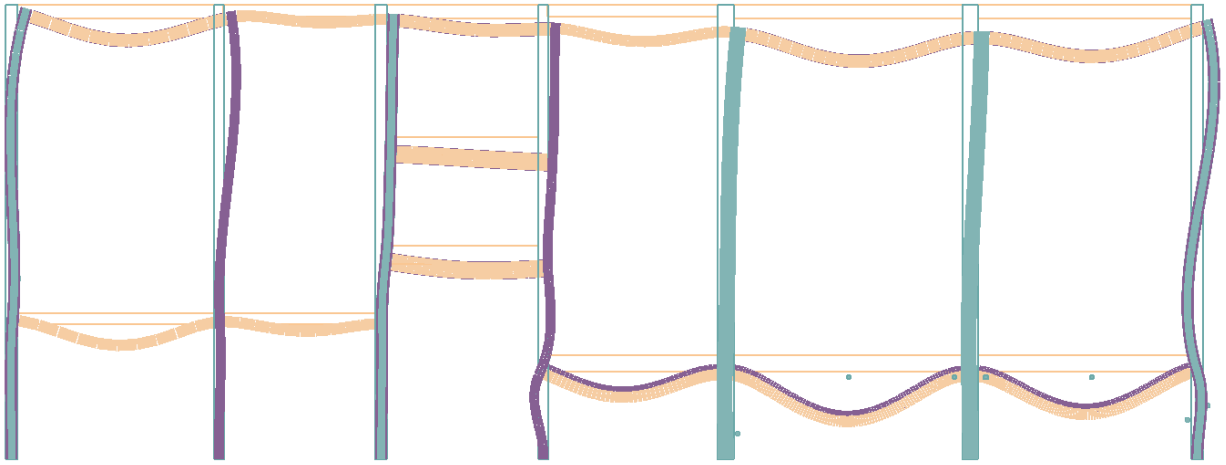

Figure 6.2: Displaced shape of Model 1 in ELS

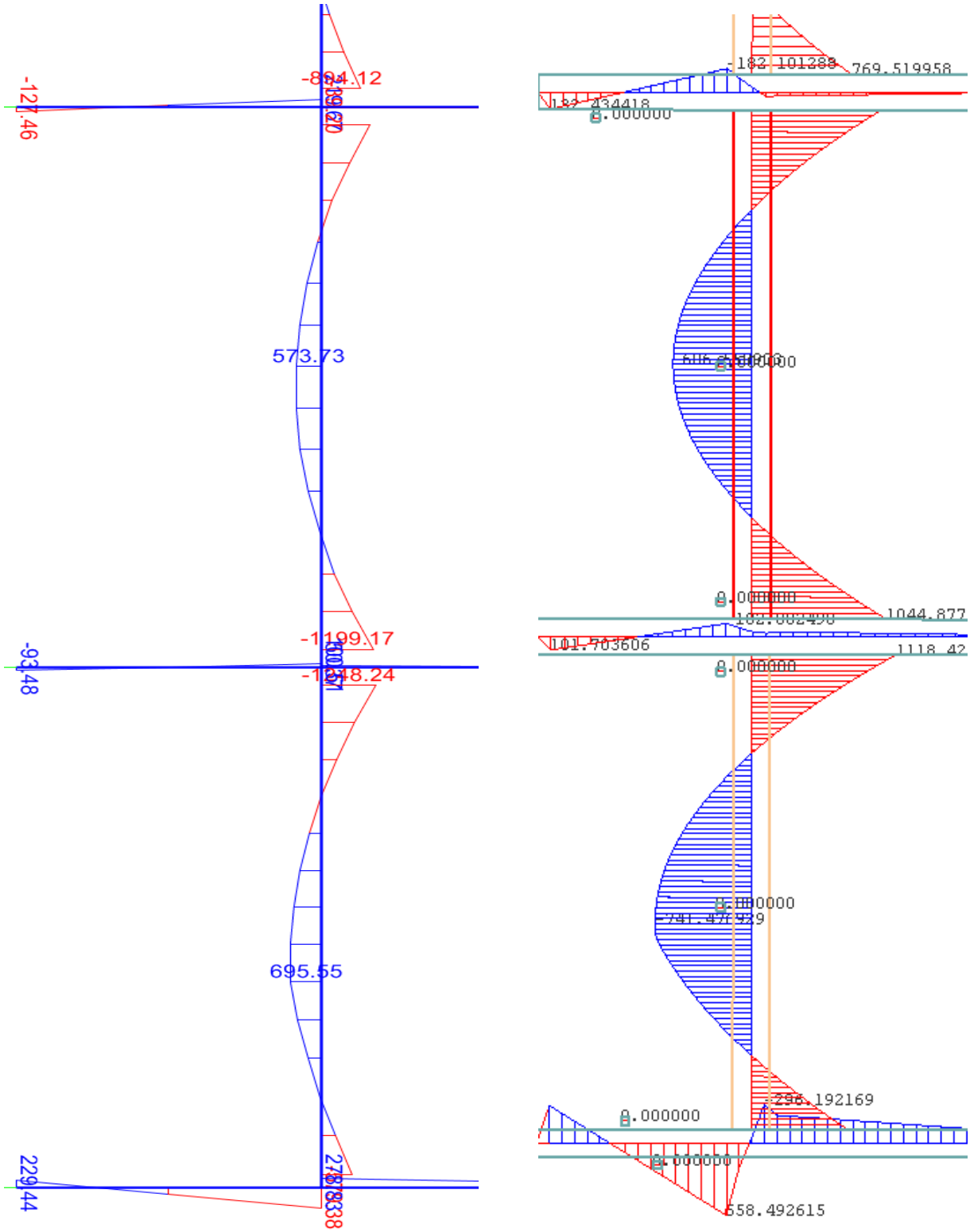

Figure 6.3: Moment diagram for test area in a) SAP2000 and b) ELS

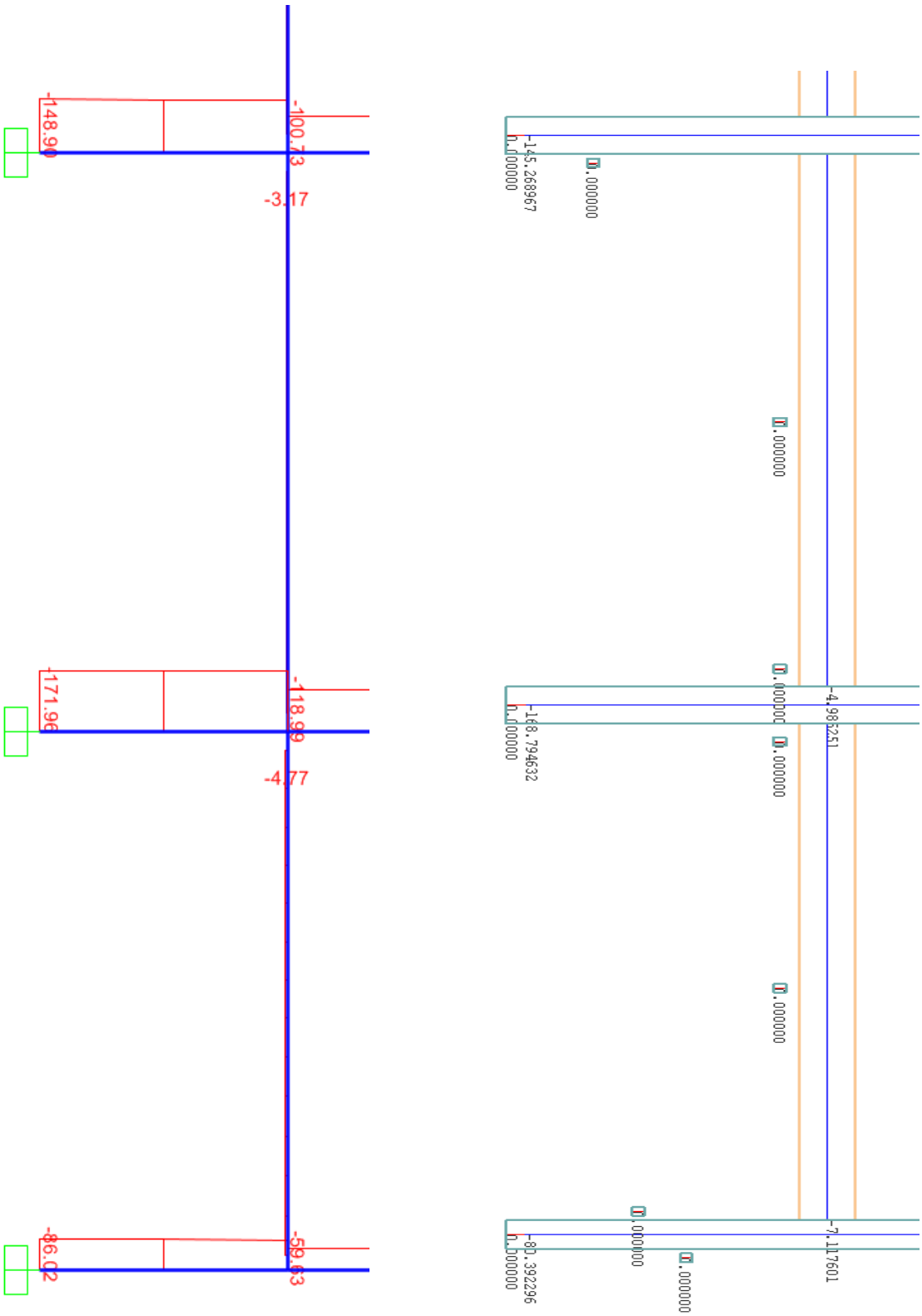

Figure 6.4: Column axial forces in Model 1, a) SAP2000, b) ELS

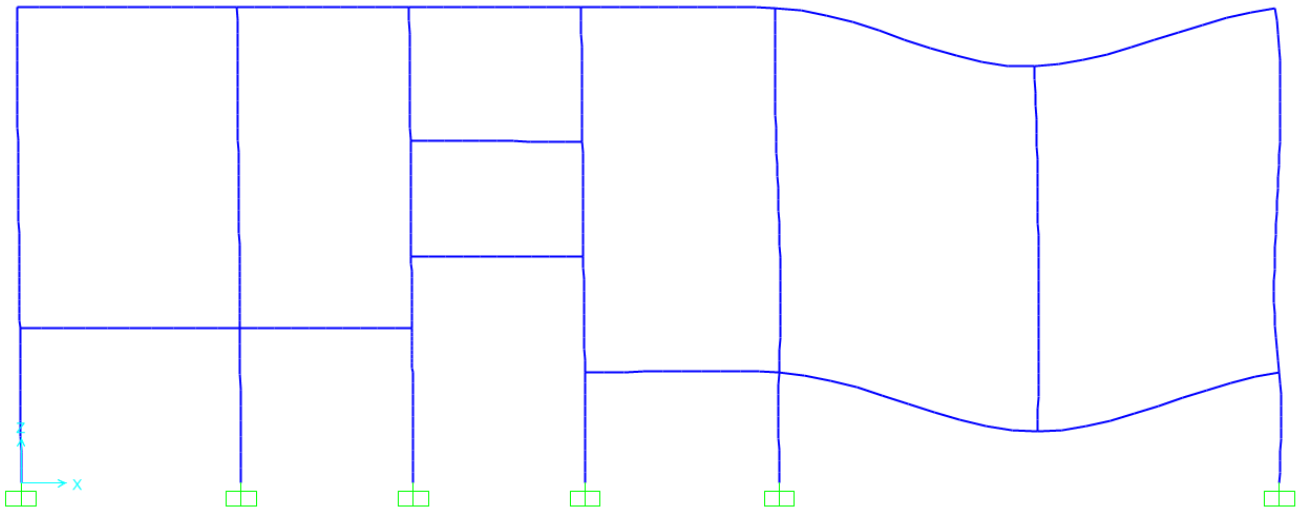

Figure 6.5: Displaced shape of Model 2 in SAP2000

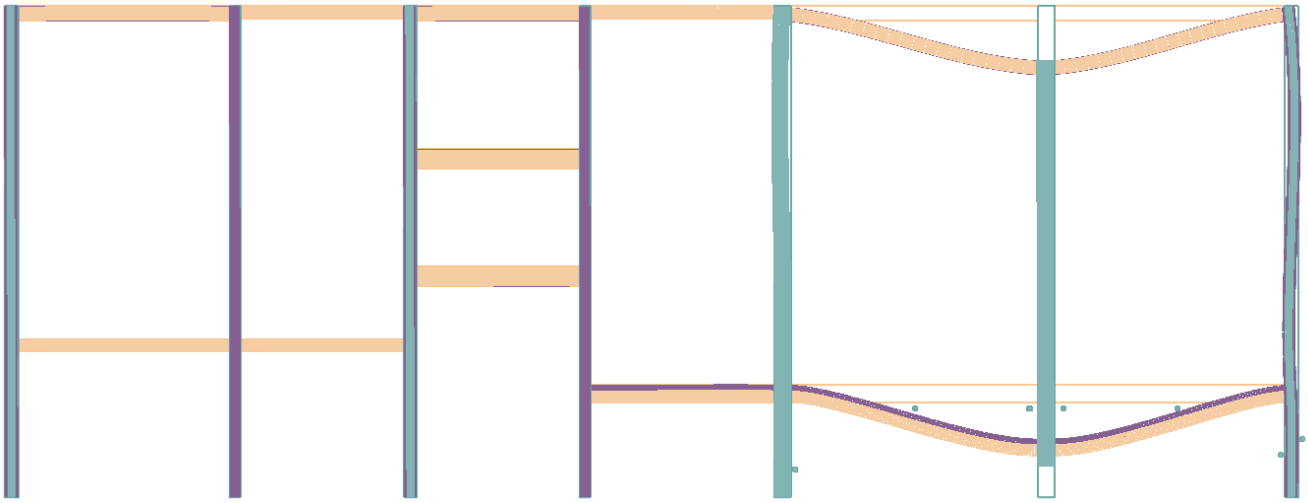

Figure 6.6: Displaced shape of Model 2 in ELS

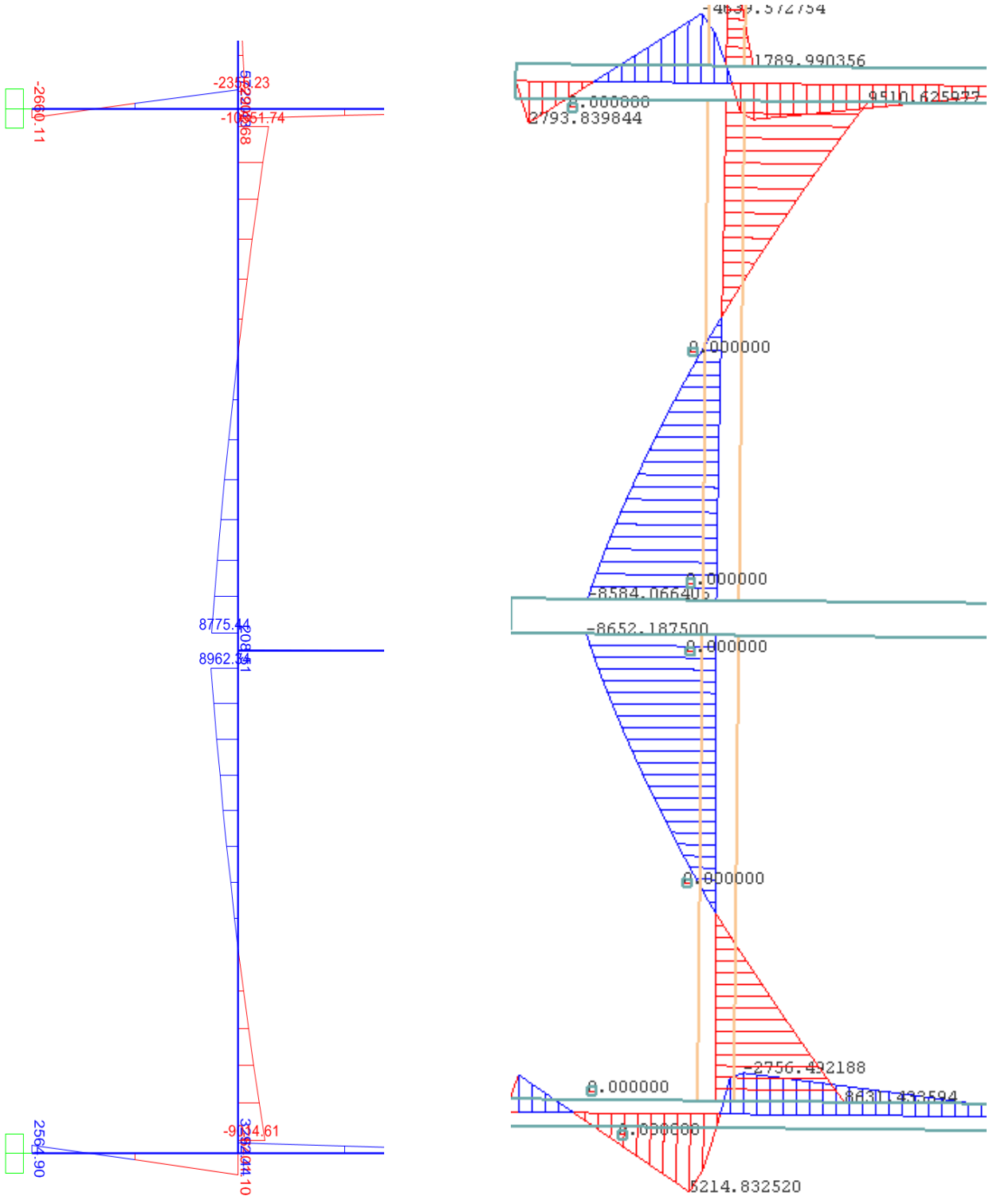

Figure 6.7: Moment diagrams in the test area for Model 2 in a) SAP2000, b) ELS

CHAPTER 7: RELATIVE STIFFNESS ANALYSIS

7.1 Introduction

In Chapter 7, the procedure and results of the Relative Stiffness Analysis are presented. The assumptions and methods used in creating the model are explained. This analysis is performed by applying loads at a certain location to match predetermined displacements at other locations. Three variations of the model of the frame are subjected to the same displacement. The forces required to develop the specified displacement varies from model to model, which allows for determination of each model's stiffness. In this chapter, the results of the analysis are presented, and the significance of the results are discussed.

7.2 Assumptions and Methods

Structural analysis in this study is conducted using the finite element method (FEM). In structural finite element theory, the response of structural elements is solved for using a form of Equation 7.1:

$$F = kd \qquad \text{Eq. 7.1}$$

where *F* is the force in an element, *k* is the stiffness of the element, and *d* is the displacement of the element or the change in position of one end with respect to the other. The term *d* in finite element theory includes the rotation of members. The equation is solved for all members in the structure, and the forces and displacements are determined for. As can be seen in the equation, the force in a member is proportional to the member's stiffness. When combining structural elements in a model, the stiffness of one member relative to other members determines the magnitude of the force that member is subjected to.

In the Relative Stiffness Model of Haskett Hall, the computer model solves Equation 7.1 for all structural members using the measured displacements as input. By displacing the structure in

the computer model to the extent measured in the experiment, strain is developed in the elements that can be compared to the experimental strain. This comparison can be used to evaluate the relative stiffness of the structure and determine sources of error. Since ELS (2012) provided slightly better results in the Capacity Model, the Relative Stiffness Analysis was conducted in ELS.

7.2.1 Application of Displacement

To perform the Relative Stiffness Analysis, a displacement load was determined from the experimental data at certain locations. These locations were on the North Beam, 1 ft 2 in. north of the removed column, and on the South beam, 2 ft 4.75 in. south of the removed column. These locations were termed control points for this analysis. The respective displacements were 0.474 in. and 0.659 in. The average displacement was equal to 0.567 in. (Table 3.3). The maximum displacement of the frame was assumed to be at the center of the removed column, where the axial load supported by the removed column was redistributed to neighboring elements including beams and columns. The maximum displacement could not be given directly to the computer model, so this value was inferred from the experimental data (Table 3.3). The joint between the removed column and the North and South beams was displaced in the computer models such that the average displacement given by the software at control points equaled the average measured displacement.

7.2.2 Model Versions

Three different versions of the computer model were created to study the effective stiffness. The first model used all the assumptions, section properties, and geometry that were used in the Capacity Model (described in Chapter 6), and this was named Model 3 (all calculated gravity loads were removed in Model 3). Because the inflection points of the moment diagram for the North and South Beams were in question, the fixity of the connections between the North and

South Beam was varied in the two subsequent models (Model 4 and 5). Varying the fixity of the connections affected the moment values at each end of the beam, adjusting the shape of the diagram.

Model 4 used extended rigid zones, effectively making the joint more stiff than Model 3. Very little information was given in the 1925 construction documents with regard to connections. Thus, the connection properties for the North and South Beams were inferred from pictures and from the limited construction drawings. Figure 7.1 shows a picture of the connection of the Test Column with the South Beam. As shown in Figure 7.1, the connections included plates that reinforced the connection of the beam with the column. These plates were assumed to create a rigid zone in the beam, where rotation of the beam would be experienced by the column as well. The picture was scaled in AutoCAD and the size of the connecting plates was measured. The length of the plate connecting the bottom flange of the beam to the column was found to be 14 in. The beam rigid zone of the connection was assumed to be half this length equal to 7.0 in. along the North and South Beam. Figure 7.2 shows the elements that were included in the beam rigid end connections at the Test Column. Similar beam rigid end zones were added to the North and South Columns as well.

Figure 7.3 shows one of several construction documents that provided details of steel connections in the building. In Model 5, the connection in Figure 7.3 was assumed to be typical, and this connection was implemented in the North and South Beams. To achieve this connection, the connectivity between the top flange of the beam and the associated column was removed. ELS includes a feature called “regions”, where the springs that connect elements are removed within a specified area. As shown in Figure 6.8, elements in ELS are connected with springs that provide structural properties. Figure 7.4 shows the beam-column connections using regions in ELS to

remove the connection springs. Without the springs, no stiffness was offered between the top flange and the column, reducing the ability of the connection to transfer moment. Essentially, the top flange is disconnected from the column. The transformed concrete section was also removed with the steel flange. Each of the created models (including the Capacity Models described in Chapter 6) is summarized in Table 7.1.

Table 7.1: Summary of Models

Model	Analysis	State of Test Column	Beam-column connection variation
1	Capacity Model	Intact	Default
2	Capacity Model	Removed	Default
3	Relative Stiffness Analysis	Removed	Default
4	Relative Stiffness Analysis	Removed	Added rigid zone
5	Relative Stiffness Analysis	Removed	Top flange removed

Each version of the model required a different maximum applied displacement to achieve the target average displacement at control joints over the removed column of 0.567 in. The displacements for each model are given in Table 7.2. Model 4 required the least amount of displacement, since the rigid connection in this model pulled down the beams' control points more effectively with the joint. Because Model 5 removed a portion of the connectivity between the beams and columns, this model required the most applied displacement to achieve the target displacement at control points.

Table 7.2: Displacement Data for Relative Stiffness Models

Model	Beam-column connection variation	Applied displacement (in.)	Average displacement at control points (in.)
3	Default	-0.580	-0.567

4	rigid zones	-0.574	-0.567
5	top flanges removed	-0.593	-0.567

7.3 Relative Stiffness Analysis Results

The typical displaced shape for the beams and columns involved in the Relative Stiffness Analysis is shown in Figure 7.5. This was the shape for Model 3, Model 4, and Model 5. Both the North and South beams bent in positive curvature at the Test Column joint, and the shape suggests that the two formed one continuous beam across the removed column. The North and South Columns bent in double curvature, indicating that they developed moment. Strain values were read from the ELS models and recorded, and the data for all models is tabulated in Appendix F. None of the members in the model reached the yield stress of the steel, so the model remained linear elastic.

7.3.1 Results for Columns

Table 7.3 provides the combined results of the Relative Stiffness Analysis for columns. Table 4.3 provides column geometry, and Section 3.2 describes the instrumentation of the strain gauges.

Table 7.3: Strain Results for Columns (where strain units are x 10^6 in./in.)

Gauge	Column, location	Height above base	Experimental change in strain, $\Delta\varepsilon_E$	Model 3 change in strain, $\Delta\varepsilon_3$	Model 4 change in strain, $\Delta\varepsilon_4$	Model 5 change in strain, $\Delta\varepsilon_5$
1	North, (S) flange	3 ft – 1 in.	-32	1.42	0.26	-3.11
2	North, (N) flange	3 ft – 1 in.	-54	-26.46	-27.52	-15.66
4	South, (S) flange	6 ft – 2 in.	-7	6.25	74.72	32.93
5	South, (E) web	6 ft – 2 in.	-61	-13.90	-16.24	-10.44
6	South, (N) flange	6 ft – 2 in.	-103	-92.12	-107.24	-53.79
7	South, (N)	4 ft – 7 in.	-93	-37.28	-57.93	-27.97

In general, most modeled data for beams reached the same order of magnitude as the experimental data, showing relatively accurate results. Additionally, most strain values measured for columns in the three models agreed with the signs of the experimental data, indicating that the model accurately captured whether the location was in tension or compression. The data for gauge 1 and 4 were exceptions to this trend. This might indicate that the assumption about the fixities of the columns or the rigid length of their base connections may be somewhat inaccurate.

7.3.2 Results for Beams

The strain values for beams for each of the three models were recorded and are presented in Appendix F. Table 7.4 provides combined results for the three models.

Table 7.4: Strain Results for Beams (where strain units are x 10^6 in./in.)

Gauge	Frame beam	Distance from Test Column	Experimental change in strain, $\Delta\varepsilon_E$	Model 3 change in strain, $\Delta\varepsilon_3$	Model 4 change in strain, $\Delta\varepsilon_4$	Model 5 change in strain, $\Delta\varepsilon_5$
11	(N) Beam	1 ft – 0.65 in.	136	531.5	605.5	369.0
12	(N) Beam	1 ft – 0.65 in.	171	531.5	605.5	369.0
13	(S) Beam	1 ft – 0.65 in.	252	533.2	608.3	302.9
14	(S) Beam	1 ft – 0.65 in.	272	533.2	608.3	302.9
15	(S) Beam	12 ft – 9 in.	81	-17.4	-17.8	-31.7
16	(N) Beam	12 ft – 9 in.	-10	11.3	20.5	27.8

Gauges 11 through 14 measured the strain closest to the removed column, and the results for the three models were all higher than the experimental values. This indicates that the beams were stiff in the models compared to the experiment, possibly because too much concrete was included in the transformed section. The values from Model 5 were the closest to matching the values from the experiment, indicating that the connections in Haskett Hall could have acted semi-rigid with respect to transferring moment to beams. Figure 7.6 shows the strain results for beams

plotted along the length of the North and South beam, clearly indicating that the results improve with reducing the rigidity of the connection.

Gauges 15 and 16 measured the strain close to the inflection point of the moment diagram of the beams, since the strains approached zero. The model data did not approach the experimental data as the connections were made semi-pinned, signifying that the inflection point of the beams was not only controlled by beam-column connectivity. Figure 4.4 shows that steel beams framed into the North and South columns close to the Test Column. These beams likely had a significant effect on the location of the inflection point in the moment diagram.

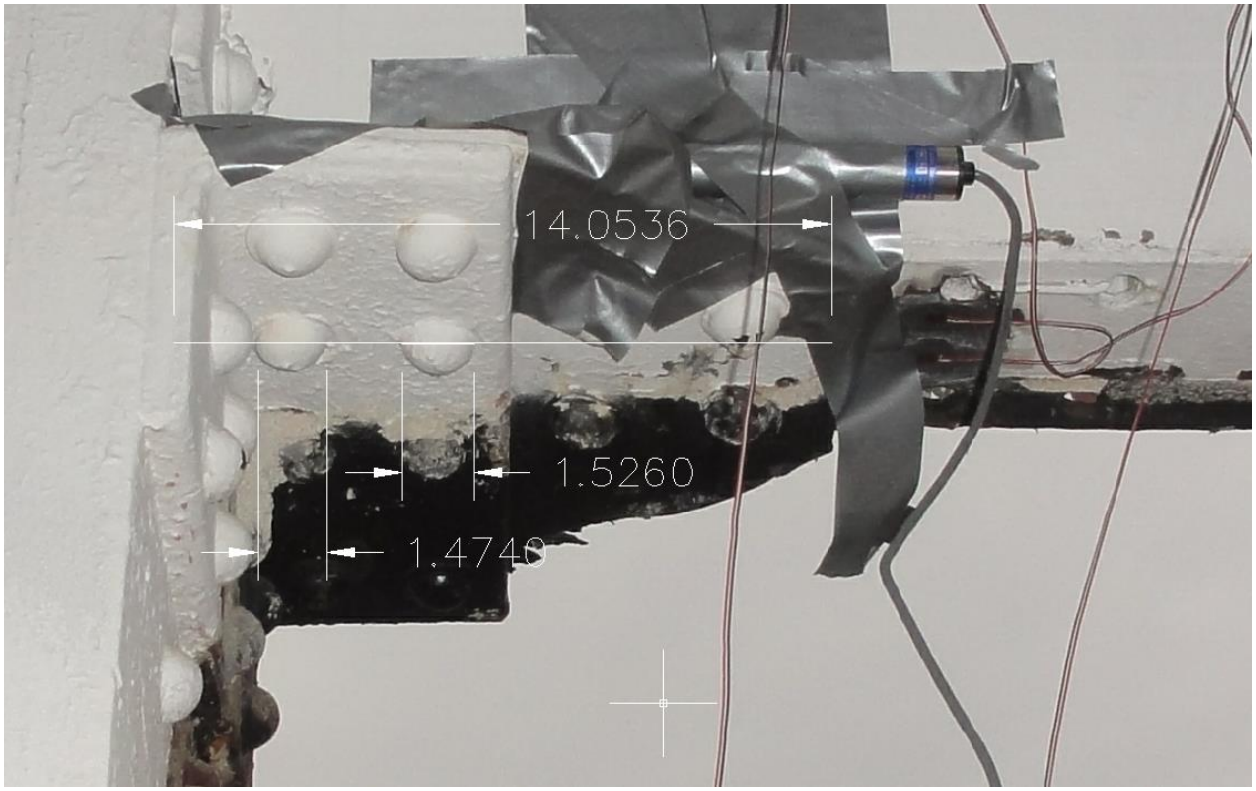

Figure 7.1: Beam-column connection of North Beam and Test Column

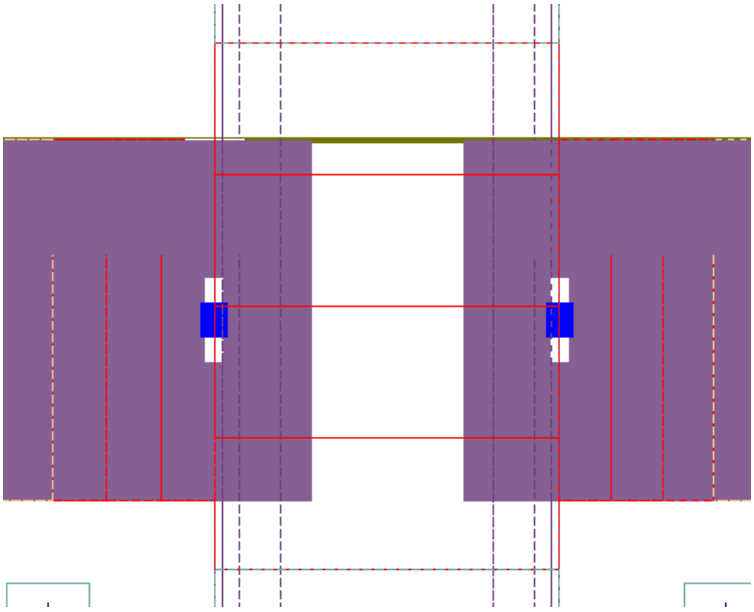

Figure 7.2: Extent of beam rigid end zone, shown in red, approximately 7.0 in. from the face of the column on either side.

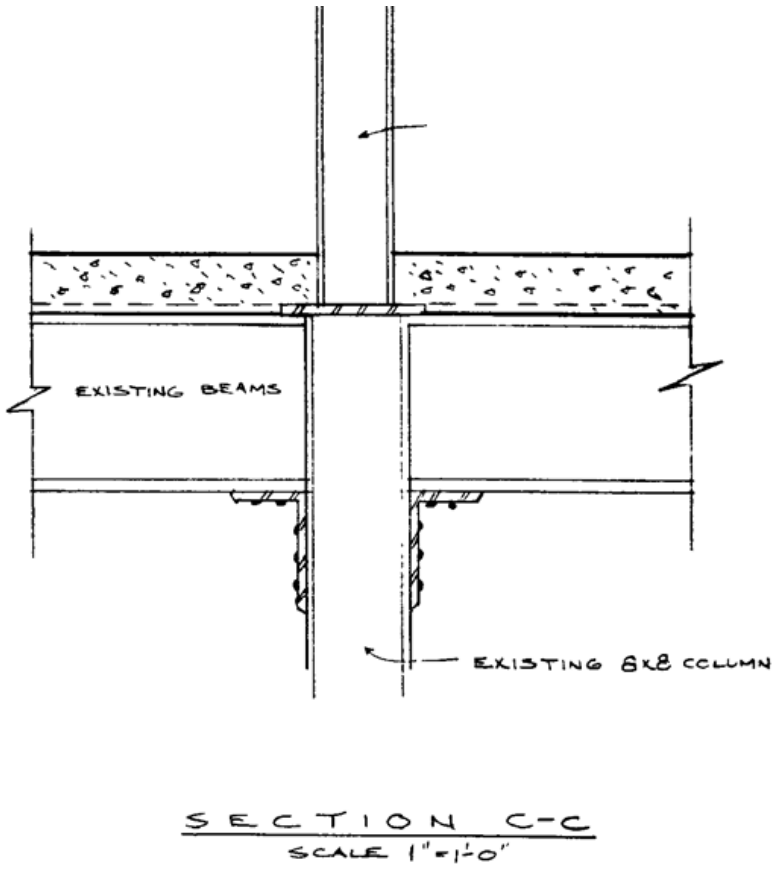

Figure 7.3: Assumed typical beam-column connection in Model 5. The top flange is disconnected from the column

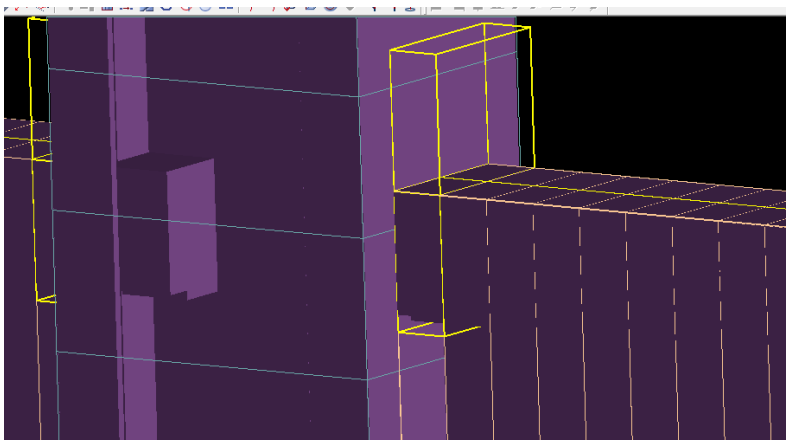

Figure 7.4: Regions created in Model 5, removing the connectivity between the top flange and the column. The transformed concrete section is also removed.

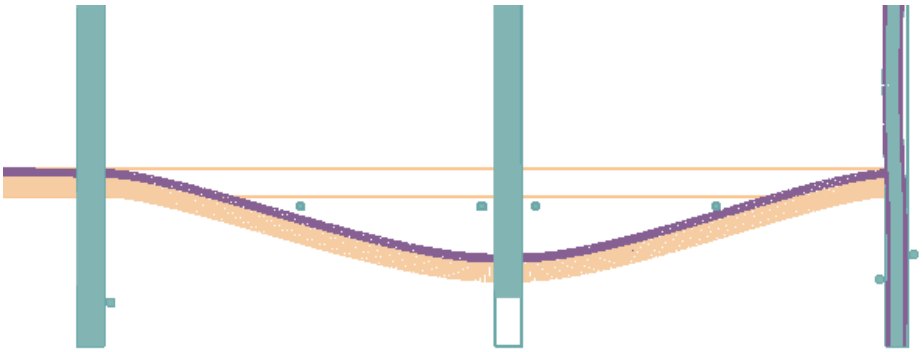

Figure 7.5: Typical displaced shape of Relative Stiffness Models 3, 4, and 5

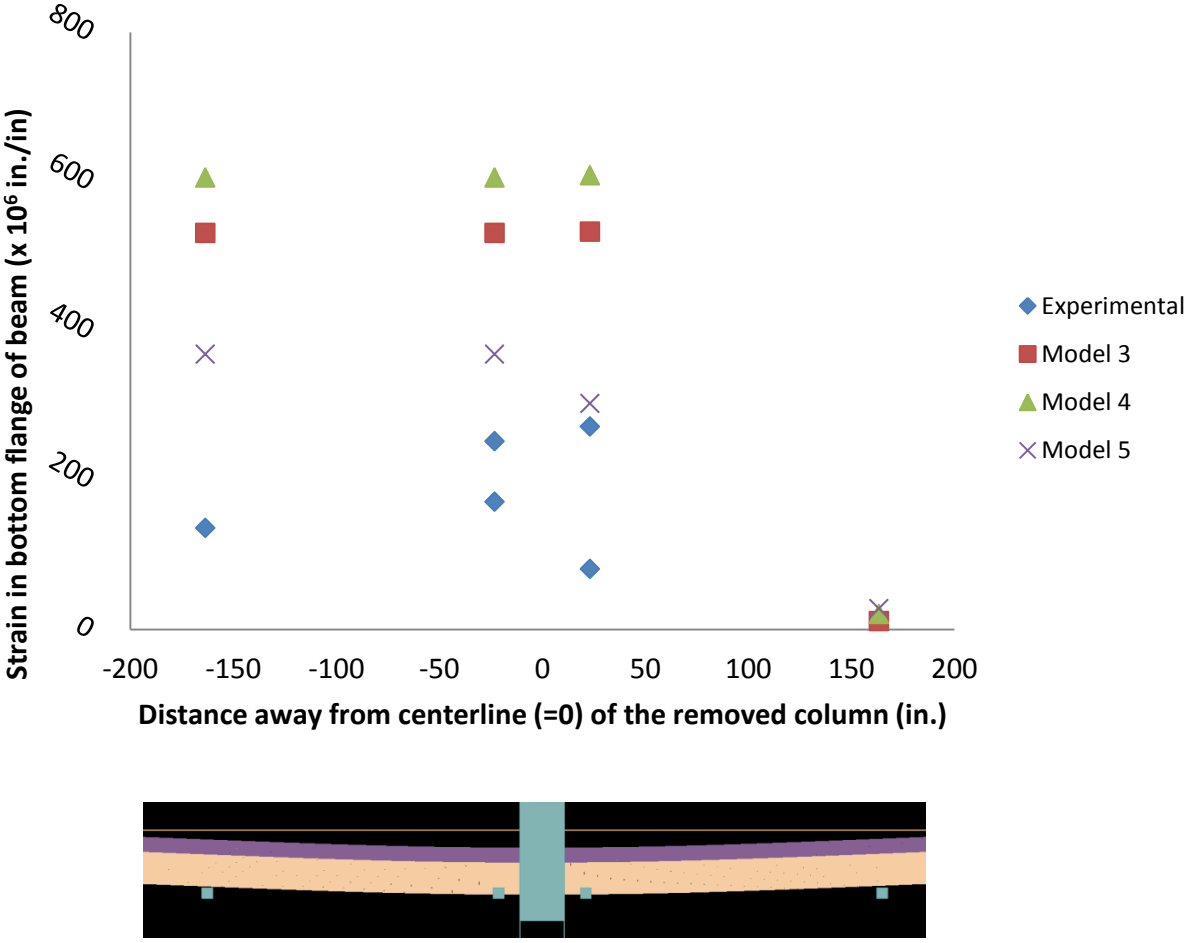

Figure 7.6: Measured and calculated strain data for beams plotted along the length of the North Beam and South Beam.

CHAPTER 8: CONCLUSION

8.1 Summary

The objective of this research was to investigate the progressive collapse potential of a constructed building from 1925. Haskett Hall was instrumented with strain gauges and displacement sensors. A column was removed at the ground story and the response of the structure was measured. After the experiment, details of the building (including structural properties and loads) were determined. These details were used to model the building in the structural analysis softwares SAP2000 and ASI EL. Two analyses were conducted using different loading scenarios to examine the effect of column removal. The experimental data was discussed in comparison to the theoretical data collected from each model, and the susceptibility of Haskett Hall to progressive collapse was evaluated.

8.2 Conclusions

While the DCR values for beams close to the removed column in Haskett Hall were exceeded, the building did not experience progressive collapse during the experiment. Additionally, the experimental error in the Capacity Model was very high. In general, the actual building seemed to have much more resistance to progressive collapse than the two-dimensional model offered.

Two softwares for progressive collapse analysis were used in this research. SAP2000 provided fast, straightforward methods to analyze Haskett Hall using elastic beam theory, and is a very utilitarian choice for progressive collapse analysis. While not explored in this research, ELS provides users with much more powerful nonlinear and composite modeling techniques that can be invaluable in collapse analyses. The two models of Haskett Hall agreed very well between the two programs, indicating their consistency in a linear static analysis.

Exact connection details were hard to determine for Haskett Hall and presented a unique challenge in the analysis. The moment-rotation relationship for the connections had a significant effect in evaluating the moments in beams. In design, special considerations should be made to ensure the capacity and behavior of beam-column connections.

The column sections selected using the Historic Sections Database proved to be adequate in modeling the effect of column removal. This validates the process of determining the section properties by measuring drawings and pictures from the experiment. However, the stiffness offered by the composite beam sections in the Relative Stiffness Model appeared too high.

8.3 Recommendations for Future Research

Future analyses of Haskett Hall and other buildings for progressive collapse should be comprehensive. Connections should be closely examined in Haskett Hall due to the significant effect they have on results. More explicit methods for modeling the slabs on steel beams should also be considered, as the stiffness offered by composite beams in the Relative Stiffness Model appeared too high. In general, three-dimensional models and infill wall modeling will likely give better results for buildings such as Haskett Hall, where a significant number of structural elements extended out of the frame. Since the plastic moment of beams in the frame may have been exceeded in the frame, a nonlinear analysis should be considered. Finally, methods to conveniently analyze and design for progressive collapse need to be further refined.

BIBLIOGRAPHY

ACI 318-08. 2008. *Building code requirements for structural concrete and commentary.* American Concrete Institute (ACI). Farmington Hills, MI.

"AISC Shapes Historic Edition." *AISC Shapes Database Version 14.0 Historic*. American Institute of Steel Construction, 2013. Web. 17 Apr. 2013. <http://www.aisc.org/WorkArea/showcontent.aspx?id=17622>.

Extreme Loading for Structures. 2012. Extreme Loading for Structures, *Version 3.1*. Applied Science International, LLC (ASI). Durham, NC, U.S.A.

ASCE 7-05. 2005. *Minimum design loads for buildings and other structures*. Report: ASCE/SEI 7-05. American Society of Civil Engineers (ASCE). Reston, VA.

DoD. 2005. *Design of buildings to resist progressive collapse*. Unified Facilities Criteria (UFC) 4-023-03, Department of Defense (DoD)

Giriunas, K. A. 2009. *Progressive collapse analysis of an existing building*. Honors Thesis. Department of Civil and Environmental Engineering and Geodetic Science. The Ohio State University, Columbus, OH.

GSA. 2003. *Progressive collapse analysis and design guidelines for new federal office buildings and major modernization projects*. General Services Administration (GSA).Washington, D.C.

Hertenstein, J. P. (1993). *Facility audit report Haskett hall, building 027* [Data file]. Retrieved from http://fod.osu.edu/bldg_audit/Haskett_Hall-93.pdf

SAP2000. 2011. SAP 2000 Advanced structural analysis program, *Version 15*. Computers and Structures, Inc. (CSI). Berkeley, CA, U.S.A.

Song, B. I. 2010. *Experimental and analytical assessment on the progressive collapse potential of existing buildings*. Master's Thesis. Department of Civil, Environmental, and Geodetic Engineering. The Ohio State University, Columbus, OH.

APPENDIX A: 1925 HASKETT HALL CONSTRUCTION DRAWINGS

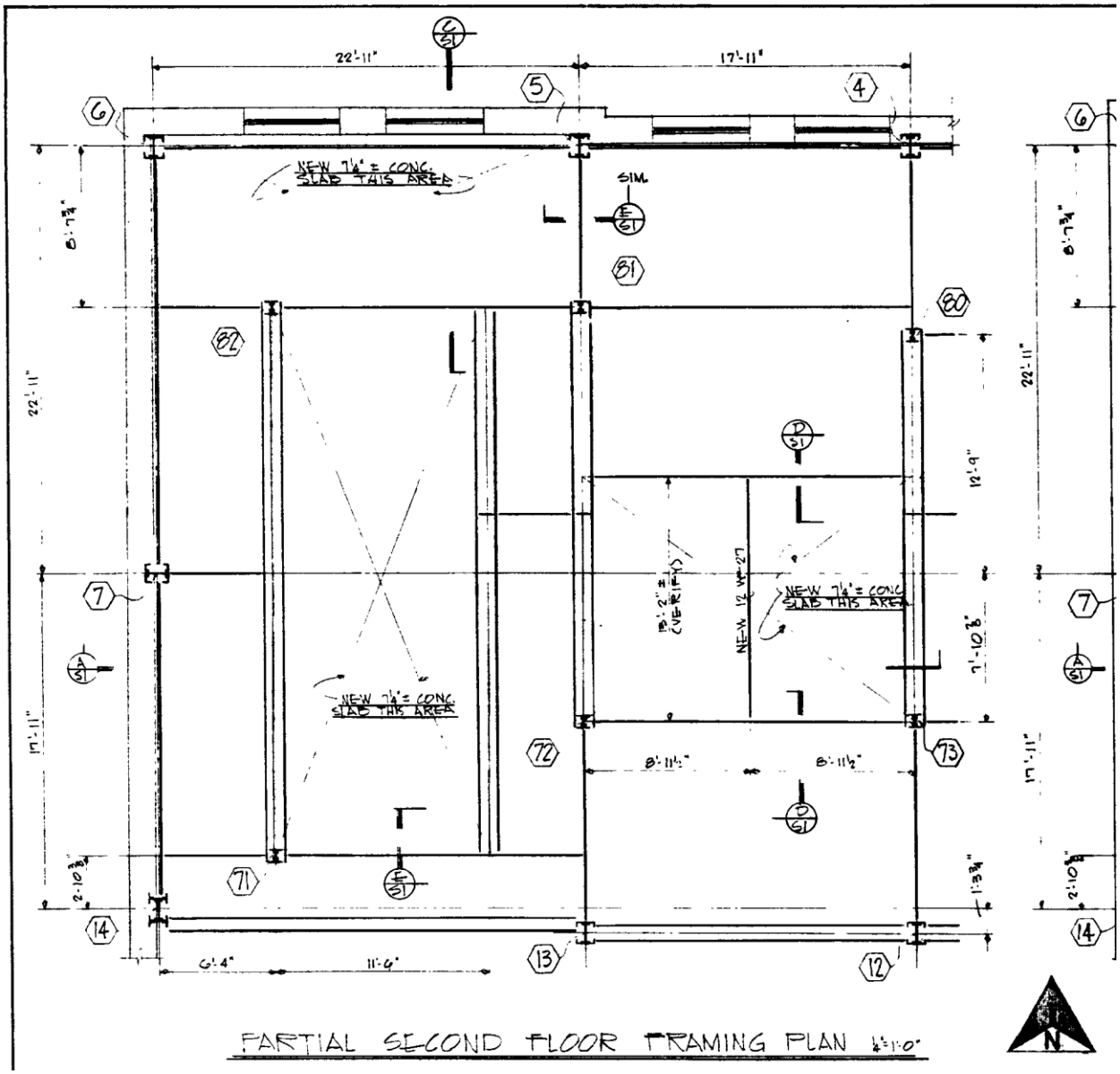

Figure A.1: Second story framing plan

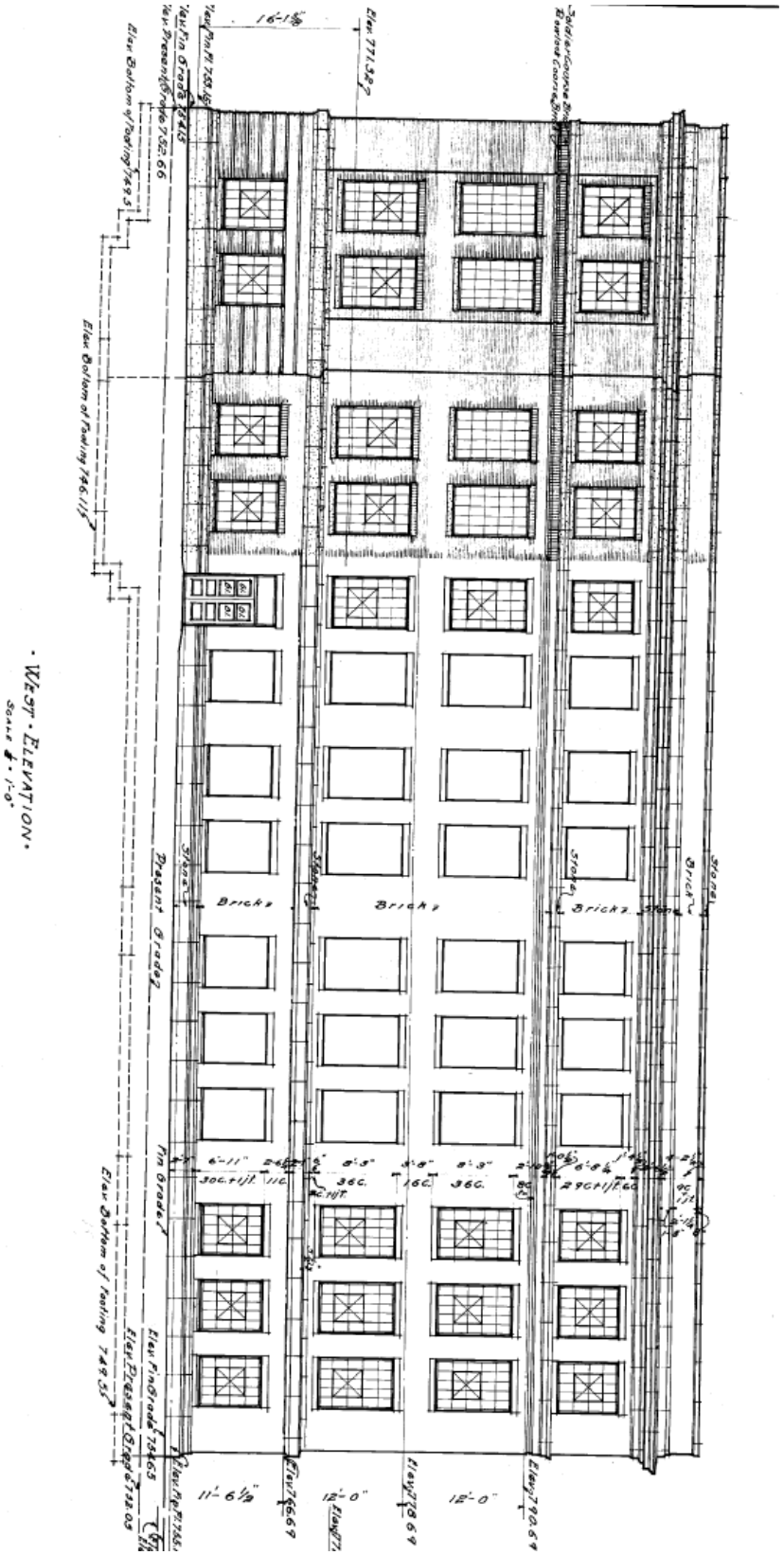

Figure A.2: West exterior, elevation view

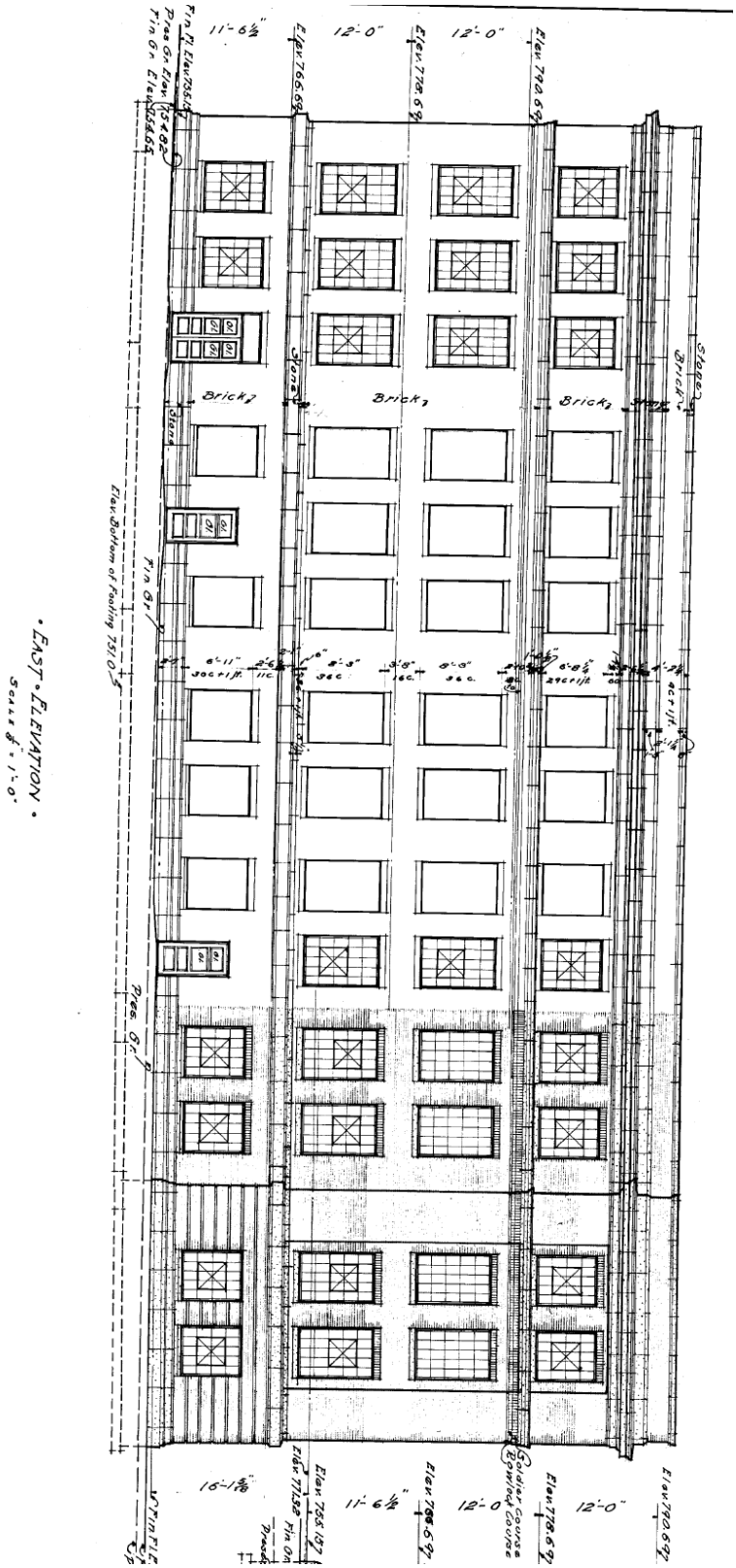

Figure A.3: East exterior, elevation view

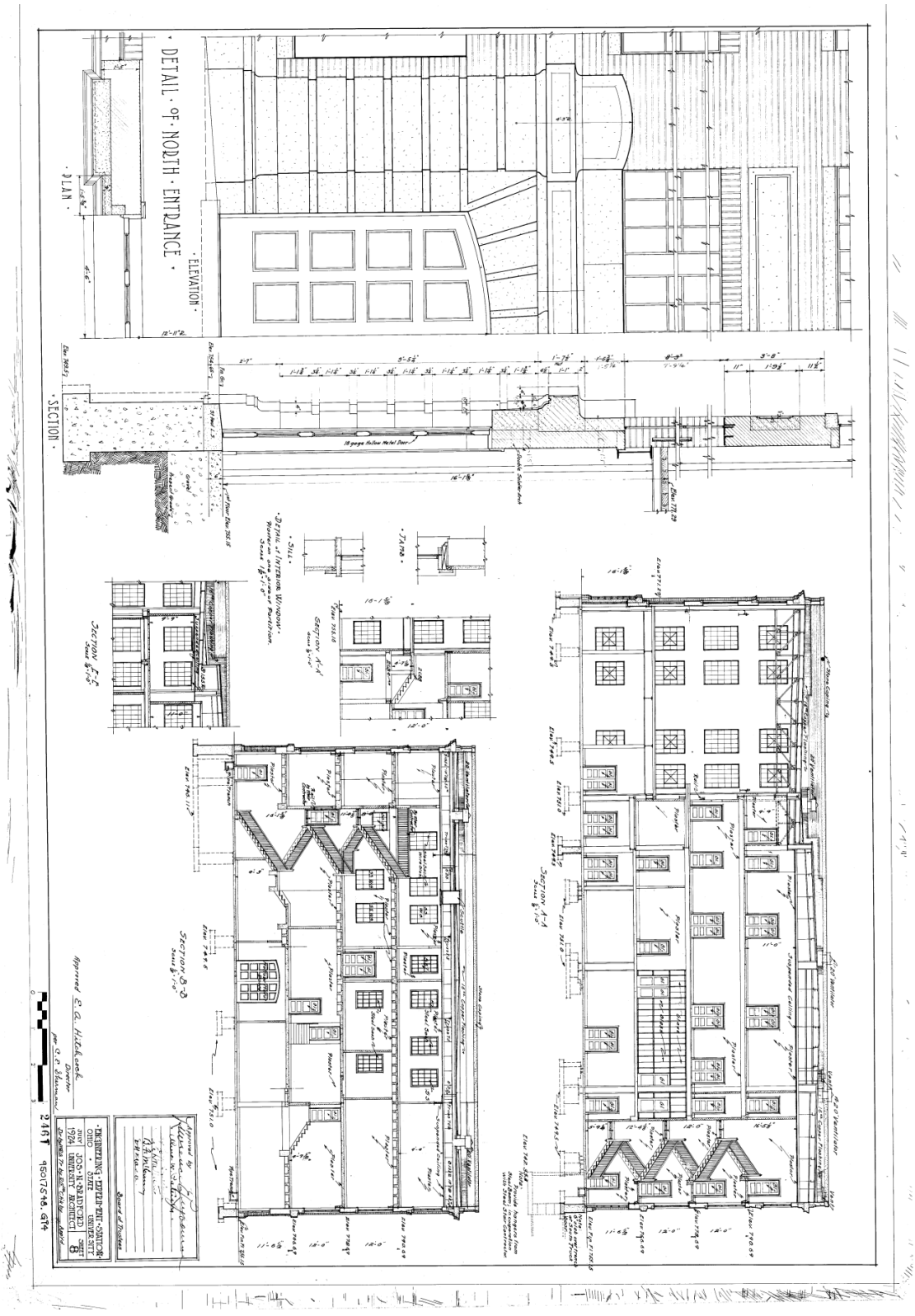

Figure A.4: Section views and elevation details

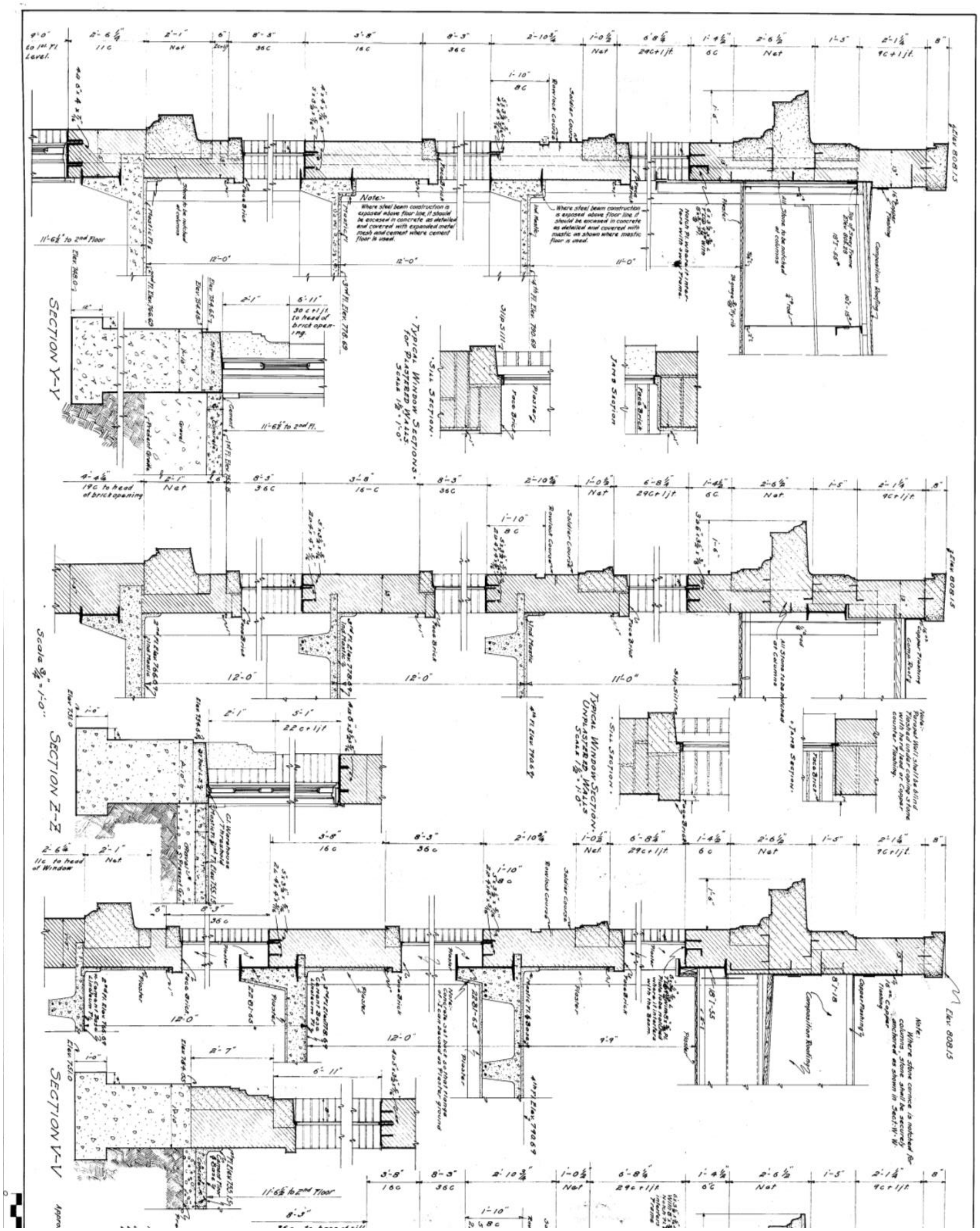

Figure A.5: Sections of exterior

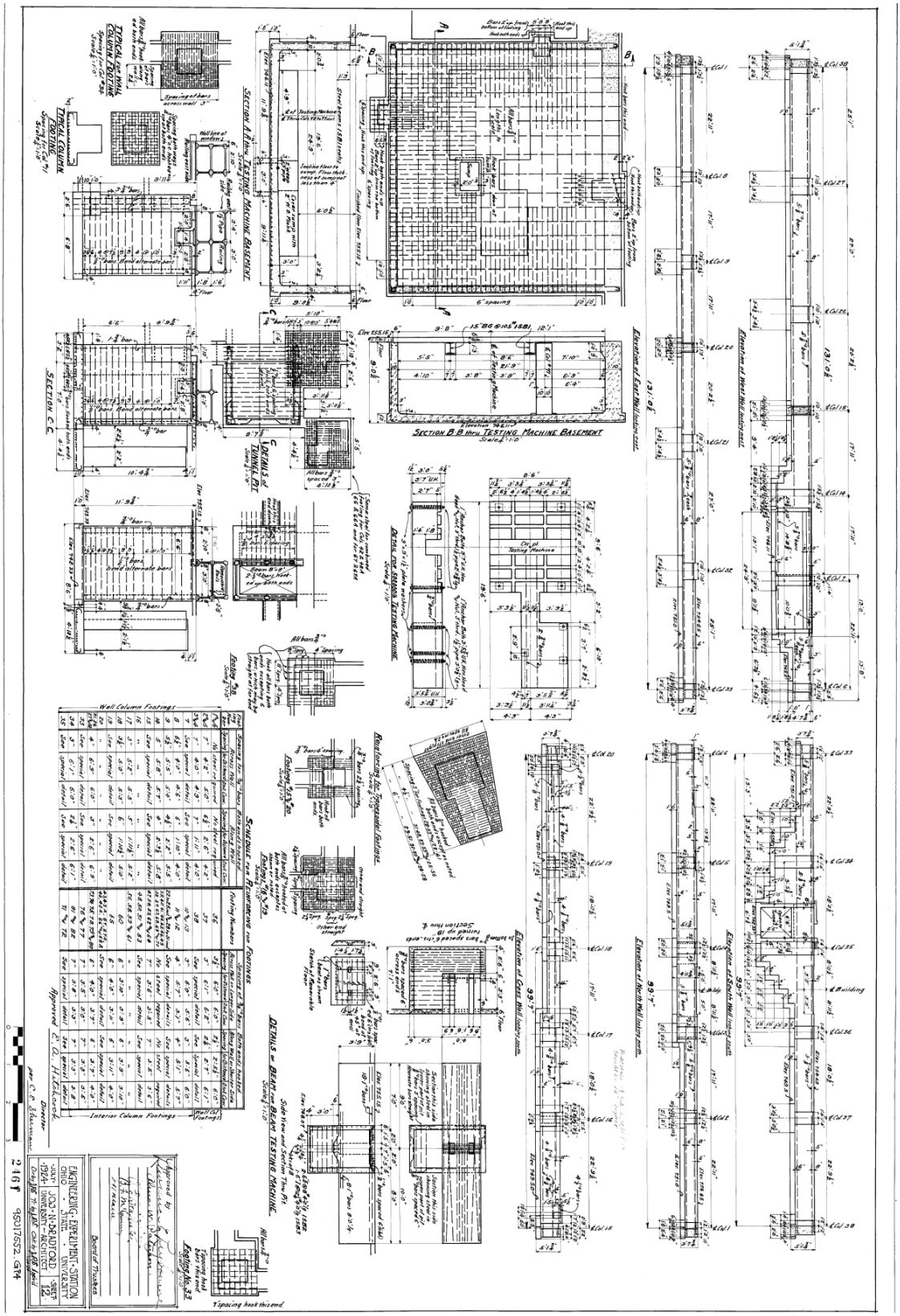

Figure A.6: Foundation Details

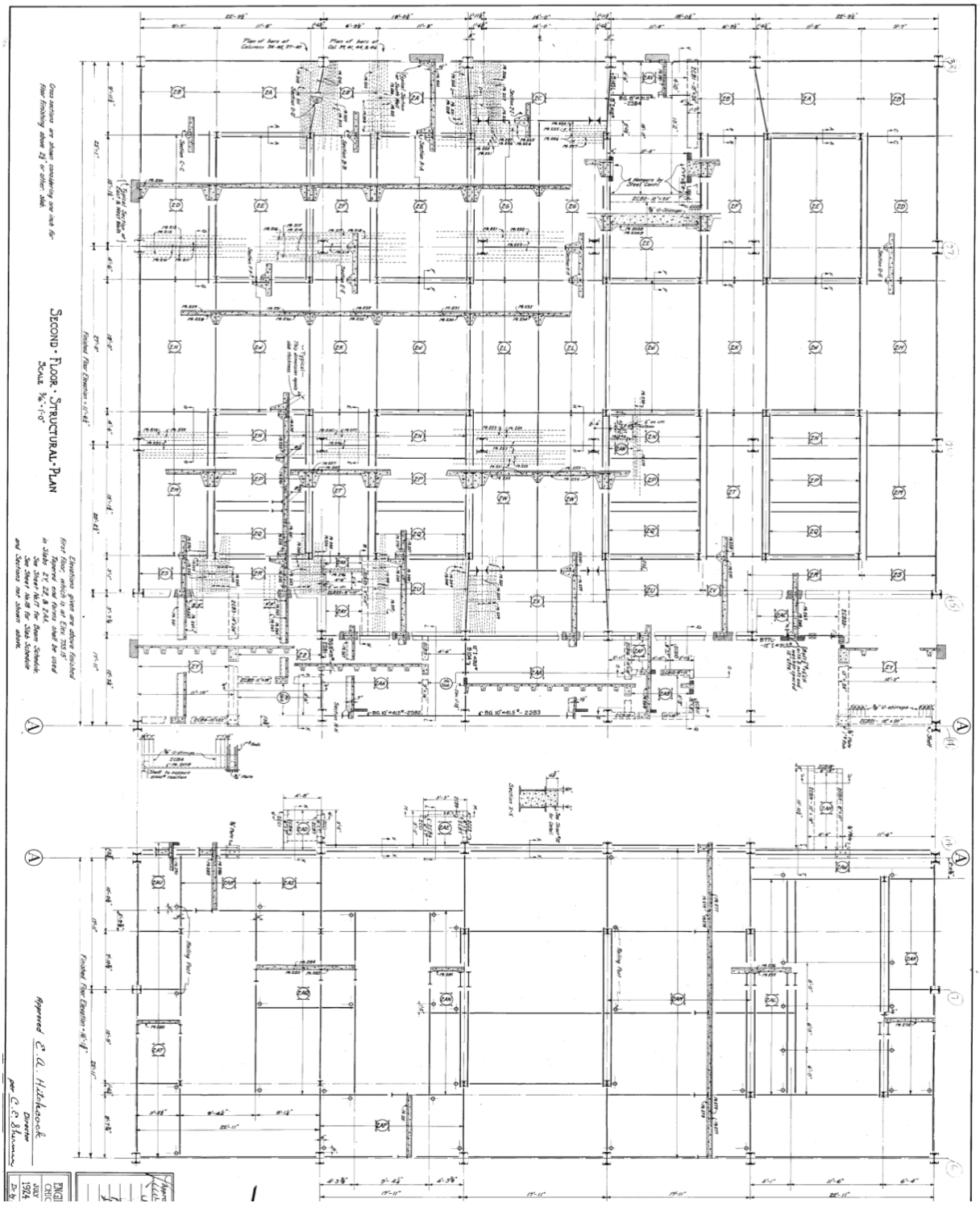

Figure A.7: Second story plan view

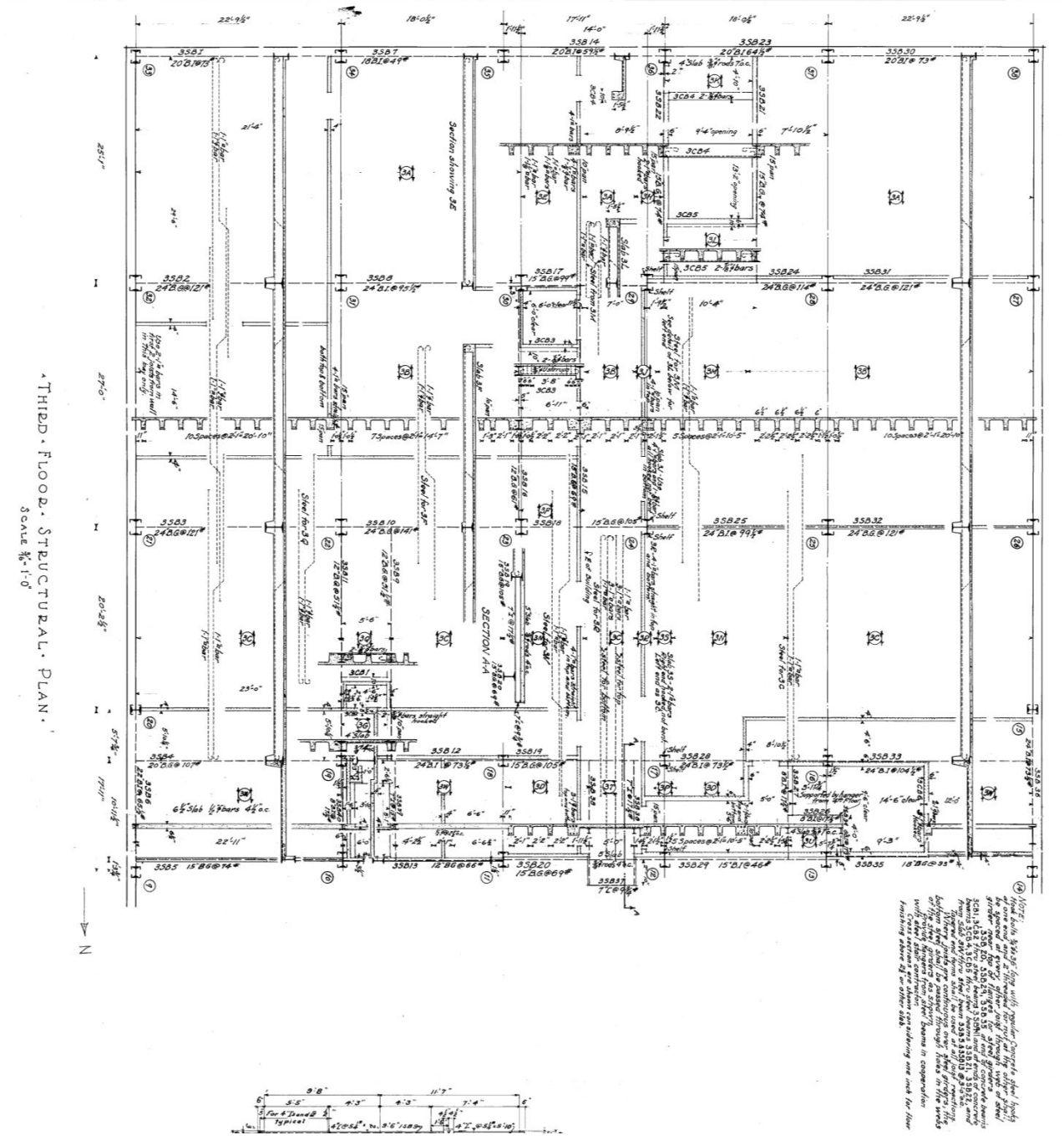

Figure A.8: Third story plan view

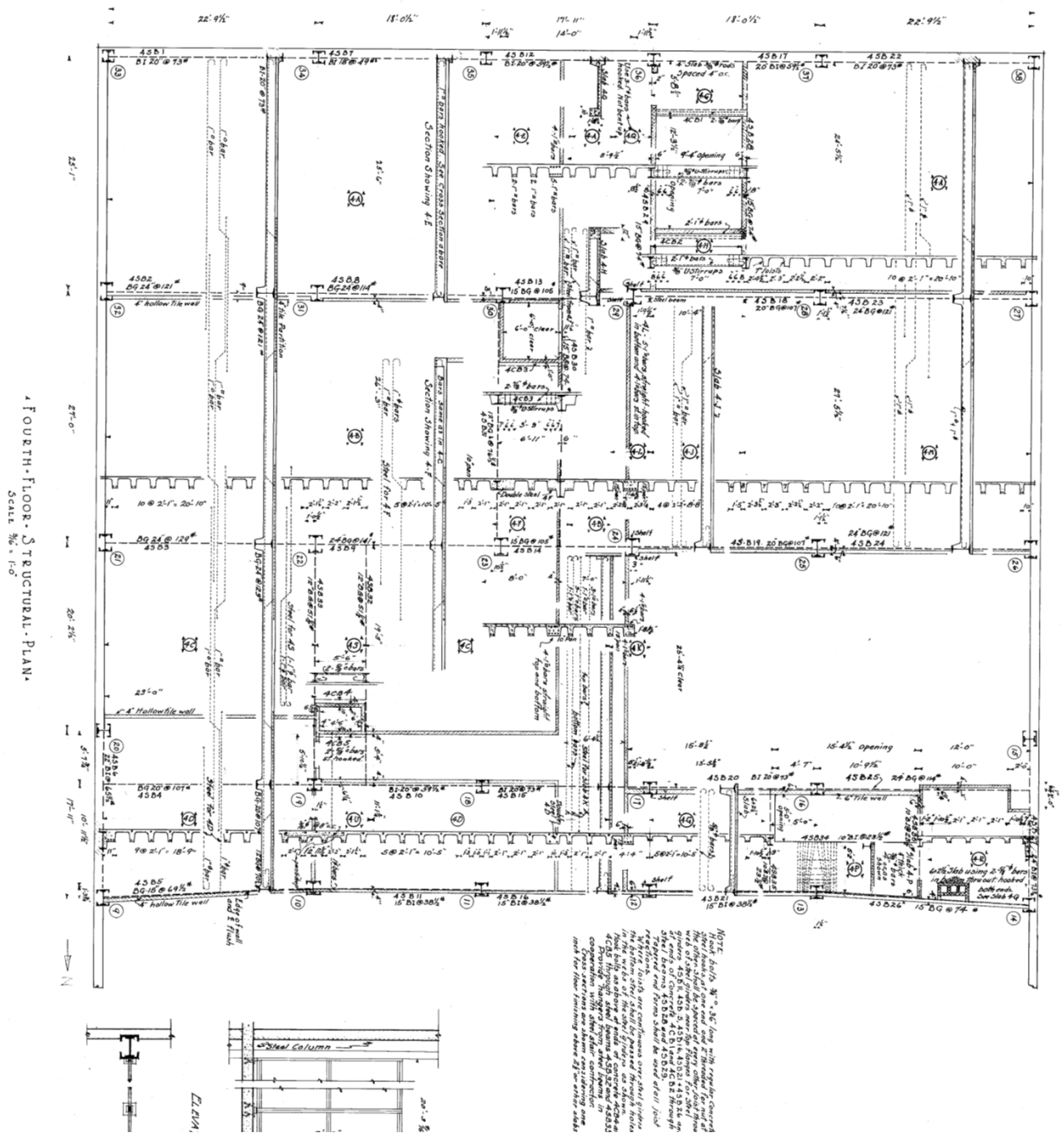

Figure A.9: Fourth story plan view

APPENDIX B: EXPERIMENTAL DATA

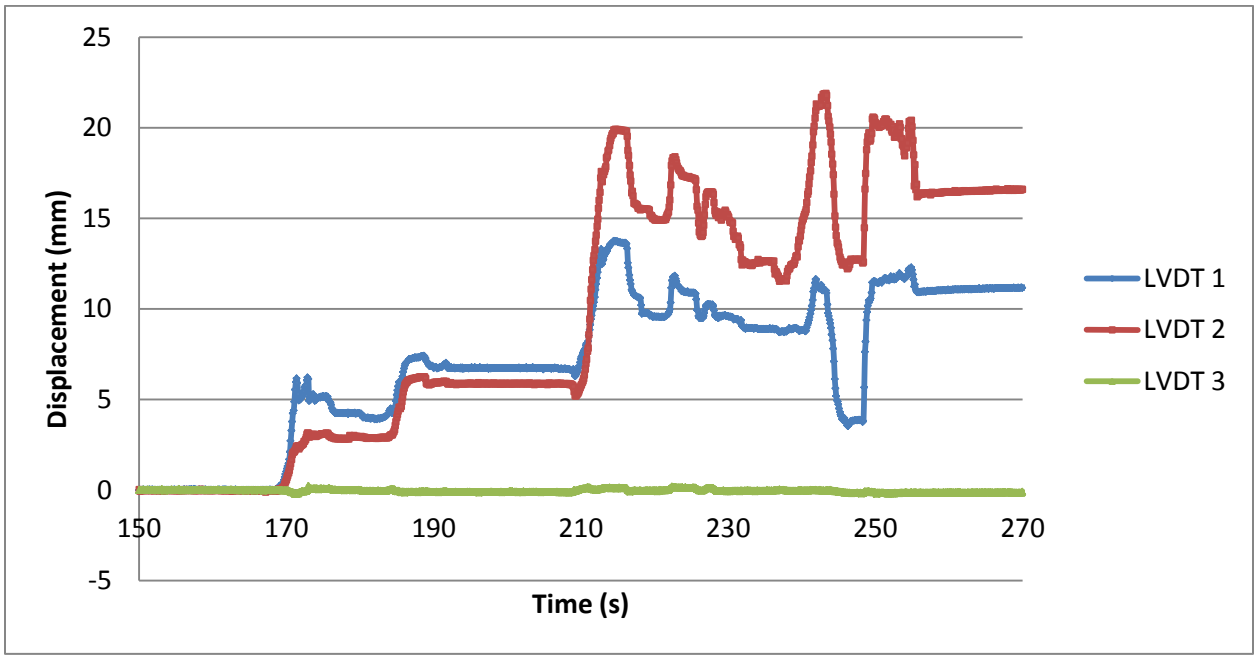

Figure B.1: Displacement data vs. time

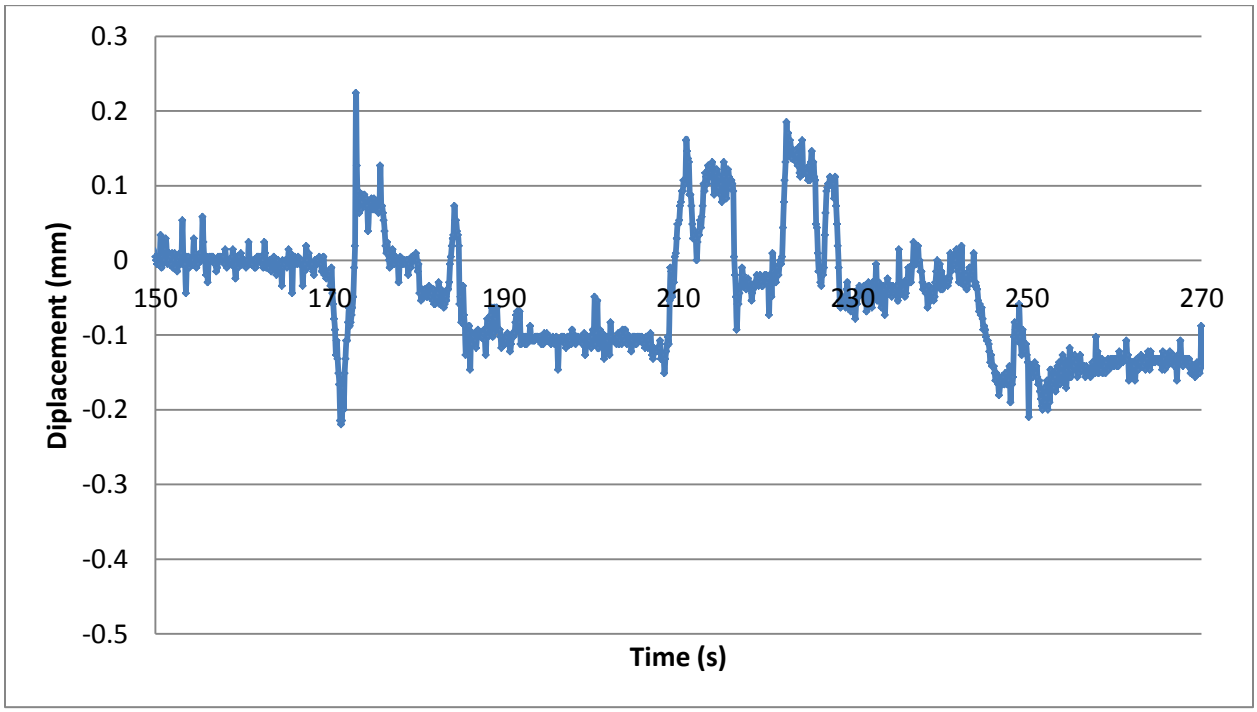

Figure B.2: Displacement data for LVDT 3 vs. time

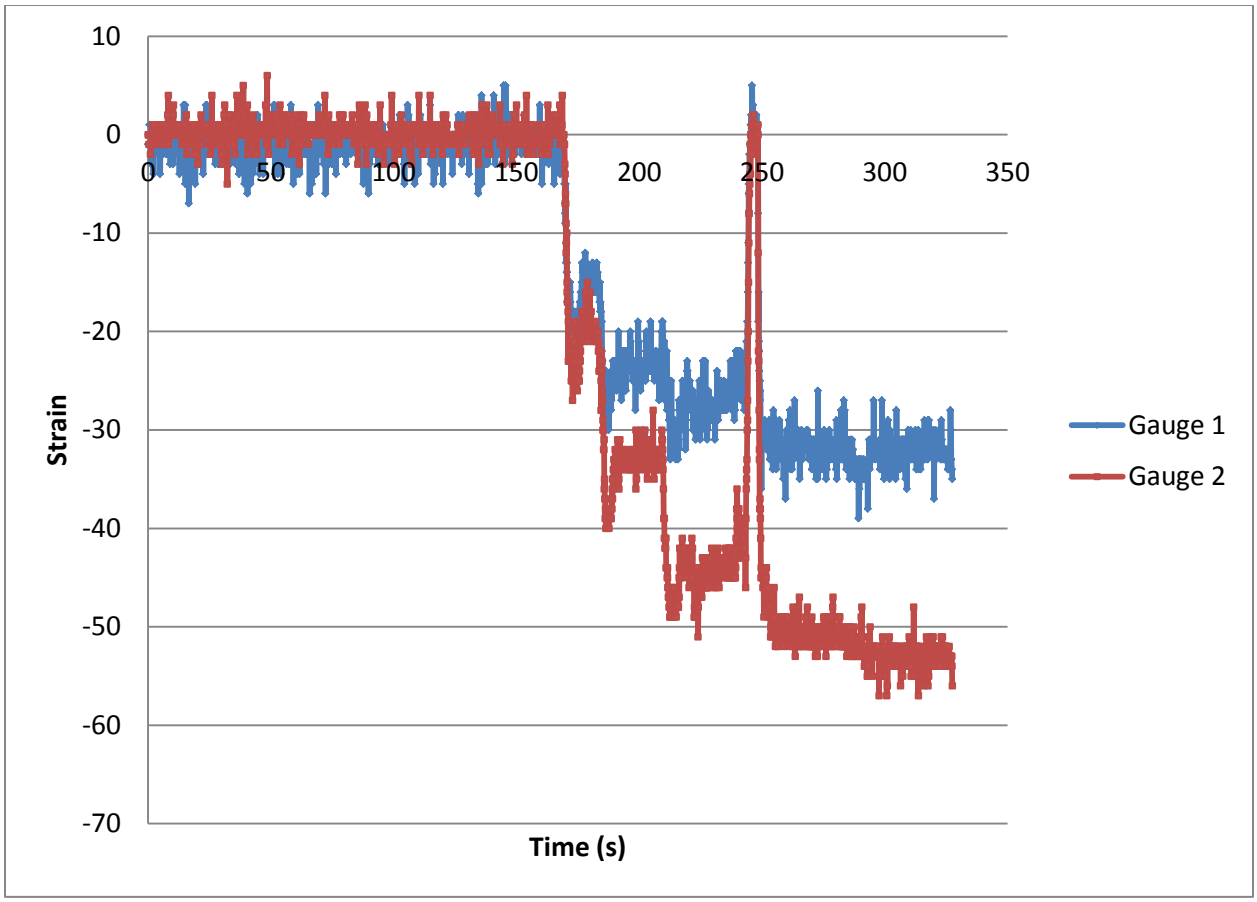

Figure B.3: Strain data for Gauges 1 and 2 vs. time

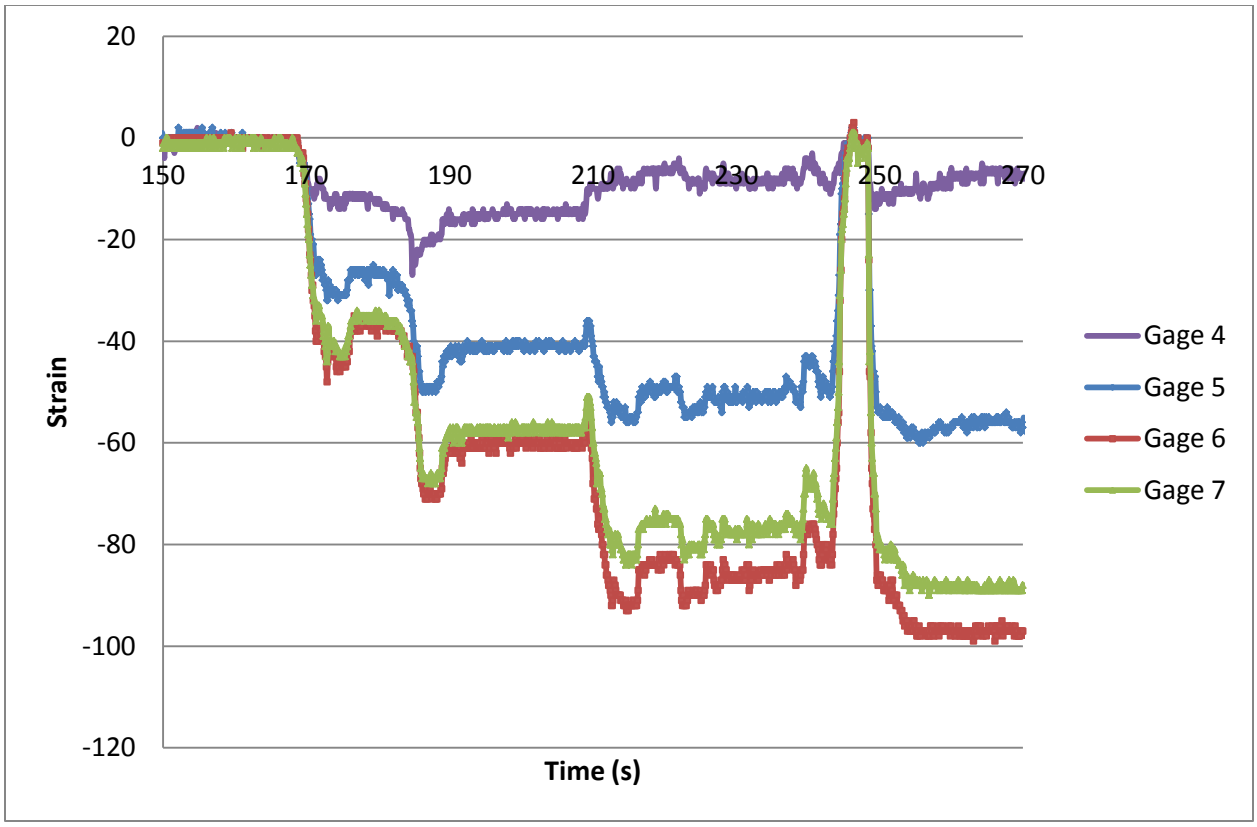

Figure B.4: Strain data for Gauges 4, 5, 6, and 7 vs. time

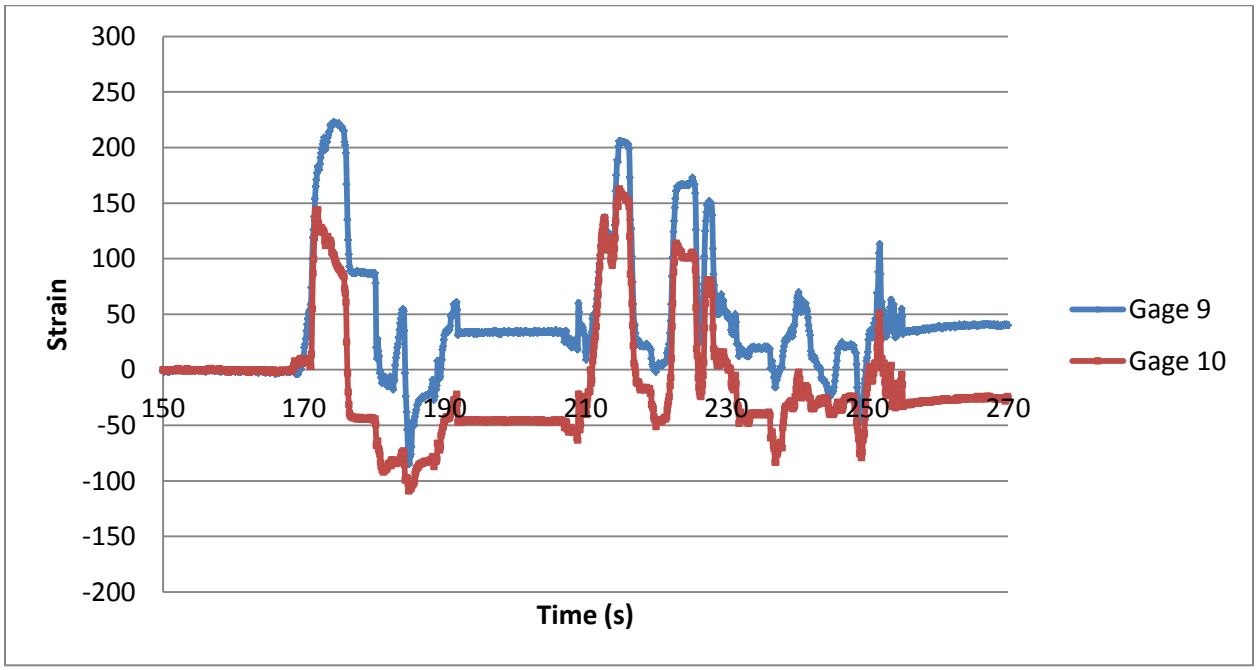

Figure B.5: Strain data for Gauges 9 and 10 vs. time

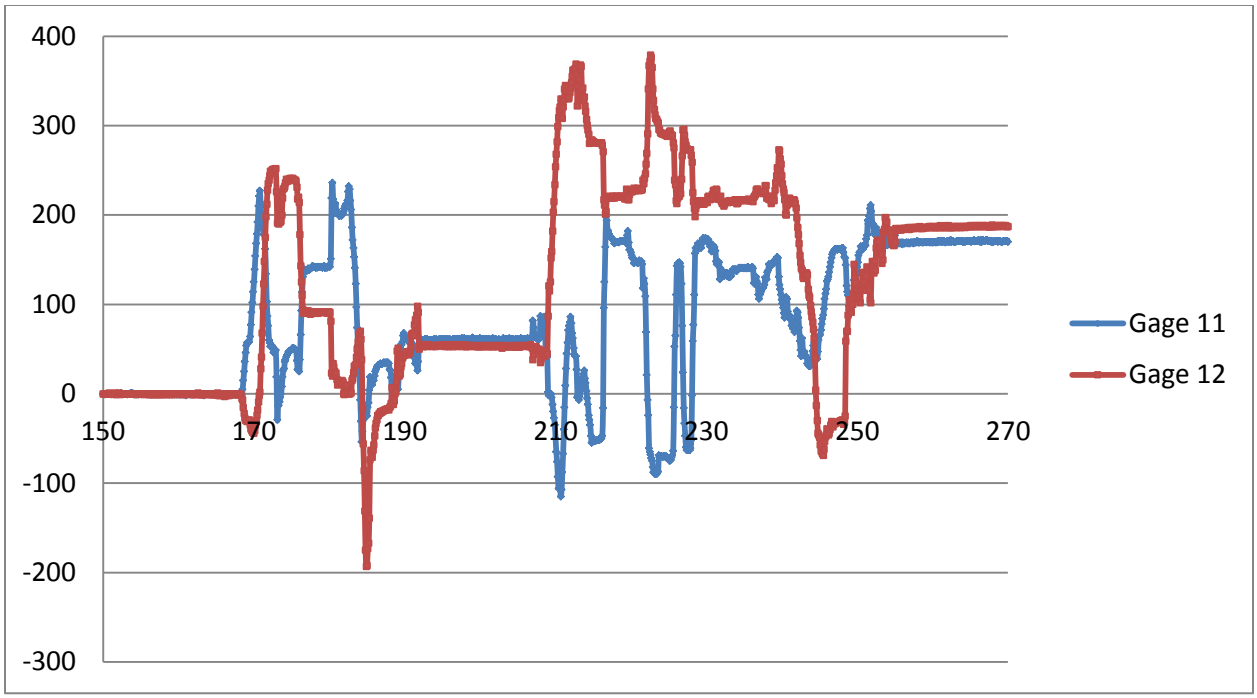

Figure B.6: Strain data for Gauges 11 and 12 vs. time

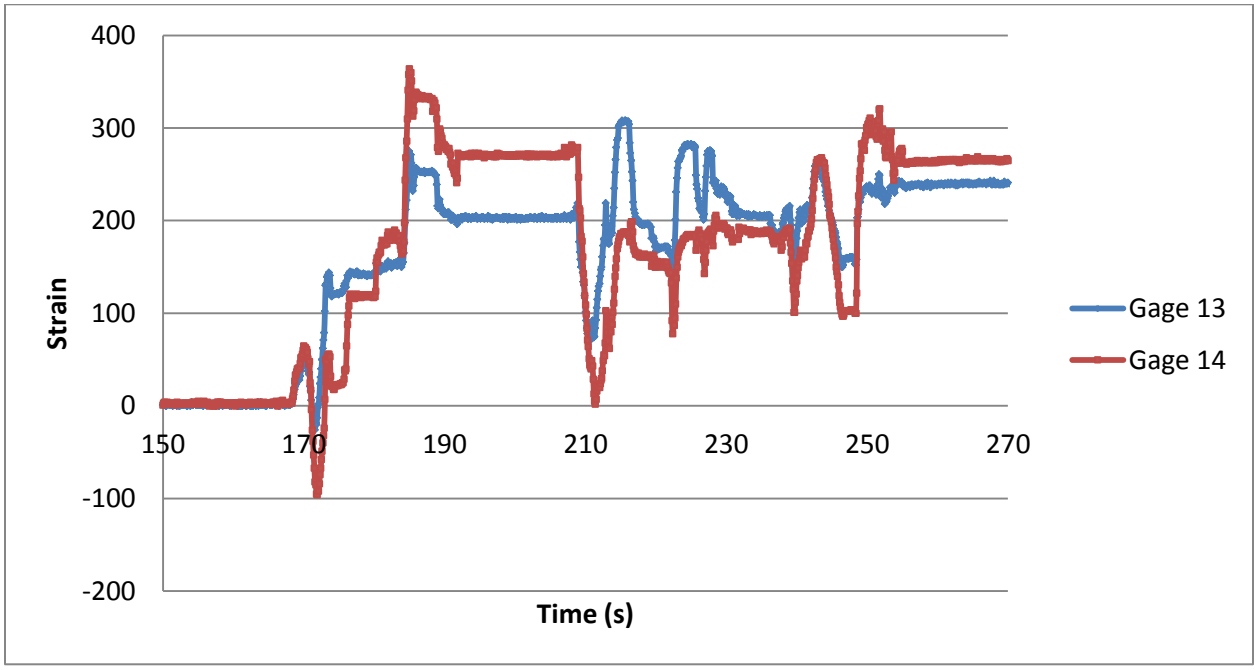

Figure B.7: Strain data for Gauges 13 and 14 vs. time

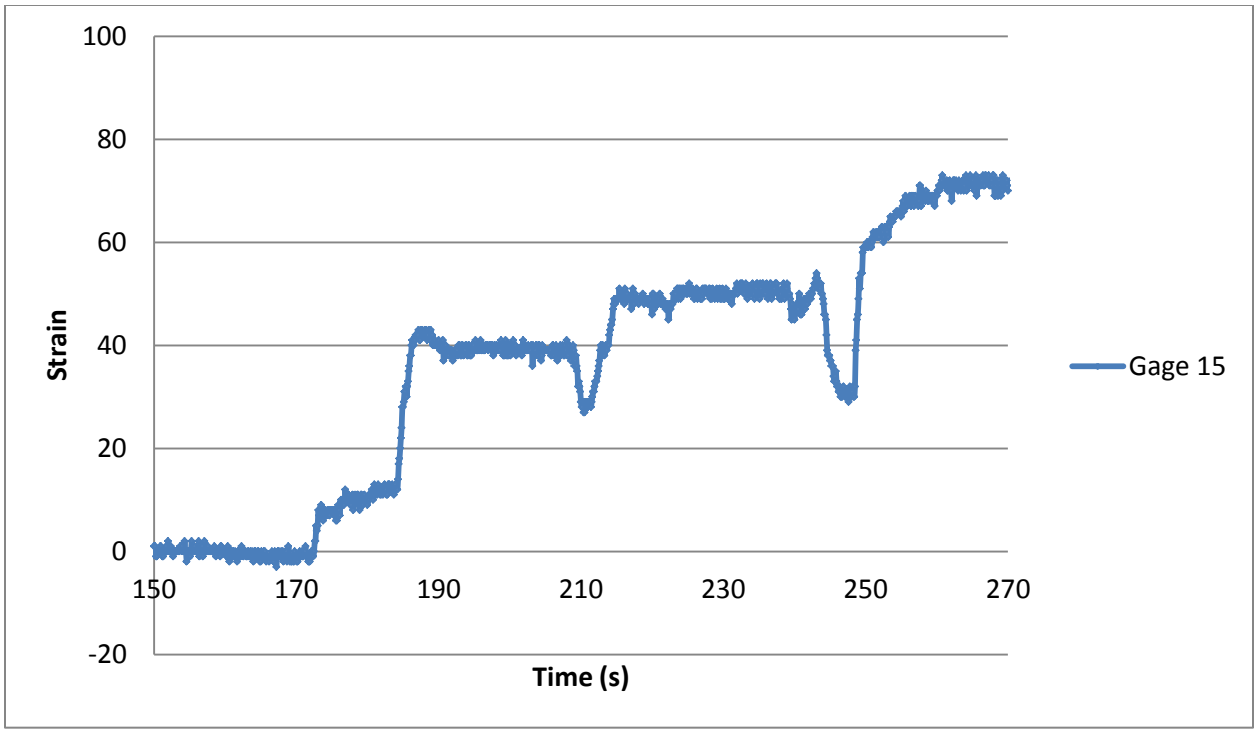

Figure B.8: Strain data for Gauge 15 vs. time

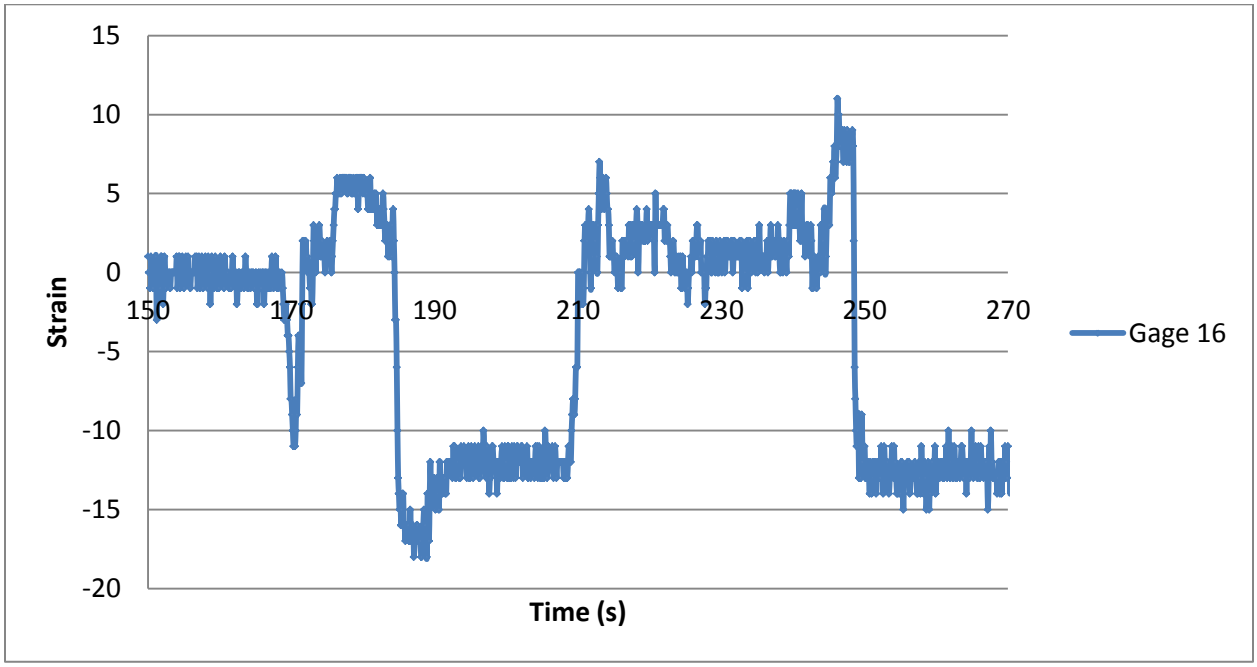

Figure B.9: Strain data for Gauge 16 vs. time

APPENDIX C: AUTOCAD MEASUREMENTS

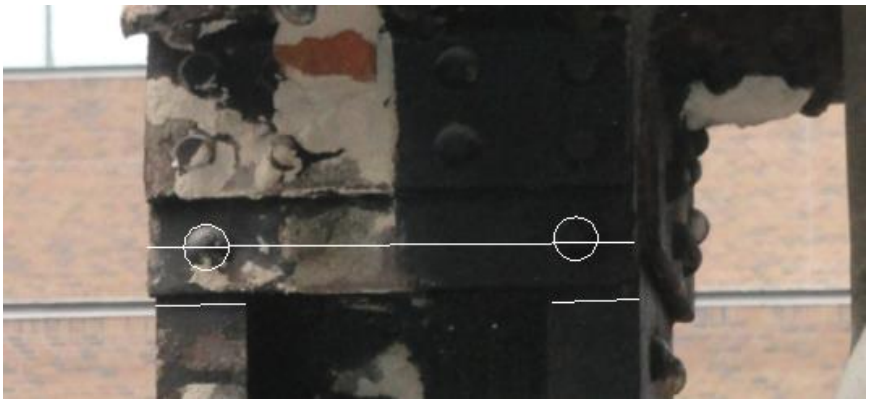

Figure C.1: Column 38 measurements, where depth is 16.6 in. and channel flange bases are 3 in.

Figure C.2: Column 38 measurements, where base is 10.3 in.

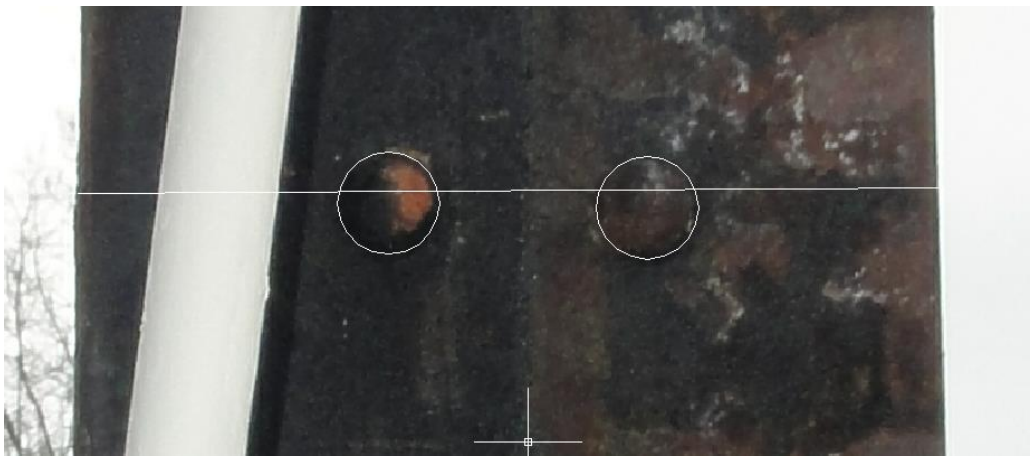

Figure C.3: Column 38 measurements, where base is 12.6 in. Note that this measurement is inconsistent with others

Figure C.4: Column 27 measurement, where base is 16.0 in.

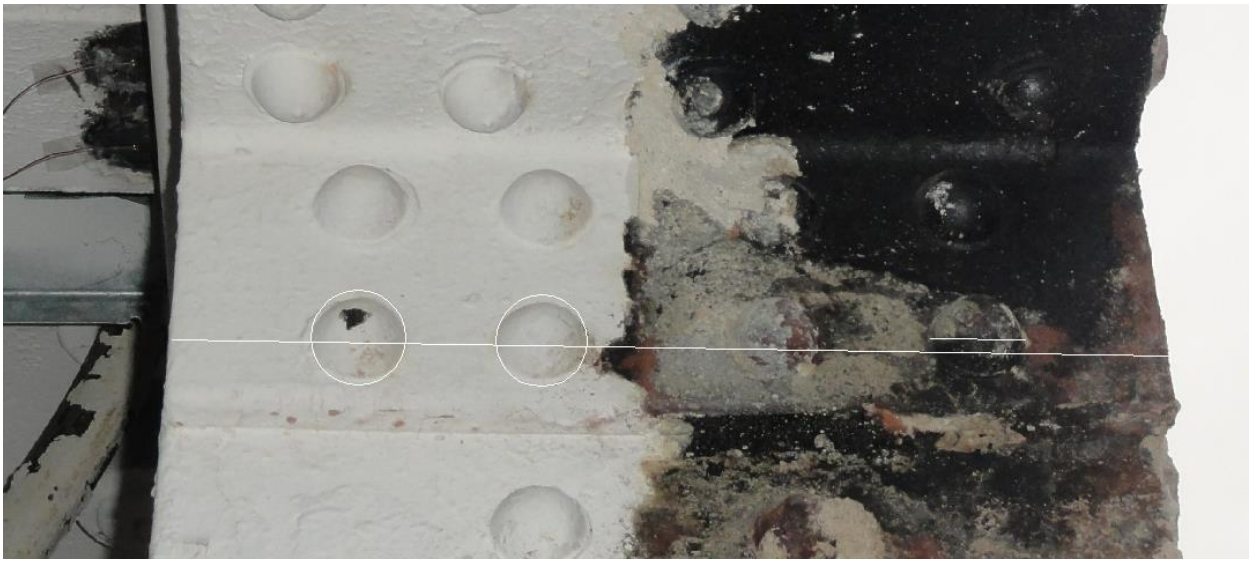

Figure C.5: Column 27 measurement, where base is 15.77 in.

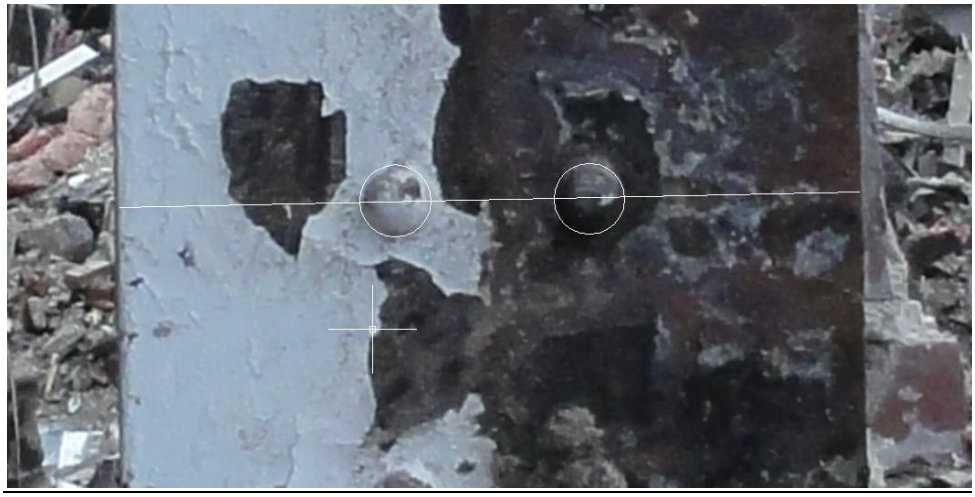

Figure C.6: Column 27 measurement, where base is 15.6 in.

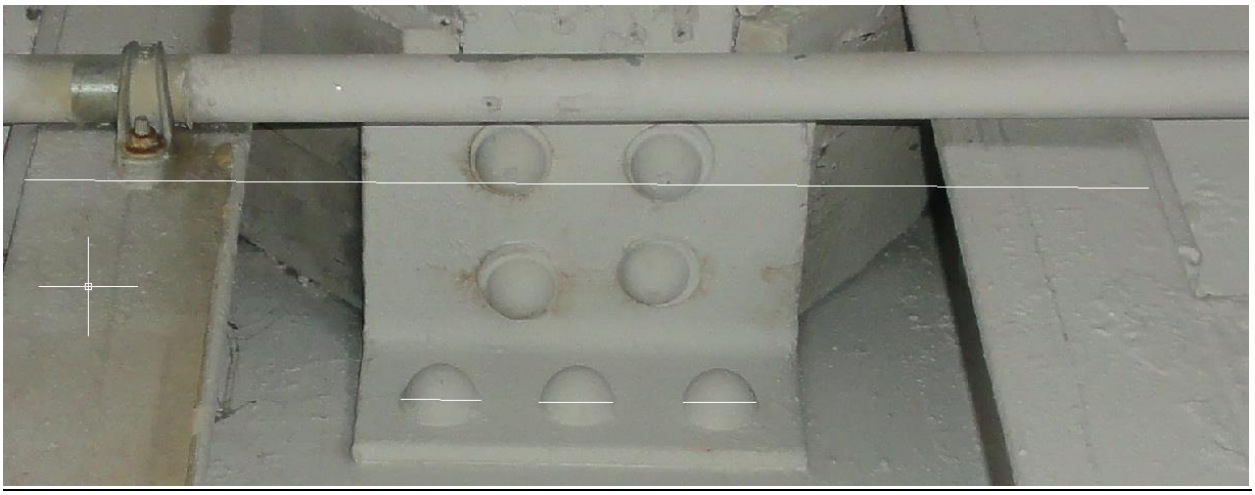

Figure C.7: Column 27 measurement, where depth is 22.5 in. (note measurement may be inflated due to skew)

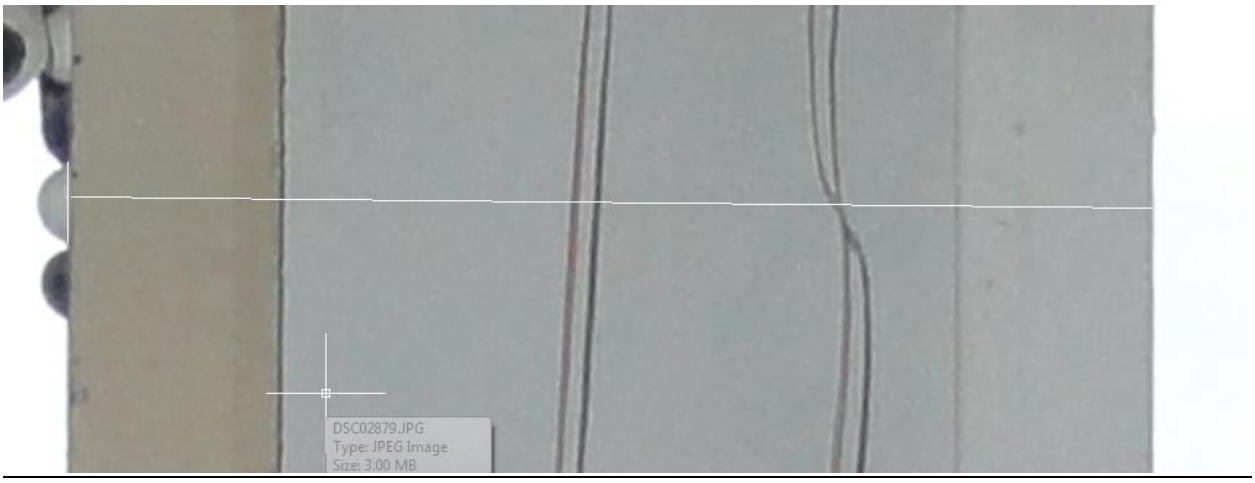

Figure C.8: Column 27 measurement, where depth is 20.5 in.

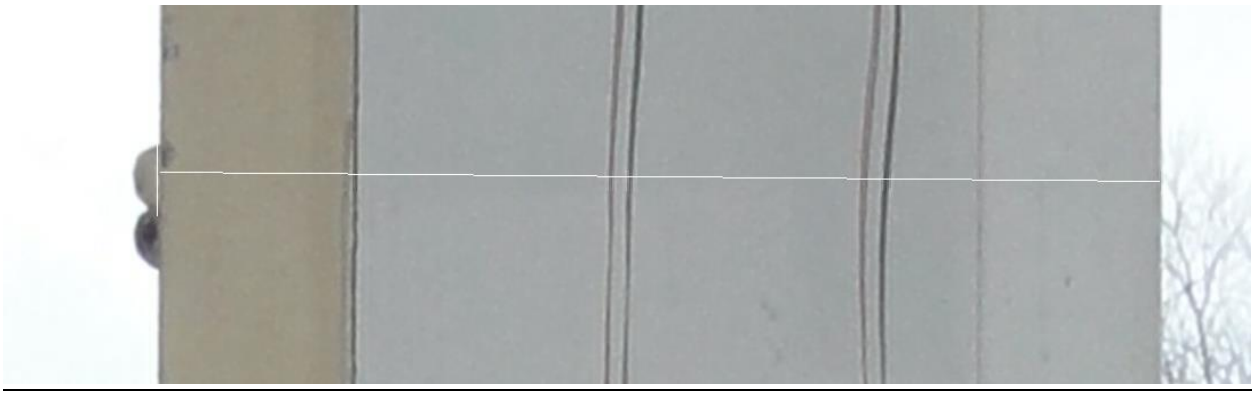

Figure C.9: Column 27 measurement, where depth is 21.26 in.

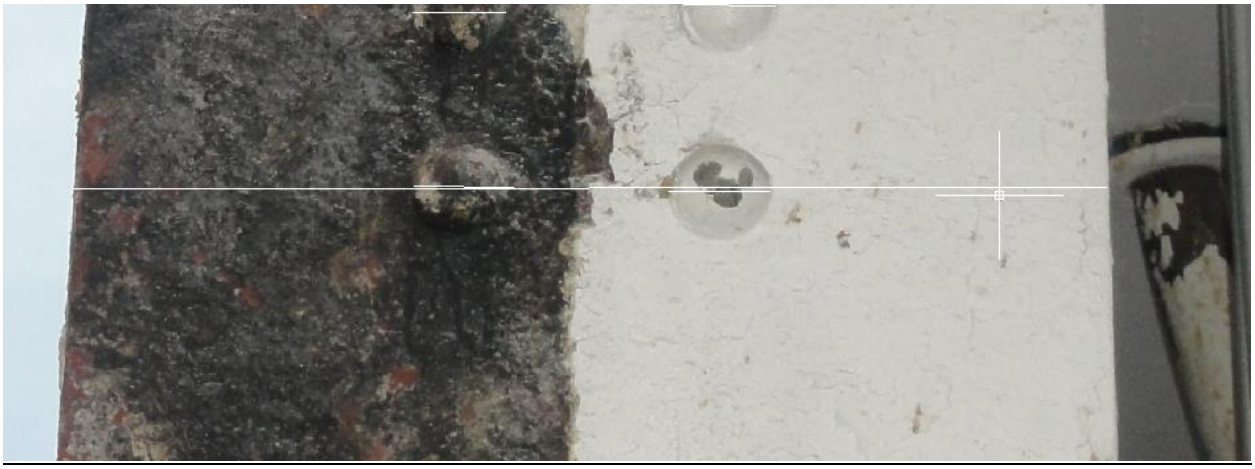

Figure C.10: Column 26 measurement, where base is 15.5 in.

Figure C.11: Column 26 measurement, where base is 15.2 in.

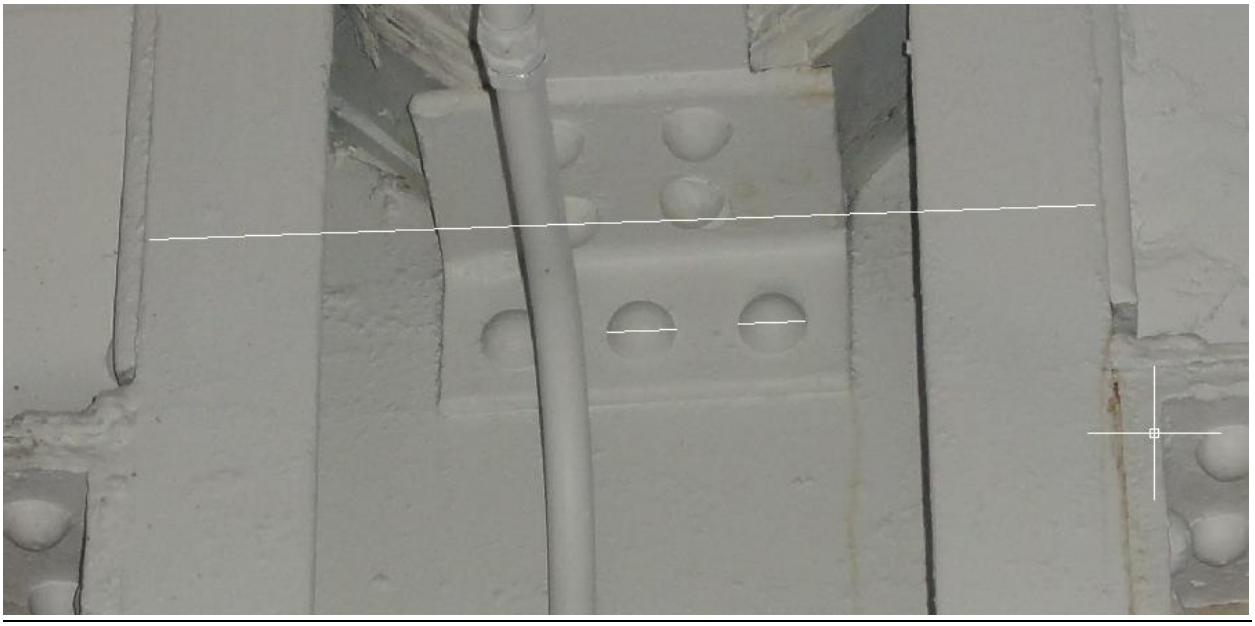

Figure C.12: Column 26 measurement, where depth is 21 in. and channel flange width is 4 in.

APPENDIX D: LOAD CALCULATIONS

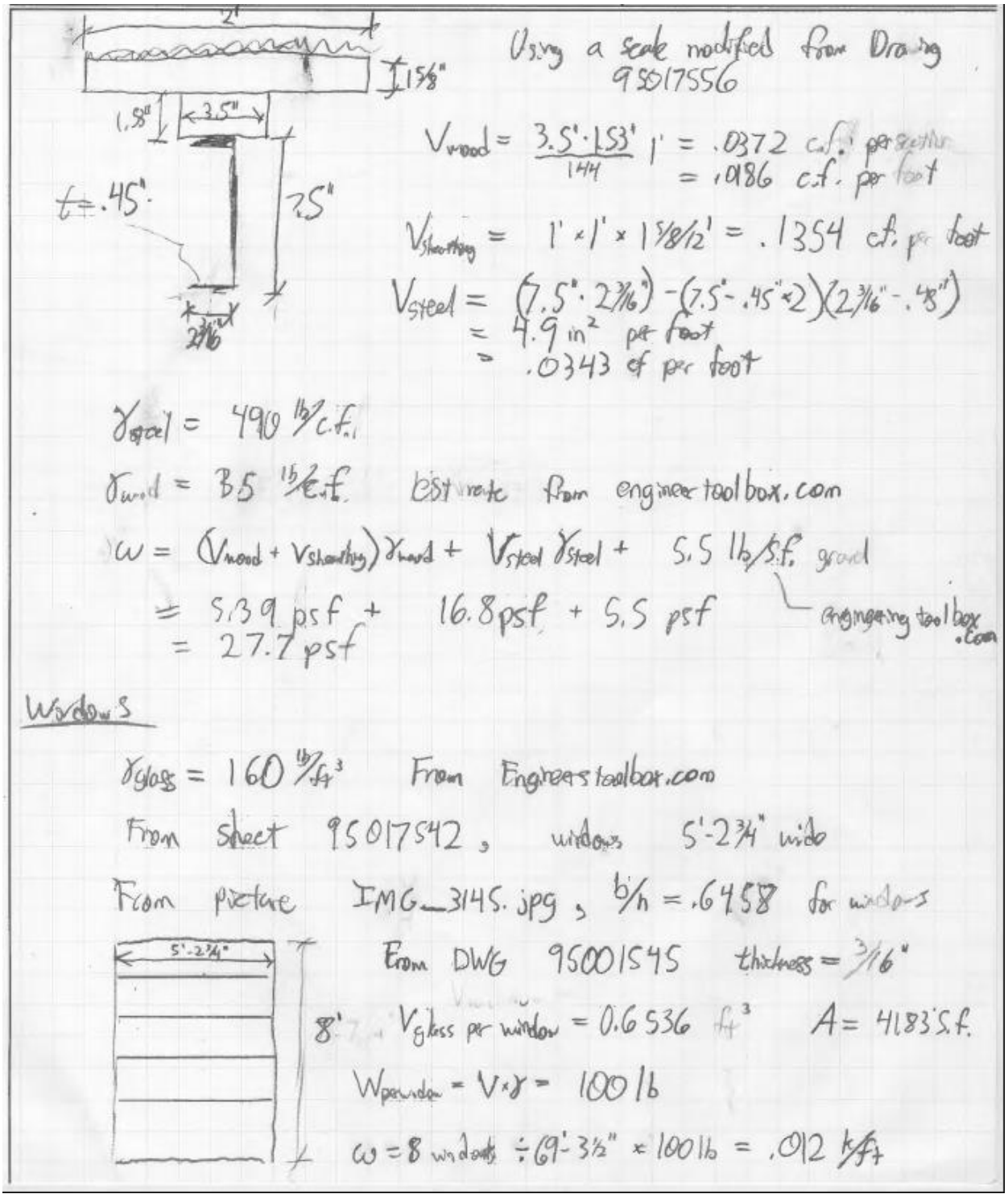

Figure D.1: Load calculations for roofing

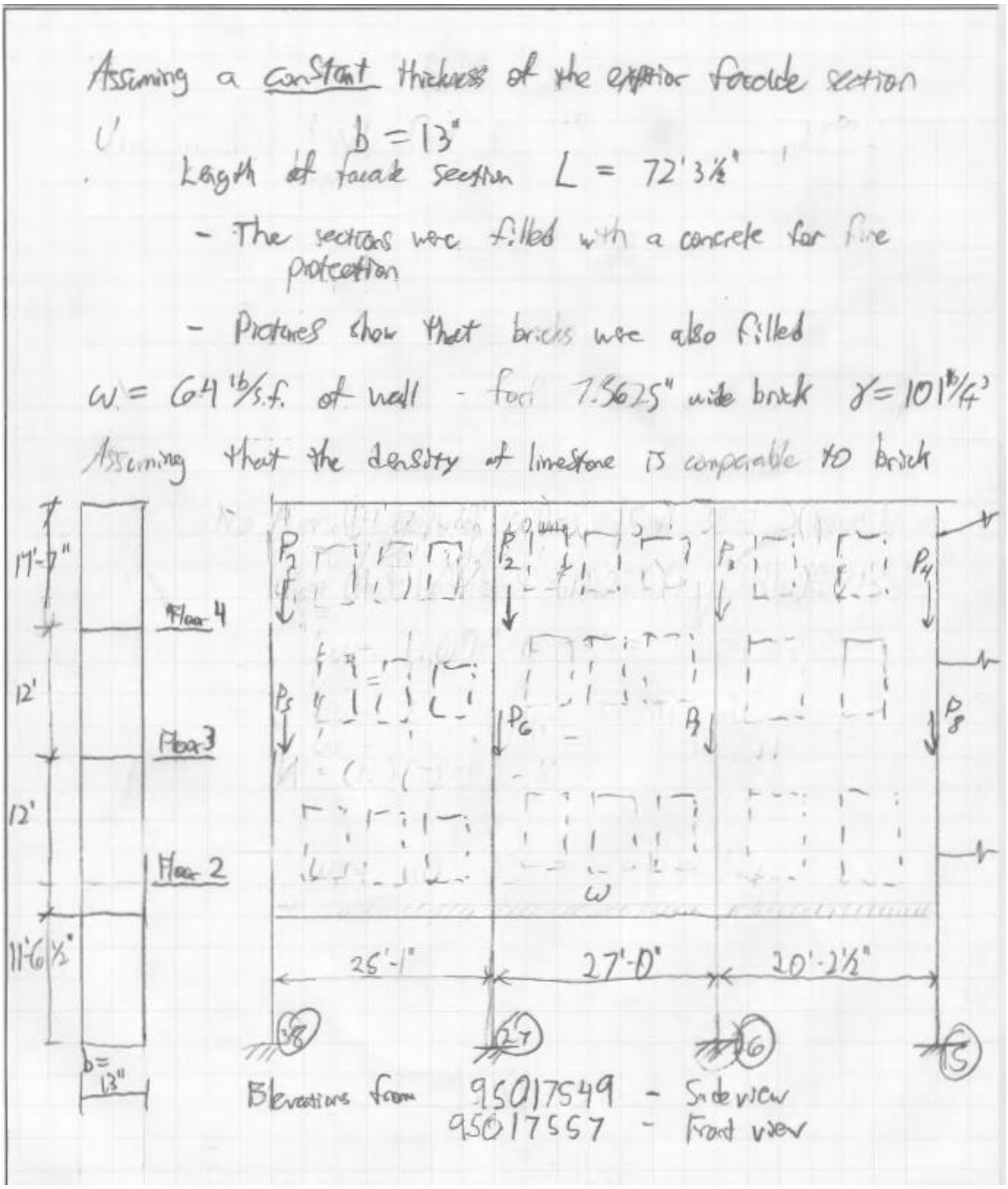

Figure D.2: Depiction of loads for brick façade

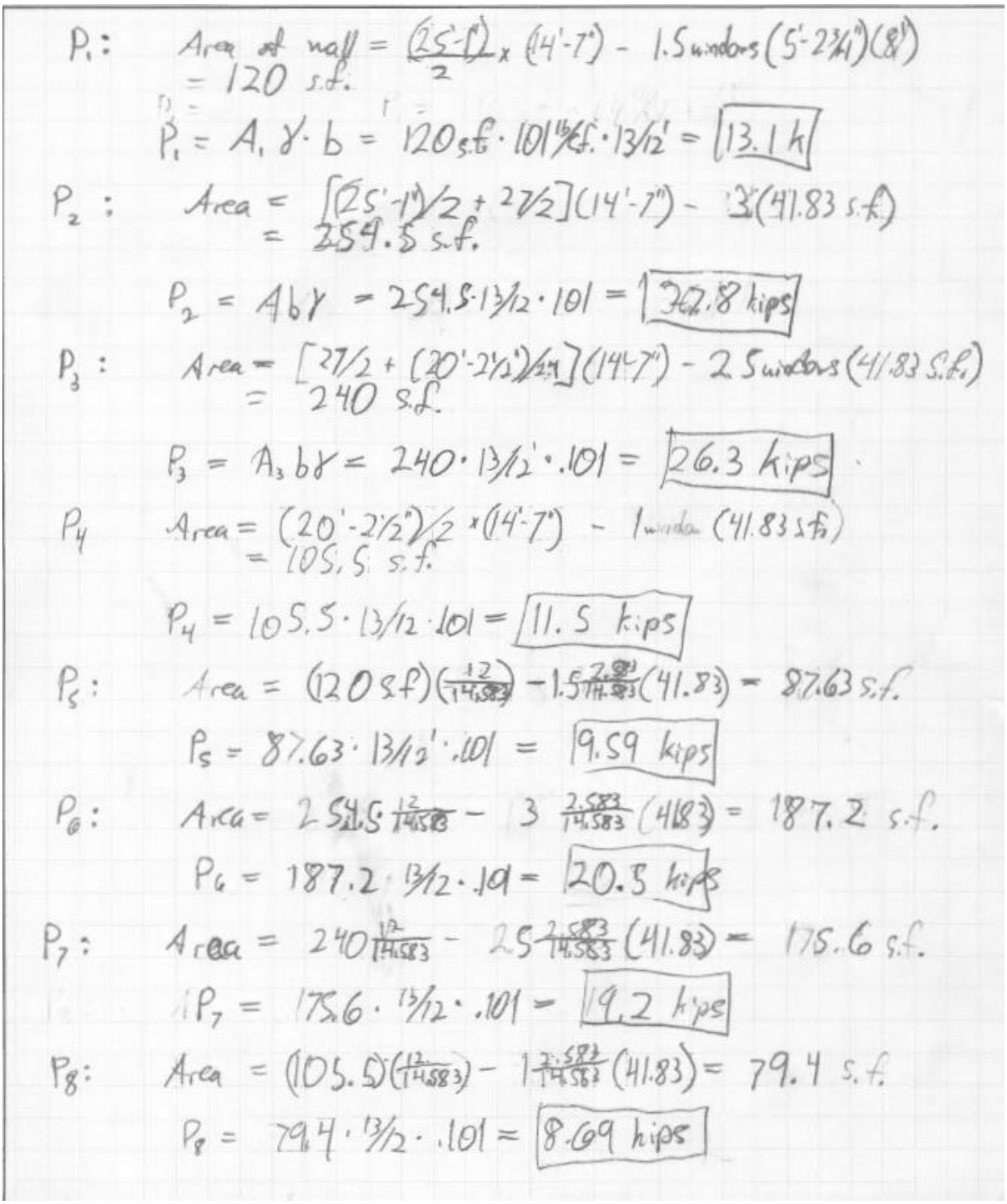

Figure D.3: Load calculations for brick façade

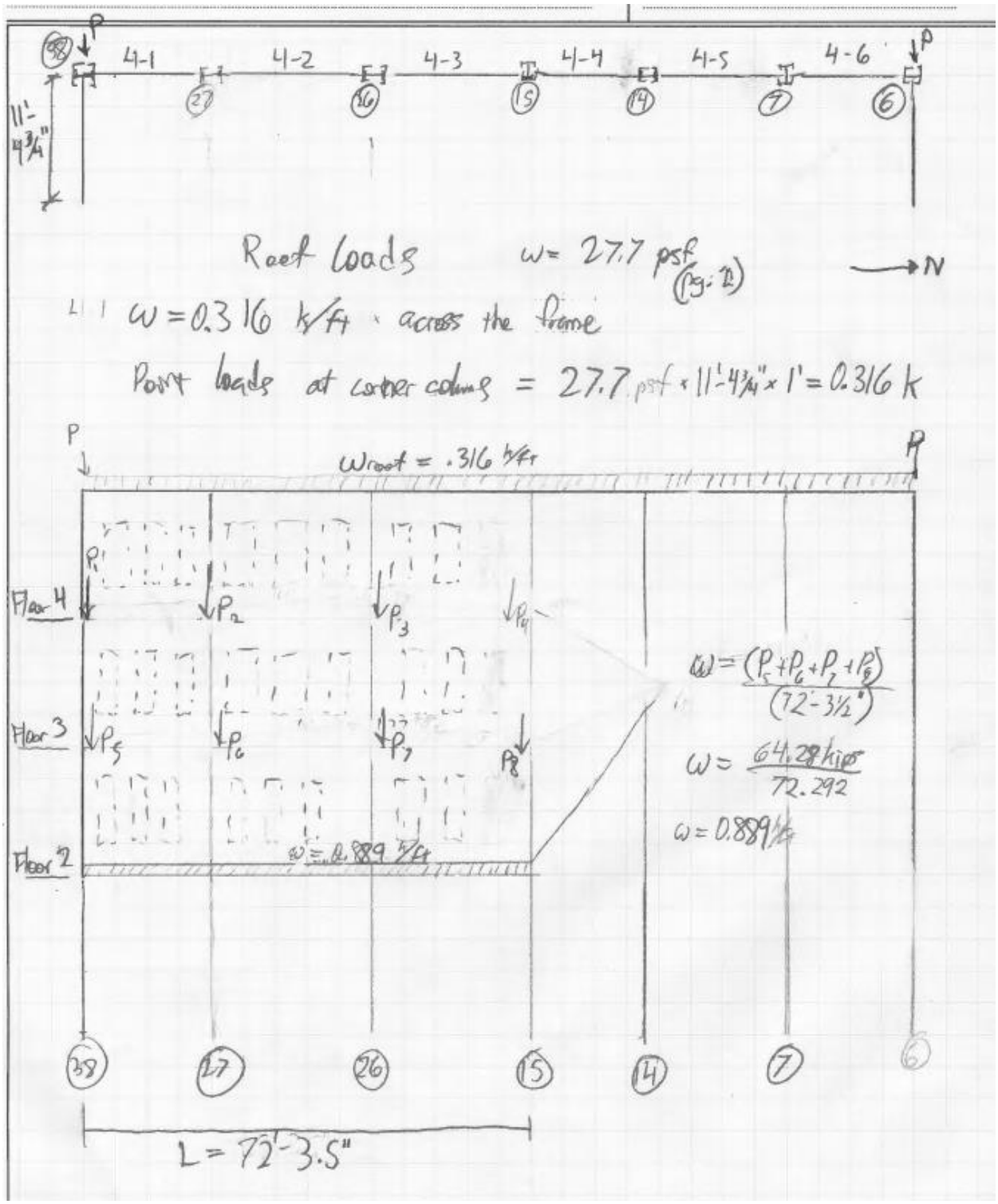

Figure D.4: Load calculations for windows

Table D.1: Point loads from East-West beams (Akah 2013)

	Column	East-West Beam (Y/N)	East-West $Weight_{beam}$ (plf)	East-West $Length_{beam}$ (ft)	East-West P_{beam} (lb)
Fourth Floor	6	Y	140	22.79	1595.42
	7	N	N/A	N/A	N/A
	14	Y	74	22.79	843.29
	15	N	N/A	N/A	N/A
	26	Y	121	22.79	1378.90
	27	Y	121	22.79	1378.90
	38	Y	73	22.79	831.90
Third Floor	6	N	N/A	N/A	N/A
	7	N	N/A	N/A	N/A
	14	Y	93	22.79	1059.81
	15	N	N/A	N/A	N/A
	26	Y	121	22.79	1378.90
	27	Y	121	22.79	1378.90
	38	Y	73	22.79	831.90
Second Floor	6	Y	42	22.79	478.63
	7	N	N/A	N/A	N/A
	14	Y	65	22.79	740.73

	15	N	N/A	N/A	N/A
	26	N	N/A	N/A	N/A
	27	N	N/A	N/A	N/A
	38	N	N/A	N/A	N/A

NOTE: Third floor East-West beam on column 14 is offset by 1 ft- 3.75in. to the South

Table D.2: Floor slab information (Akah 2013)

Slab	Between Columns (#, #)	$Width_{slab}$ (ft)	$Length_{slab}$ (ft)	Direction	Joists (Y/N)	t_{slab} (in.)	#-way
4R	**14, 15**	10.96	12.00	E-W	Y	2.5	1
4M	26, 27	22.79	27.00	N-S	Y	2.5	1
4A	27, 38	22.79	25.08	N-S	Y	2.5	1
3W	**14, 15**	10.96	12.00	E-W	N	6.0	2
3C	15, 26	20.21	22.79	E-W	Y	2.5	1
3B	26, 27	22.79	27.00	N-S	Y	2.5	1
3A	27, 38	22.79	25.08	N-S	Y	2.5	1
2AK	**6, 14**	6.33	29.32	N-S	N	5.0	1
2AJ	**7, 14**	2.86	22.92	E-W	N	5.0	1
2Y	14, 15	10.92	17.92	N-S	Y	2.5	1
2S-2R	**15, 26**	5.08	22.79	E-W	N	7.0	1
2M	**15, 27**	9.58	19.63	N-S	N	7.0	1
2H	**26, 27**	9.58	18.00	N-S	N	7.0	2
2D	**27, 38**	9.58	19.63	N-S	N	7.0	1
2A-2B	**27, 38**	9.96	22.79	E-W	N	7.0	1

NOTE: A bolded column location indicates that a beam existed on the frame to support distributed loads

Table D.3: Floor slab peak distributed loads and point load values (Akah 2013)

Slab	Between Columns (#, #)	$Width_{slab}$ (ft)	$Length_{slab}$ (ft)	t_{slab} (in.)	#-way	γ (pcf)	w_{peak} (plf)	P_{slab} (lb)	$P_{triangle}$ (lb)
4R	**14, 15**	10.96	12.00	2.5	1	150	187	N/A	N/A
4M	26, 27	22.79	27.00	2.5	1	150	356	4807	N/A
4A	27, 38	22.79	25.08	2.5	1	150	356	4466	N/A
3W	**14, 15**	10.96	12.00	6.0	2	150	410	2465	2251
3C	15, 26	20.21	22.79	2.5	1	150	315	3598	N/A
3B	26, 27	22.79	27.00	2.5	1	150	356	4807	N/A
3A	27, 38	22.79	25.08	2.5	1	150	356	4466	N/A
2AK	**6, 14**	6.33	29.32	5.0	1	150	197	N/A	N/A
2AJ	**7, 14**	2.86	22.92	5.0	1	150	89.5	1025	N/A
2Y	14, 15	10.92	17.92	2.5	1	150	170	1528	N/A
2S-2R	**15, 26**	5.08	22.79	7.0	1	150	222	2534	N/A
2M	**15, 27**	9.58	19.63	7.0	1	150	419	N/A	N/A
2H	**26, 27**	9.58	18.00	7.0	2	150	419	N/A	2009
2D	**27, 38**	9.58	19.63	7.0	1	150	419	N/A	N/A
2A-2B	**27, 38**	9.96	22.79	7.0	1	150	435	4964	N/A

Table D.4: Joist point loads (Akah 2013)

Slab	Between Columns (#, #)	$Length_{slab}$ (ft)	t_{slab} (in.)	Joist Depth (in.)	Joist area (ft^2)	N (joists)	γ (pcf)	w_{joists} (plf)	P_{joists} (lb)
4R	**14, 15**	12.00	2.5	6.00	0.313	5	150	117	N/A
4M	26, 27	27.00	2.5	12.00	0.625	10	150	N/A	12656
4A	27, 38	25.08	2.5	12.00	0.625	10	150	N/A	11757
3C	15, 26	22.79	2.5	12.00	0.625	10	150	N/A	10683
3B	26, 27	27.00	2.5	12.00	0.625	10	150	N/A	12656
3A	27, 38	25.08	2.5	12.00	0.625	10	150	N/A	11757
2Y	14, 15	17.92	2.5	10.00	0.521	5	150	N/A	3499

Table D.5: Floor slab layouts and load distributions (Akah 2013)

Slab	Distribution	Between Columns (#, #)	Beam Length (in.)	Start Point (in.)	Distr. Peak Start (in.)	Distr. Peak End (in.)	End Point (in.)
4R	Uniform	**14, 15**	215	0	0	131.5	131.5
4M	Points	26, 27	324	0	N/A	N/A	324
4A	Points	27, 38	301	0	N/A	N/A	301
3W	Triangle	**14, 15**	215	15.75	81.5	81.5	147.25
3C	Points	15, 26	242.5	0	N/A	N/A	242.5
3B	Points	26, 27	324	0	N/A	N/A	324
3A	Points	27, 38	301	0	N/A	N/A	301
2AK	Uniform	**6, 7**	275	103.75	103.75	275	275
2AK	Uniform	**7, 14**	215	0	0	180.625	180.625
2AJ	Points	**7, 14**	215	180.625	N/A	N/A	215
2Y	Points	14, 15	215	0	N/A	N/A	215
2S-2R	Points	**15, 26**	242.5	0	N/A	N/A	61
2M	Uniform	**15, 26**	242.5	61	61	242.5	242.5
2M	Uniform	**26, 27**	324	0	0	54	54
2H	Trapezoid	**26, 27**	324	54	111.5	212.5	270

2D	Uniform	**26, 27**	324	270	270	324	324
2D	Uniform	**27, 38**	301	0	0	181.5	181.5
2A- 2B	Points	**27, 38**	301	181.5	N/A	N/A	301

NOTE: Measurements are in reference to the North end of the beam.

Table D.6: Total floor slab distributed loads on perimeter frame beams (Akah 2013)

Floor	Between Columns (#, #)	Beam Length (in.)	Distr. Load Start (k/in.)	Distr. Peak (k/in.)	Distr. Load End (k/in.)	Source
Fourth	14, 15	215	0.0254		0.0254	Slab 4R
Third	14, 15	215	0	0.0342	0	Slab 3W
Second	6, 7	275	0.0165		0.0165	Slab 2AK
	7, 14	215	0.0165		0.0165	Slab 2AK
	15, 26	242.5	0.0349		0.0349	Slab 2M
	26, 27	324	0.0349		0.0349	Slab 2M
	26, 27	324	0	0.0349	0	Slab 2H
	26, 27	324	0.0349		0.0349	Slab 2D
	27, 38	301	0.0349		0.0349	Slab 2D

NOTE: Refer to Table C.2.5 to determine location of distributive loads on beams. A superimposed dead load of 0.0142 k/in. existed on each beam. A wall distributed load of 0.0741 k/in. existed on second floor beams located between columns 15 through 38.

Table D.7: Total point loads on perimeter frame beams (Akah 2013)

Floor	Between Columns (#, #)	Beam Length (in.)	Location (in.)	Point Load (kips)	Point Source
Third	14, 15	215	15.75	3.53	E-W Beam
Second	7, 14	215	180.625	1.03	Slab 2AJ
	15, 26	243	61	2.53	Slab 2S-2R
	26, 27	324	54	2.01	Slab 2H
	26, 27	324	270	2.01	Slab 2H
	27, 38	301	181.5	4.96	Slab 2A-2B

NOTE: Measurements are in reference to the North end of the beam

Table D.8: Total point loads on perimeter frame columns (Akah 2013)

Floor	Column	E-W P_{beam} (lb)	P_{slab} (lb)	P_{joist} (lb)	P_{wall} (lb)	$P_{superimposed}$ (lb)	P_{total} (lb)	P_{total} (kips)
Fourth	6	1595	N/A	N/A	N/A	N/A	1595	1.60
	7	N/A	N/A	N/A	N/A	N/A	0	0
	14	843	N/A	N/A	N/A	N/A	843	0.84
	15	N/A	N/A	N/A	11500	N/A	11500	11.50
	26	1379	4808	6328	26300	2308	41122	41.12
	27	1379	9274	12207	27800	4451	55111	55.11
	38	832	4466	5879	13100	2144	26421	26.42
Third	6	N/A	N/A	N/A	N/A	N/A	0	0
	7	N/A	N/A	N/A	N/A	N/A	0	0
	14	1060	N/A	N/A	N/A	N/A	1060	1.06
	15	N/A	3598	5342	8690	1727	19357	19.36
	26	1379	8406	11670	19200	4035	44690	44.69
	27	1379	9274	12207	20500	4451	47811	47.81
	38	832	4466	5879	9590	2144	22911	22.91
Second	6	479	N/A	N/A	N/A	N/A	479	0.48
	7	N/A	N/A	N/A	N/A	N/A	0	0
	14(N)	741	1026	N/A	N/A	N/A	1766	1.77

	14(S)	N/A	1528	1750	N/A	1531	4809	4.81
	15	N/A	4062	1750	N/A	1531	7343	7.34
	26	N/A	N/A	N/A	N/A	N/A	0	0
	27	N/A	N/A	N/A	N/A	N/A	0	0
	38	N/A	4965	N/A	N/A	N/A	4965	4.96

NOTE: On the second floor there existed two elevations for slabs running into column 14

APPENDIX E: COMPUTER MODEL INPUT INFORMATION

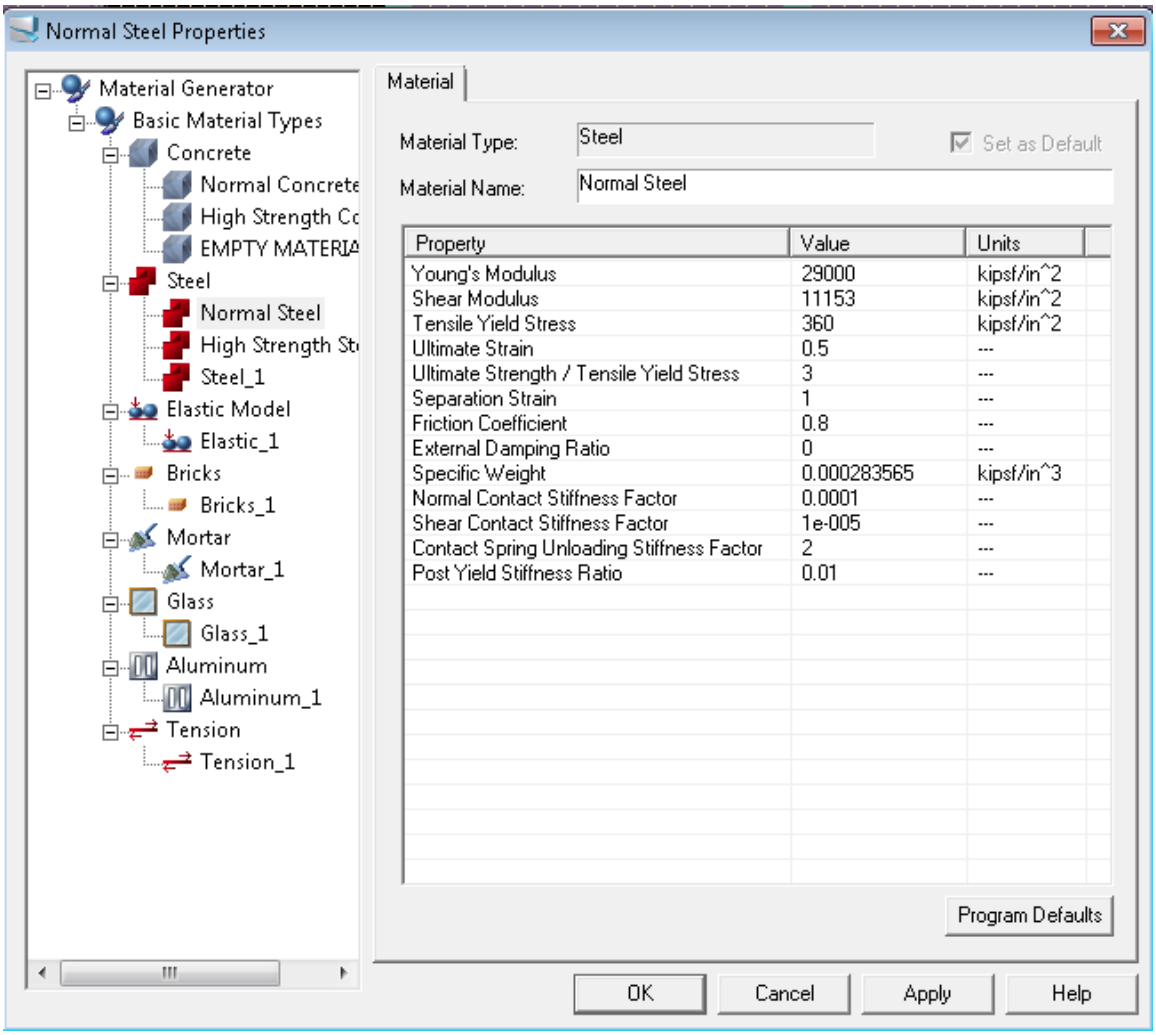

Figure E.1: Steel material properties in ELS

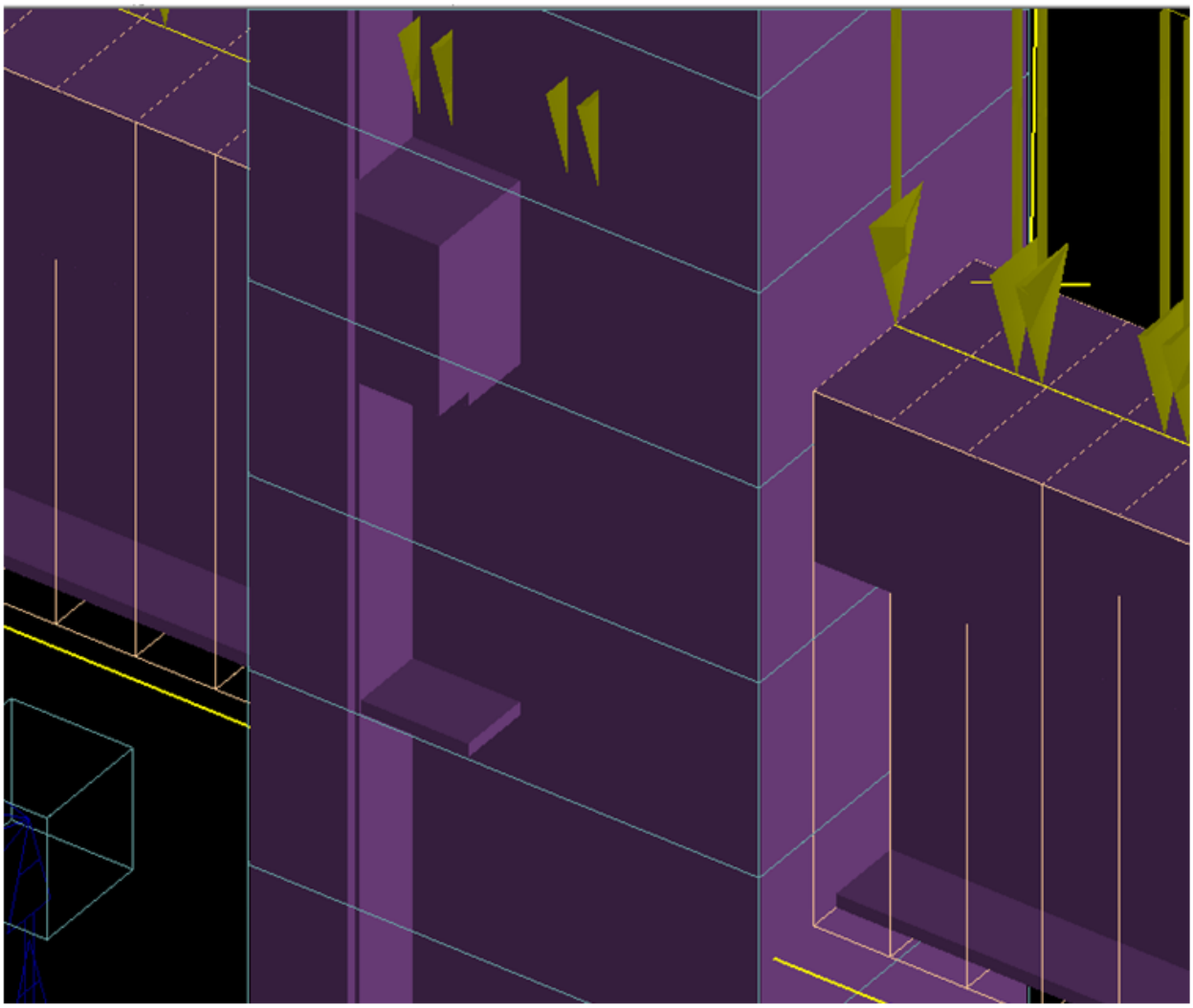

Steel Section	
Visible	☑
Display Mode	Solic
Color	
Steel Section Start Extension	5.90 in
Steel Section End Extension	5.90 in

Figure E.2: Rigid connection type in ELS. Beams extend into the column supporting them

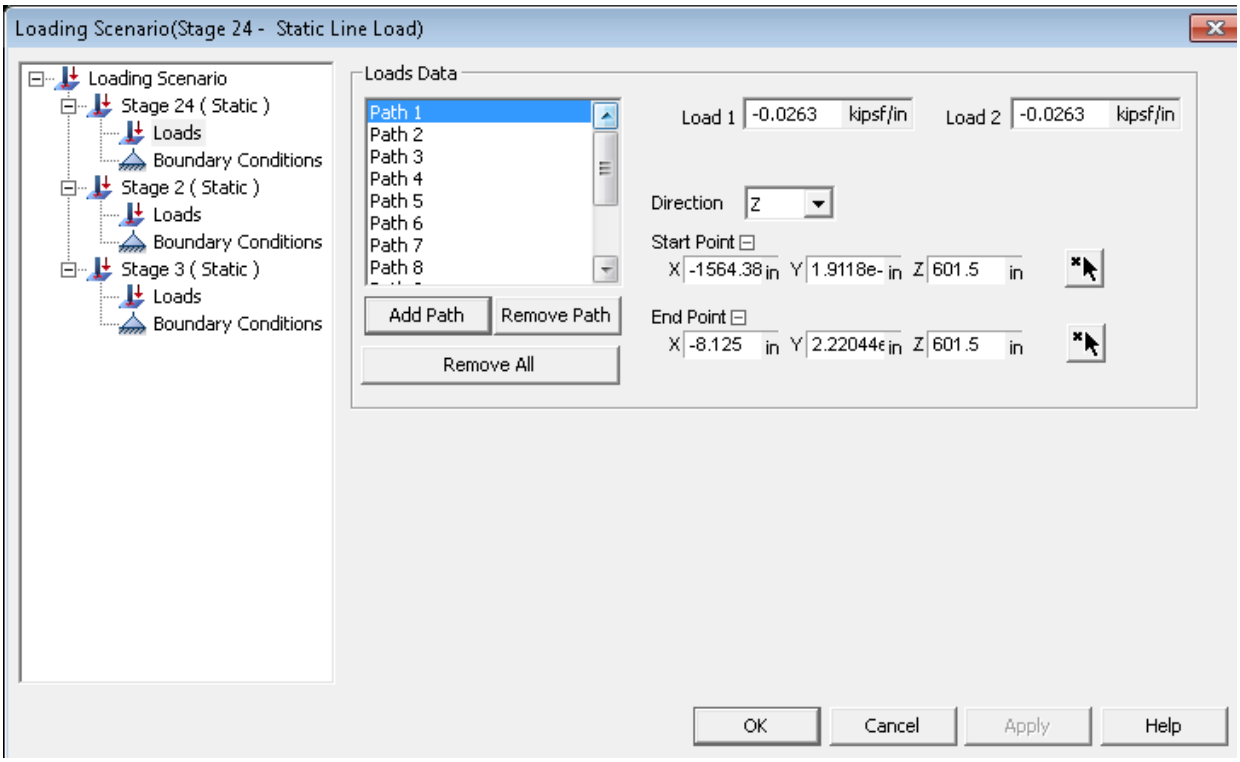

Figure E.3: Sample of line loads input to ELS

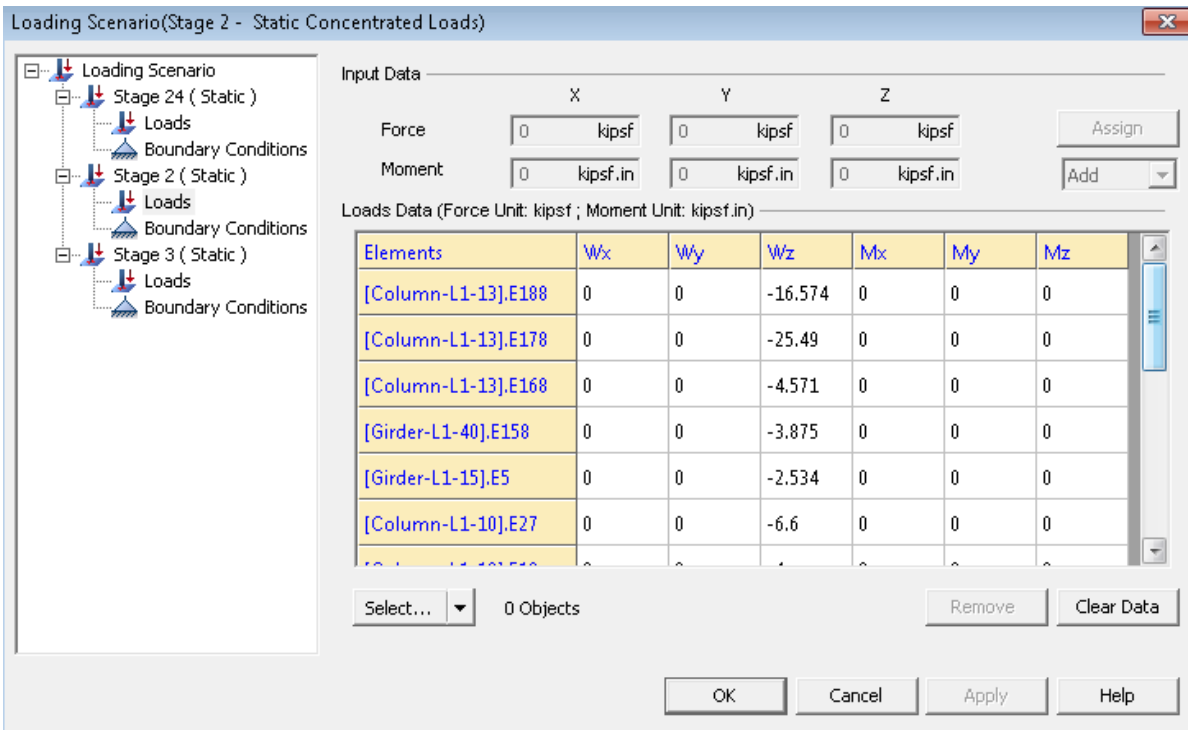

Figure E.4: Sample of point loads input to ELS

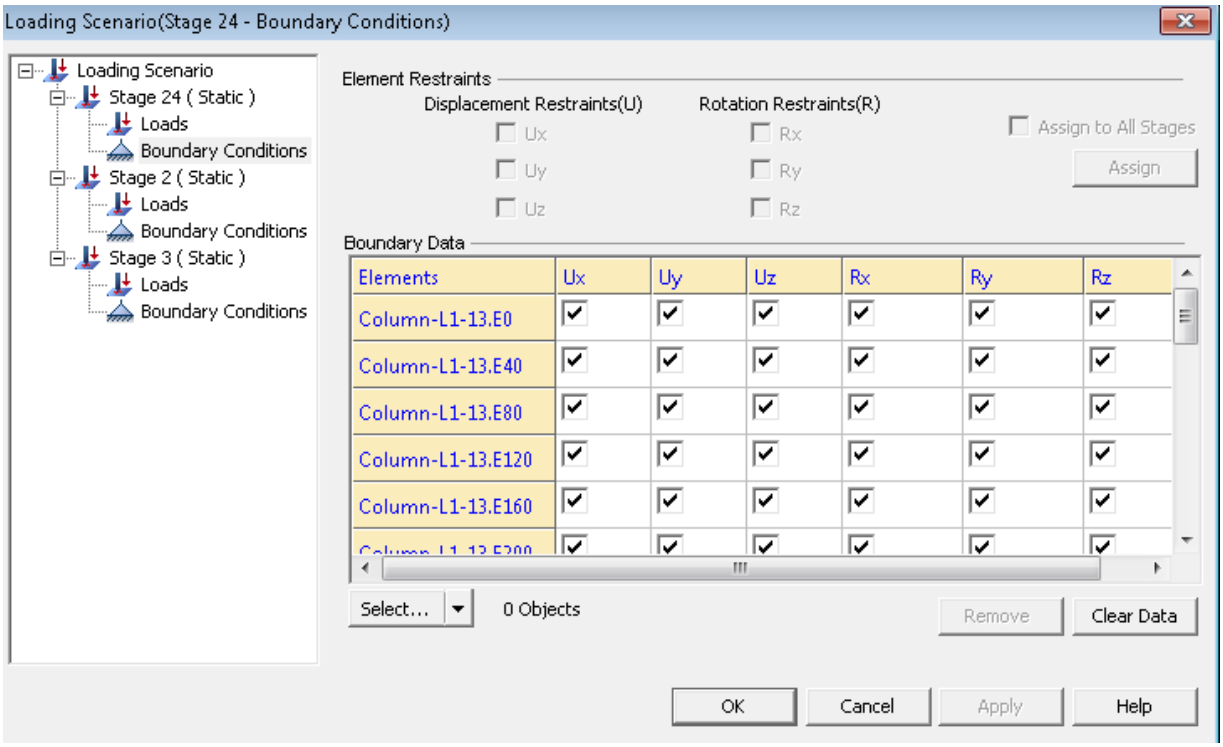

Figure E.5 Sample of boundary conditions (fixed column bases) in ELS

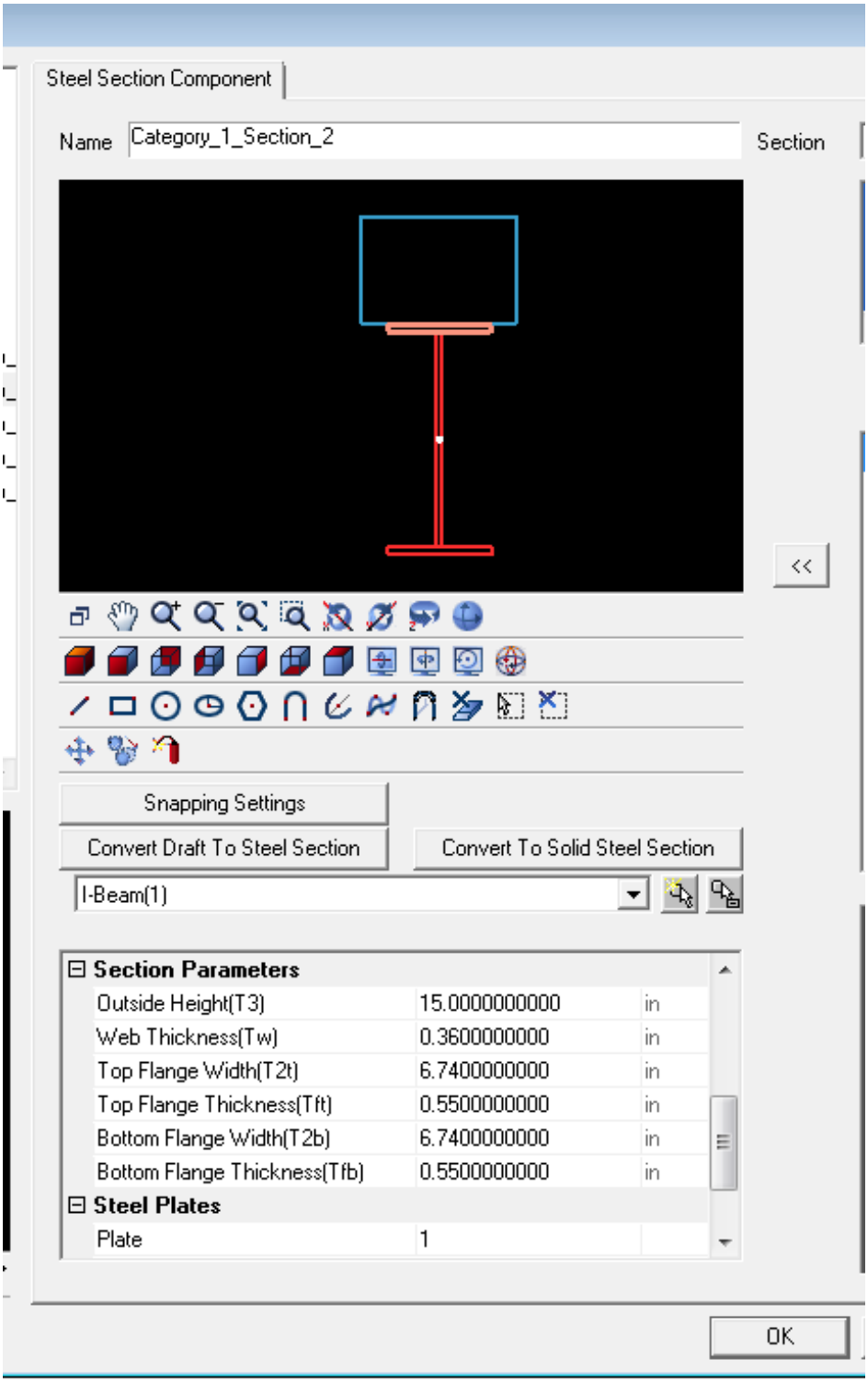

Figure E.6: Section properties of typical composite beam in ELS

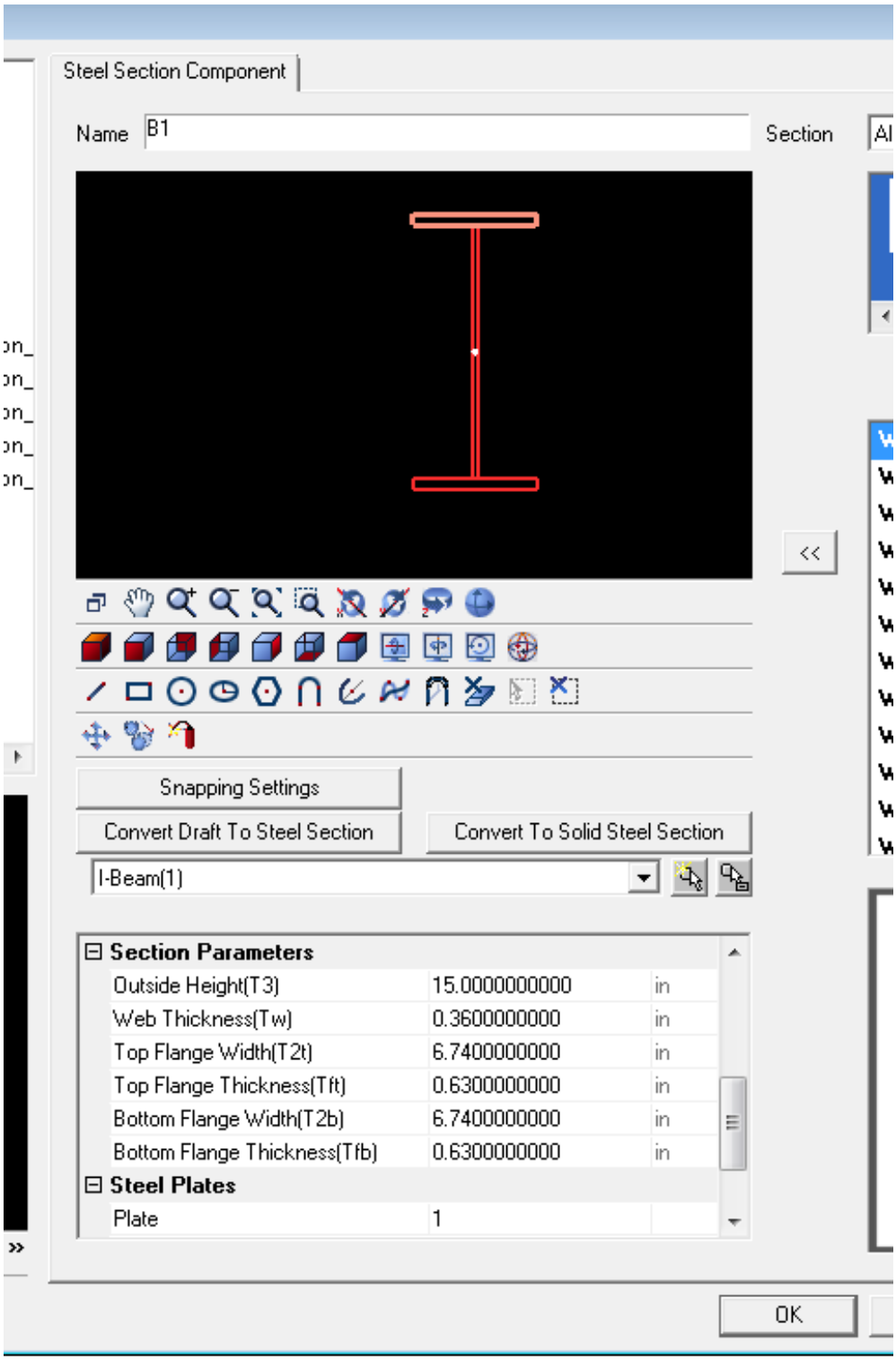

Figure E.7: Section properties of 15 in. deep beam in ELS

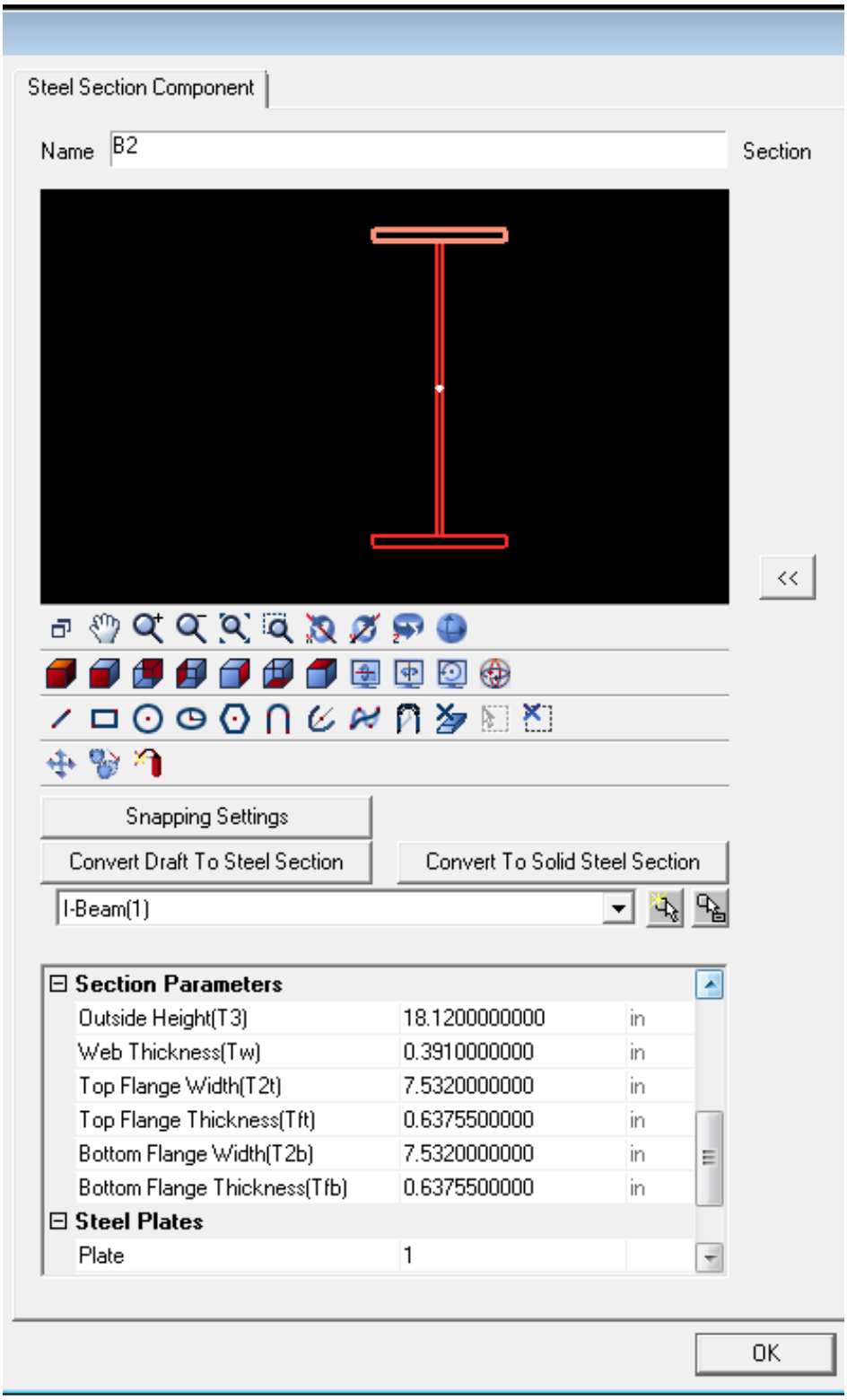

Figure E.8: Section properties of 18.12 in. deep beam in ELS

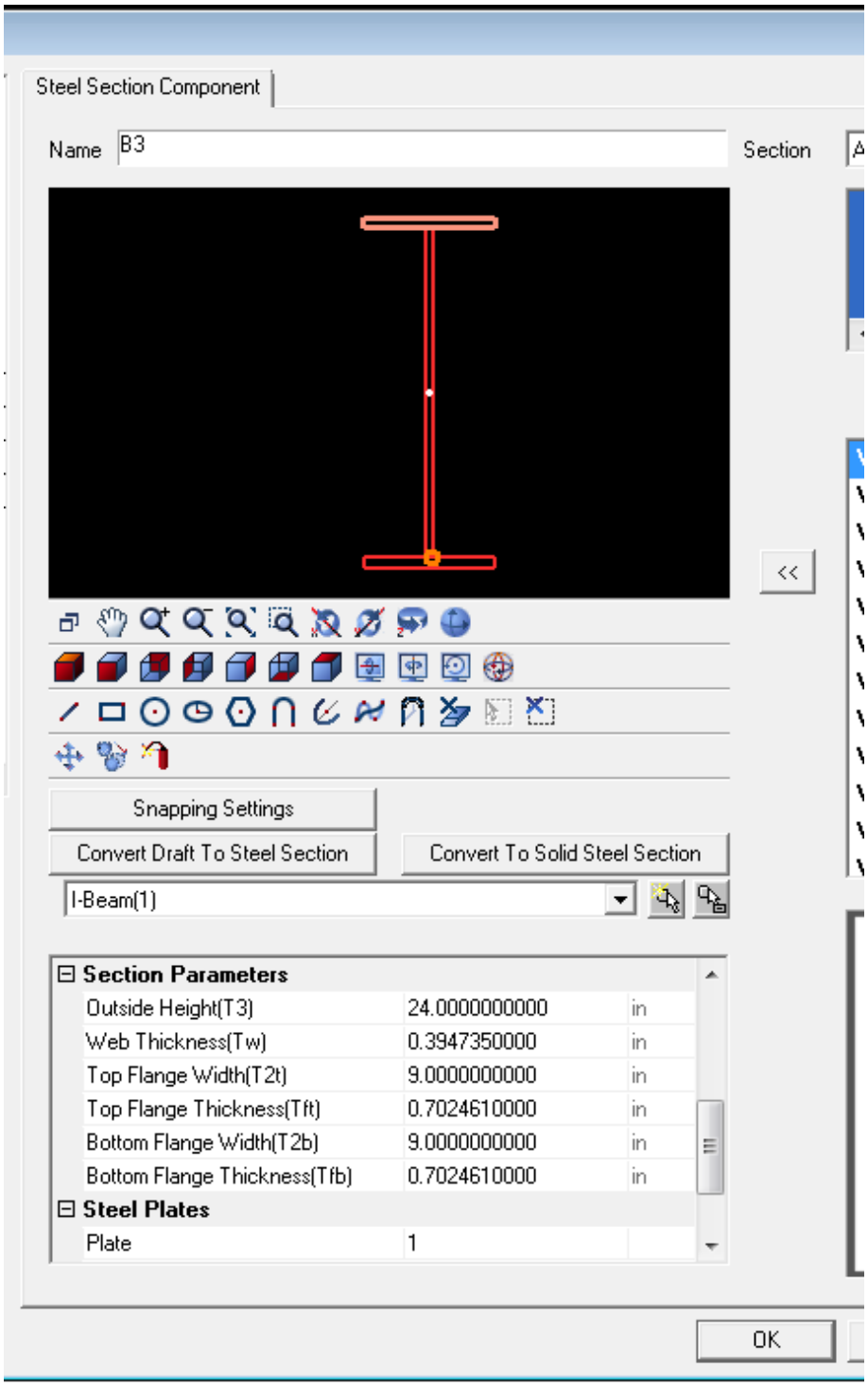

Figure E.9: Section properties of 24 in. deep beam in ELS

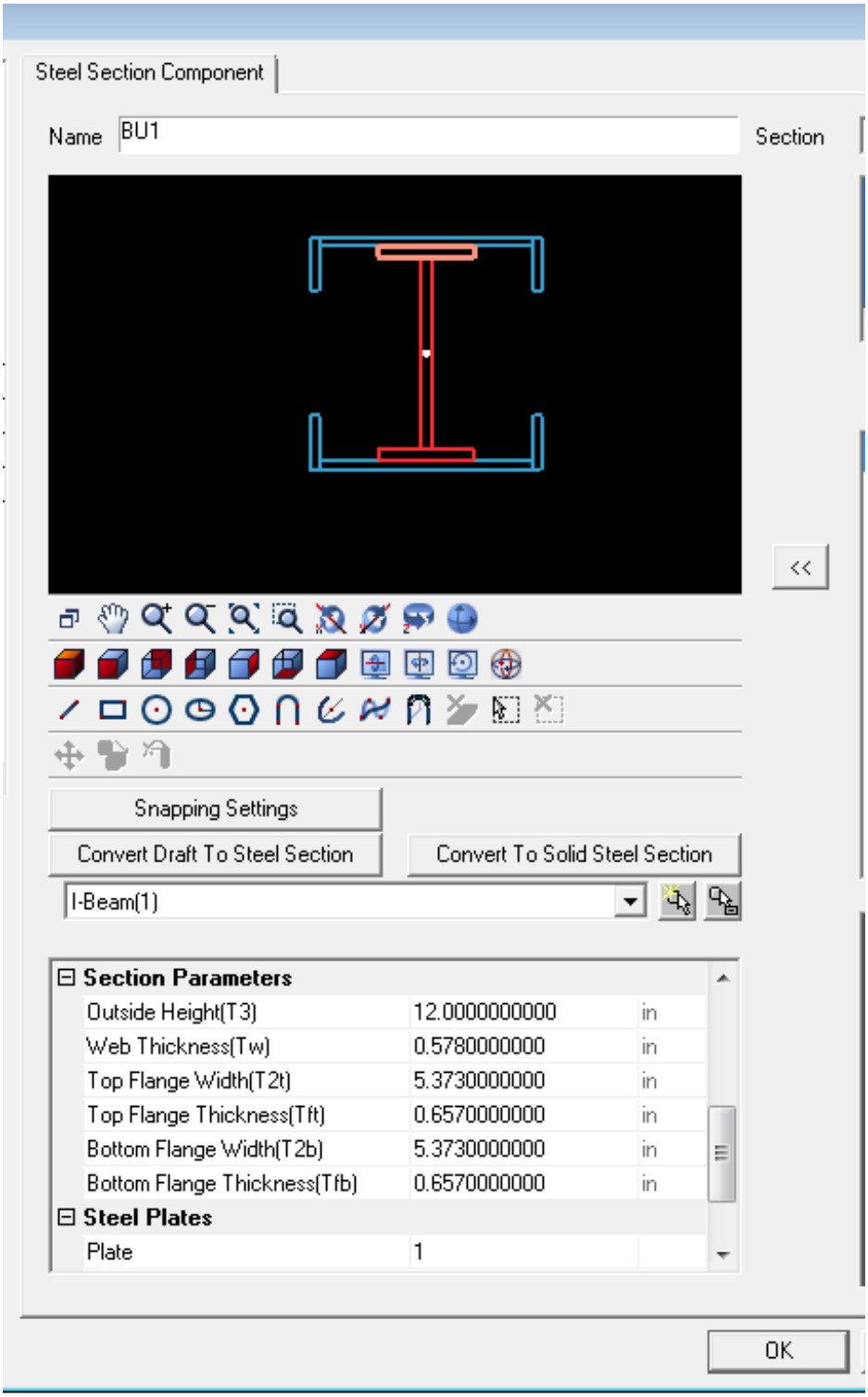

Figure E.10: Section properties of 12 in. deep built-up column in ELS

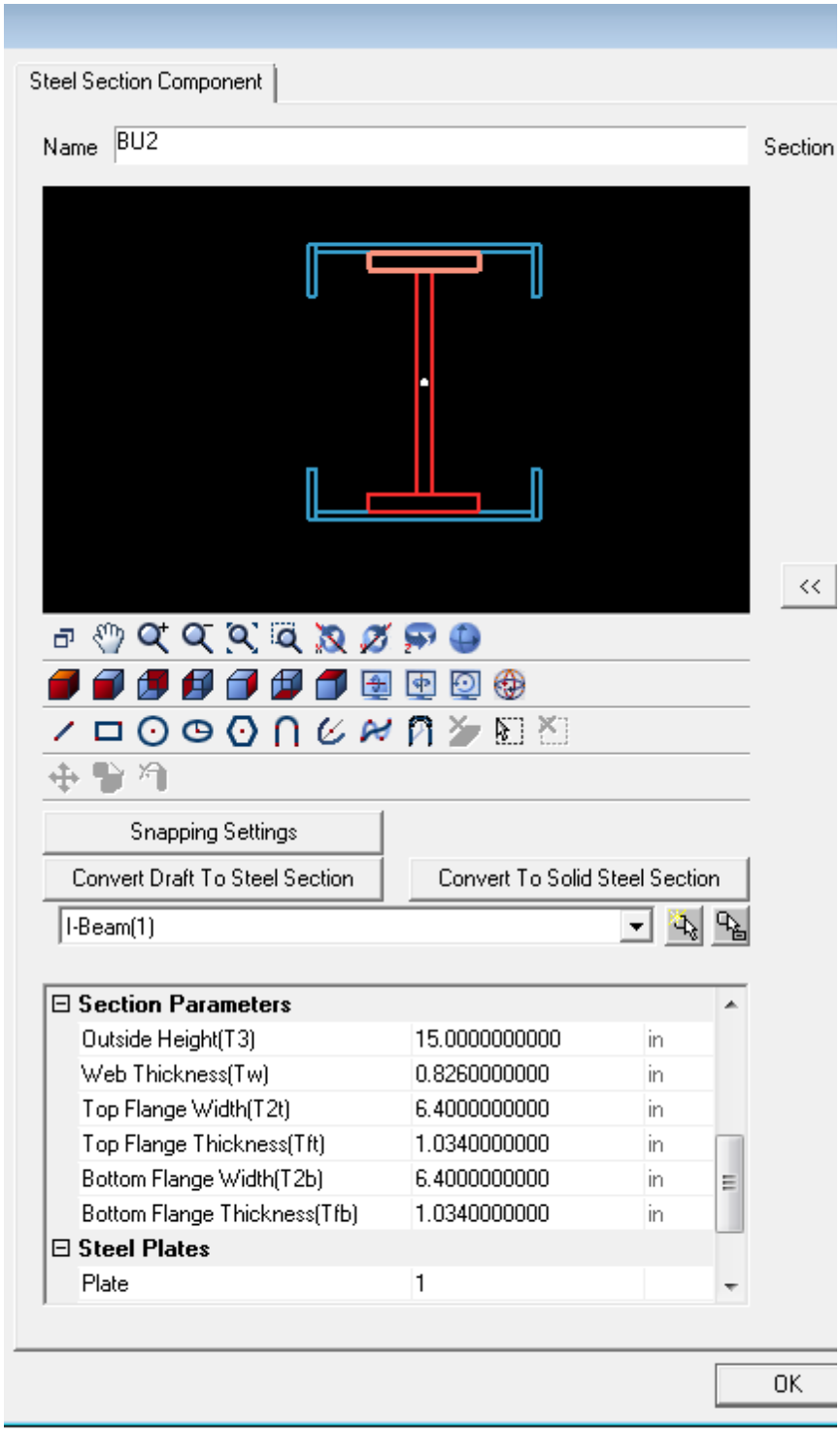

Figure E.11: Section properties of 15 in. deep built-up column in ELS

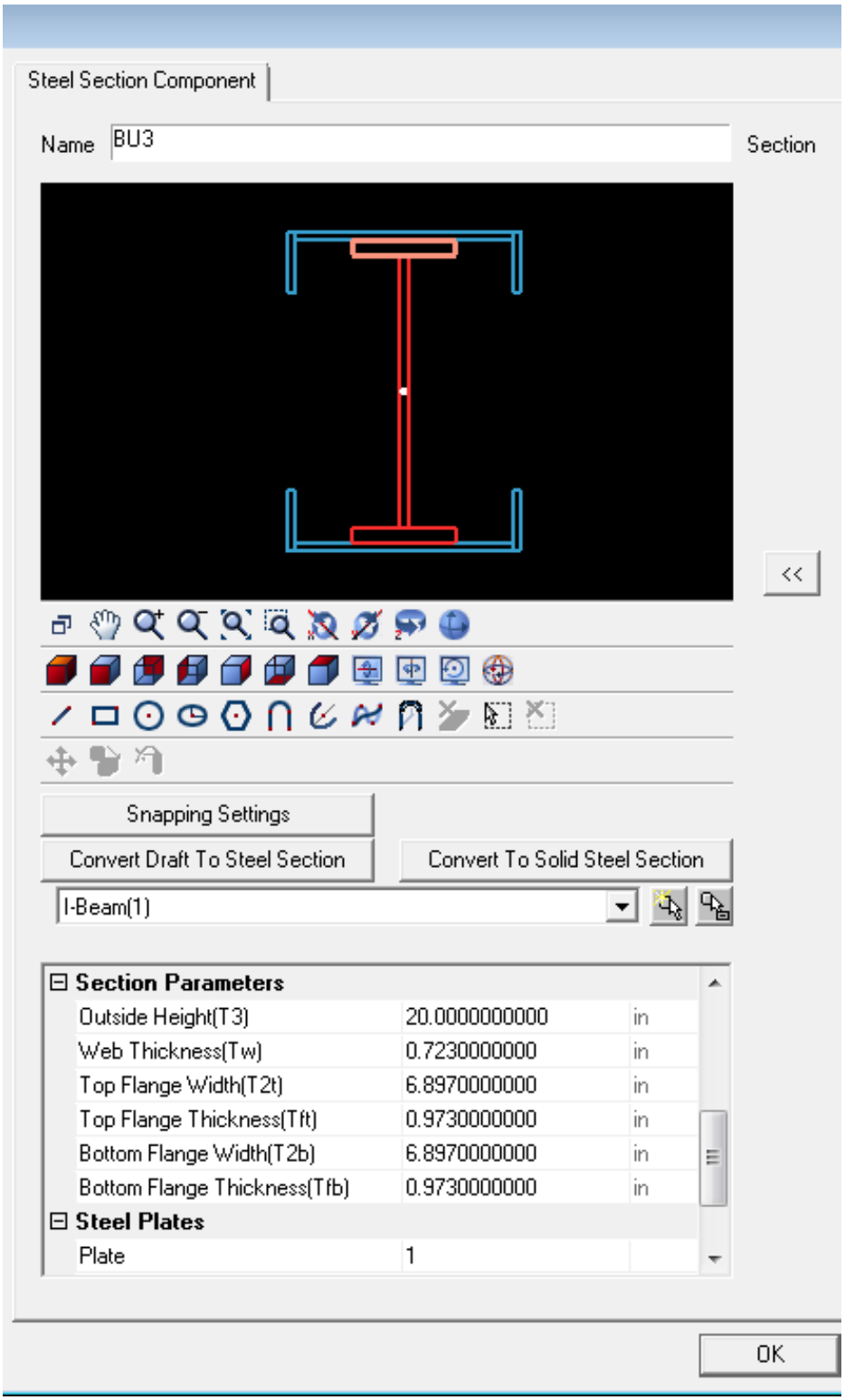

Figure E.12: Section properties of 20 in. deep built-up column in ELS

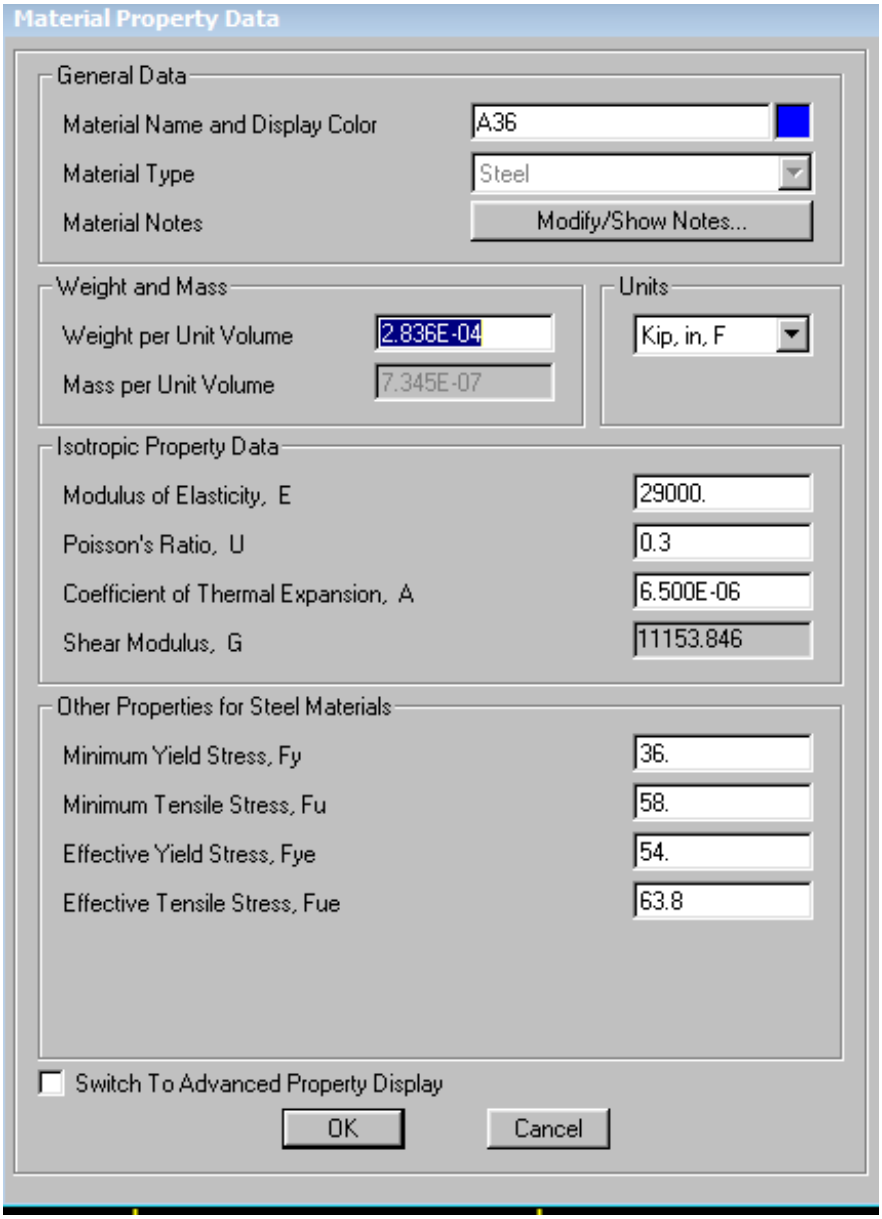

Figure E.13: Steel material properties input to SAP2000

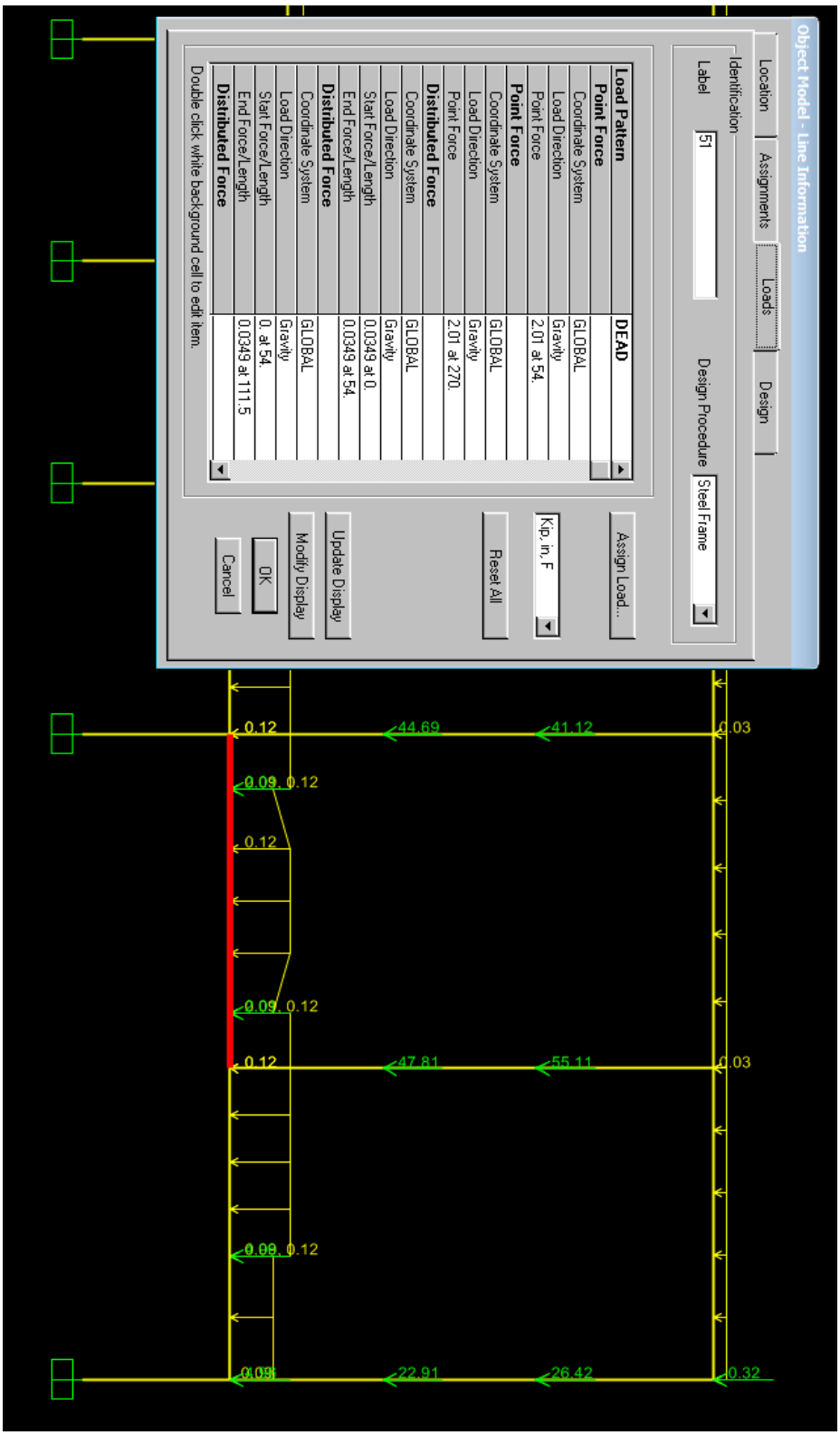

Figure E.14: Sample of loads in SAP2000

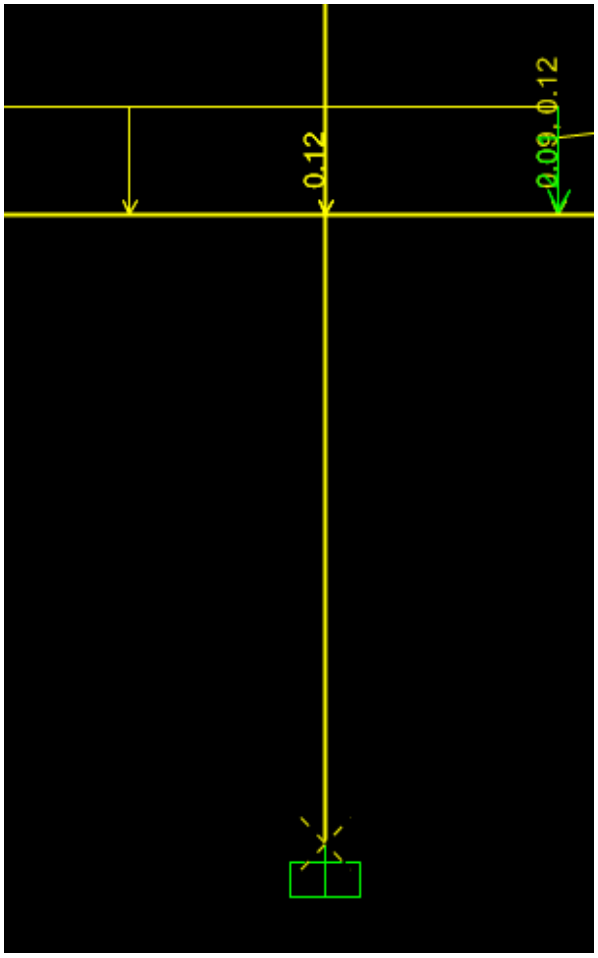

Figure E.15: Fixed Column Base in SAP2000, typical of all columns

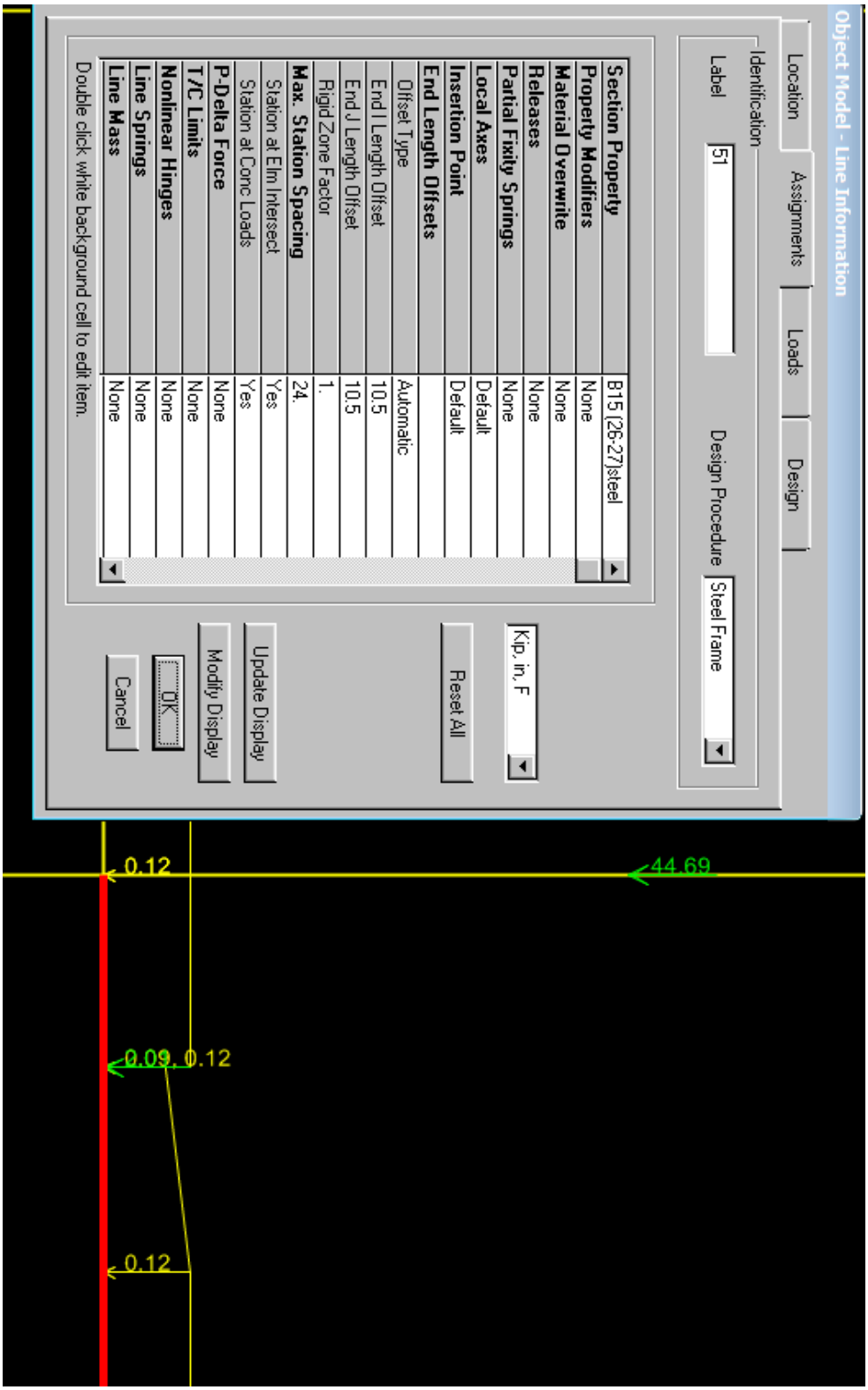

Figure E.16: Rigid end zones in SAP2000

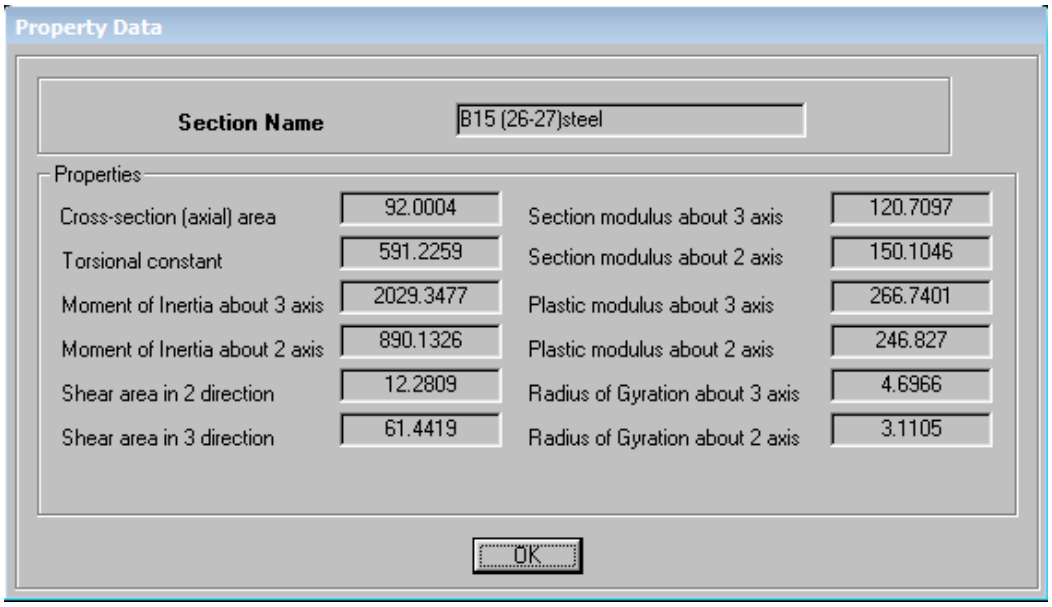

Figure E.17: Section properties of one 15 in. deep composite beam calculated in SAP2000

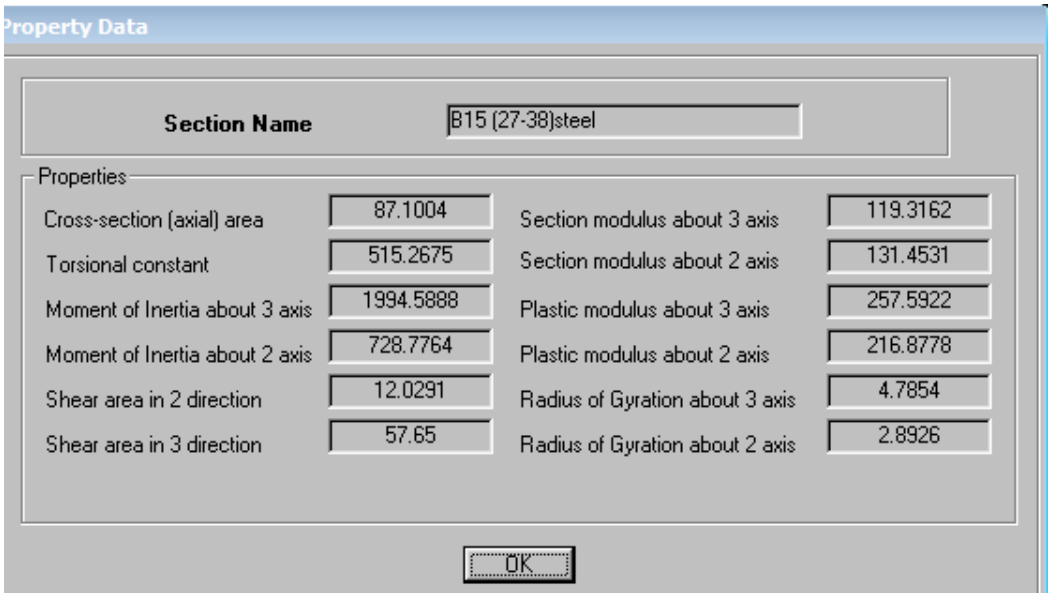

Figure E.18: Section properties of one 15 in. deep composite beam calculated in SAP2000

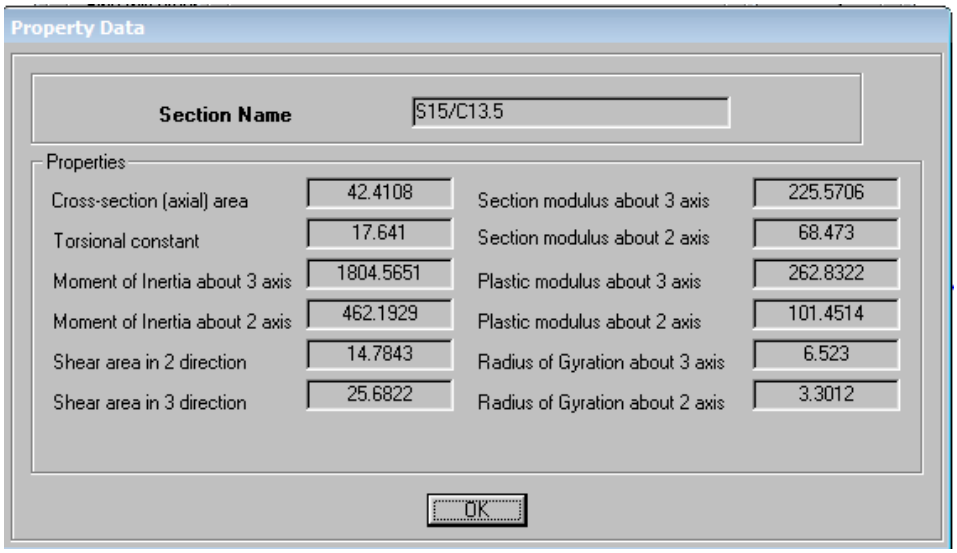

Figure E.19: Section properties of 15 in. deep column calculated in SAP2000

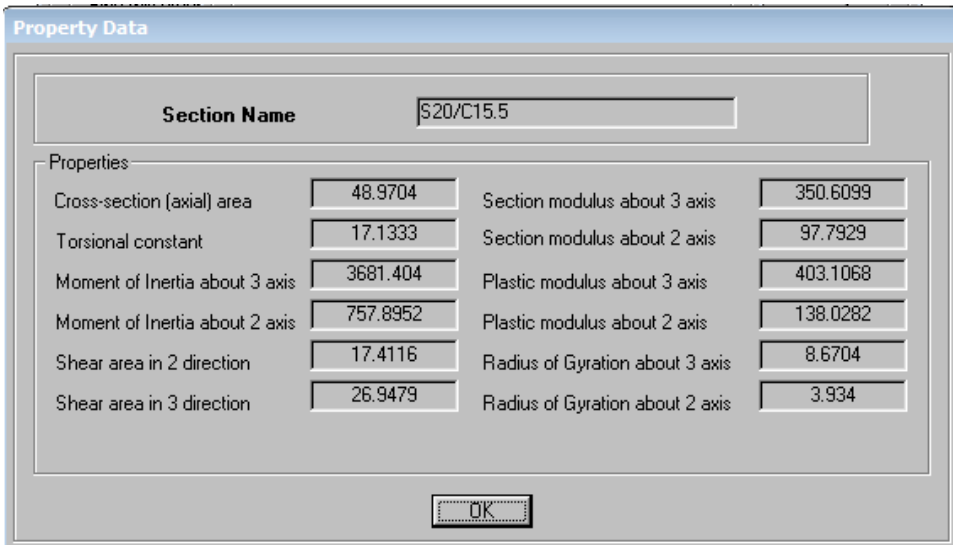

Figure E.20: Section properties of 20 in. deep column calculated in SAP2000

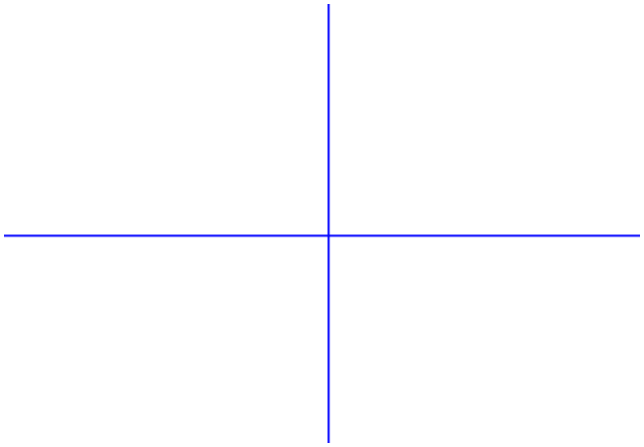

Figure E.21: SAP2000 Element connection

APPENDIX F: SOFTWARE STRESS AND STRAIN RESULTS FOR CAPACITY MODELS

The stress at locations of strain gauges was measured in Models 1 and 2, and recorded as σ_1 and σ_2, respectively.

Table F.1: SAP2000 Column Stress Results

Gauge	Column, location	Height above base	σ_1 (psi)	σ_2 (psi)	Change in stress, $\Delta\sigma$ (psi)
1	North, (S) flange	3 ft – 1 in.	-2.79	-3.65	-0.86
2	North, (N) flange	3 ft – 1 in.	-3.27	-6.05	-2.78
4	South, (S) flange	6 ft – 2 in.	-1.11	5.75	8.66
5	South, (E) web	6 ft – 2 in.	-2.01	-4.11	-2.10
6	South, (N) flange	6 ft – 2 in.	-2.91	-13.98	-12.87
7	South, (N) flange	4 ft – 7 in.	-2.42	-8.53	-6.11

Table F.2: Strains calculated in columns in SAP2000 model

Gauge	Column, location	Height above base	$\Delta\varepsilon = \Delta\sigma / E$	Measured strain	Percent difference (%)
1	North, (S) flange	3 ft – 1 in.	-29.66	-32.00	-92.67
2	North, (N) flange	3 ft – 1 in.	-95.86	-54.00	-177.52

4	South, (S) flange	6 ft – 2 in.	236.55	-7.00	3379.31
5	South, (E) web	6 ft – 2 in.	-72.41	-61.00	-118.71
6	South, (N) flange	6 ft – 2 in.	-381.72	-103.00	-370.61
7	South, (N) flange	4 ft – 7 in.	-210.69	-93.00	-226.55

Table F.3: ELS Column Stress Results

Gauge	Column, location	Height above base	σ_1 (psi)	σ_2 (psi)	Change in stress, $\Delta\sigma$ (psi)
1	North, (S) flange	3 ft – 1 in.	-2.83	-3.41	-0.58
2	North, (N) flange	3 ft – 1 in.	-3.13	-7.92	-4.80
4	South, (S) flange	6 ft – 2 in.	-0.85	3.35	4.20
5	South, (E) web	6 ft – 2 in.	-1.98	-4.00	-2.02
6	South, (N) flange	6 ft – 2 in.	-3.15	-13.98	-10.83
7	South, (N) flange	6 ft – 2 in.	-2.45	-8.75	-6.30

Table F.4: Strains calculated in columns in ELS model

Gauge	Column, Location	Height above base	$\Delta\varepsilon = \Delta\sigma / E$	Measured Strain	Percent Difference (%)

1	North, (S) flange	3 ft – 1 in.	-19.88	-32.00	-37.88
2	North, (N) flange	3 ft – 1 in.	-165.34	-54.00	206.19
4	South, (S) flange	6 ft – 2 in.	144.87	-7.00	-2169.61
5	South, (E) web	6 ft – 2 in.	-69.66	-61.00	14.19
6	South, (N) flange	6 ft – 2 in.	-373.45	-103.00	262.57
7	South, (N) flange	6 ft – 2 in.	-217.24	-93.00	133.59

Table F.5: SAP2000 Beam Stress Results

Gauge	Frame beam	Distance from removed column	σ_1 (psi)	σ_2 (psi)	Change in stress, $\Delta\sigma$ (psi)
11	(N) Beam	1 ft – 0.65 in.	-7.63	67.88	75.51
12	(N) Beam	1 ft – 0.65 in.	-7.63	67.88	75.51
13	(S) Beam	1 ft – 0.65 in.	-8.14	69.97	78.11
14	(S) Beam	1 ft – 0.65 in.	-8.14	69.97	78.11
15	(S) Beam	12 ft – 9 in.	5.73	6.72	0.99
16	(N) Beam	12 ft – 9 in.	4.69	6.49	1.80

Table F.6: Calculated strains in beams in SAP2000

Gauge	Frame beam	Distance from removed column	$\Delta\varepsilon = \Delta\sigma / E$	Experimental value	Percent difference (%)
11	(N) Beam	1 ft – 0.65 in.	2603.79	136.00	1814.55
12	(N) Beam	1 ft – 0.65 in.	2603.79	171.00	1422.69
13	(S) Beam	1 ft – 0.65 in.	2693.38	252.00	968.80
14	(S) Beam	1 ft – 0.65 in.	2693.38	272.00	890.21
15	(S) Beam	12 ft – 9 in.	34.14	81.00	-57.85
16	(N) Beam	12 ft – 9 in.	62.07	-10.00	-720.69

Table F.7: ELS Beam Stress Results

Gauge	Frame beam	Distance from removed column	σ_1 (psi)	σ_2 (psi)	Change in stress, $\Delta\sigma$ (psi)
11	(N) Beam	1 ft – 0.65 in.	-6.61	64.18	70.79

12	(N) Beam	1 ft – 0.65 in.	-6.61	64.18	70.79
13	(S) Beam	1 ft – 0.65 in.	-7.29	65.51	72.80
14	(S) Beam	1 ft – 0.65 in.	-7.29	65.51	72.80
15	(S) Beam	12 ft – 9 in.	5.75	4.91	-0.84
16	(N) Beam	12 ft – 9 in.	4.81	6.46	1.65

Table F.8: Calculated strains in beams in ELS

Gauge	Frame beam	Distance from removed column	$\Delta\varepsilon = \Delta\sigma / E$	Experimental value	Percent difference (%)
11	(N) Beam	1 ft – 0.65 in.	2440.86	136.00	1694.75
12	(N) Beam	1 ft – 0.65 in.	2440.86	171.00	1327.40
13	(S) Beam	1 ft – 0.65 in.	2510.47	252.00	896.22
14	(S) Beam	1 ft – 0.65 in.	2510.47	272.00	822.97
15	(S) Beam	12 ft – 9 in	-28.84	81.00	-135.61
16	(N) Beam	12 ft – 9 in	56.90	-10.00	-668.97

Table F.9: Model 3, calculated strain results in columns

Gauge	Column, location	Height above base	Theoretical change in strain, $\Delta\varepsilon_T$	Experimental change in strain, $\Delta\varepsilon_E$	Percent difference (%)	$\Delta\varepsilon_T - \Delta\varepsilon_E$
1	North, (S) flange	3 ft – 1 in.	1.42	-32	2350.85	33.42
2	North, (N) flange	3 ft – 1 in.	-26.46	-54	104.05	27.54
4	South, (S) flange	6 ft – 2 in.	6.25	-7	212.04	13.25
5	South, (E) web	6 ft – 2 in.	-13.90	-61	338.95	47.10
6	South, (N) flange	6 ft – 2 in.	-92.12	-103	11.81	10.88
7	South, (N) flange	4 ft – 7 in.	-37.28	-93	149.46	55.72

Table F.10: Model 3, calculated strain results in beams

Gauge	Frame beam	Distance from removed column	Theoretical change in strain, $\Delta\varepsilon_T$	Experimental change in strain, $\Delta\varepsilon_E$	Percent difference (%)	$\Delta\varepsilon_T - \Delta\varepsilon_E$
11	(N) Beam	1 ft – 0.65 in.	531.50	136	74.41	395.50

12	(N) Beam	1 ft – 0.65 in.	531.50	171	67.83	360.50
13	(S) Beam	1 ft – 0.65 in.	533.22	252	52.74	281.22
14	(S) Beam	1 ft – 0.65 in.	533.22	272	48.99	261.22
15	(S) Beam	12 ft – 9 in	-17.41	81	565.12	-98.41
16	(N) Beam	12 ft – 9 in	11.29	-10	188.54	21.29

Table F.11: Model 4, calculated strain results in columns

Gauge	Column, location	Height above base	Theoretical change in strain, $\Delta\varepsilon_T$	Experimental change in strain, $\Delta\varepsilon_E$	Percent difference (%)	$\Delta\varepsilon_T - \Delta\varepsilon_E$
1	North, (S) flange	3 ft – 1 in.	0.26	-32	12640.54	32.26
2	North, (N) flange	3 ft – 1 in.	-27.52	-54	96.19	26.48
4	South, (S) flange	6 ft – 2 in.	74.72	-7	109.37	81.72
5	South, (E) web	6 ft – 2 in.	-16.24	-61	275.58	44.76
6	South, (N) flange	6 ft – 2 in.	-107.24	-103	3.95	-4.24
7	South, (N) flange	4 ft – 7 in.	-57.93	-93	60.54	35.07

Table F.12: Model 4, calculated strain results in beams

Gauge	Column, location	Distance from removed column	Theoretical change in strain, $\Delta\varepsilon_T$	Experimental change in strain, $\Delta\varepsilon_E$	Percent difference (%)	$\Delta\varepsilon_T - \Delta\varepsilon_E$
11	(N) Beam	1 ft – 0.65 in.	605.52	136	77.54	469.52
12	(N) Beam	1 ft – 0.65 in.	605.52	171	71.76	434.52
13	(S) Beam	1 ft – 0.65 in.	608.28	252	58.57	356.28
14	(S) Beam	1 ft – 0.65 in.	608.28	272	55.28	336.28
15	(S) Beam	12 ft – 9 in	-17.77	81	555.76	-98.77
16	(N) Beam	12 ft – 9 in	20.51	-10	148.76	30.51

Table F.13: Model 5, calculated strain results in columns

Gauge	Column, location	Height above base	Theoretical change in strain, $\Delta\varepsilon_T$	Experimental change in strain, $\Delta\varepsilon_E$	Percent difference (%)	$\Delta\varepsilon_T - \Delta\varepsilon_E$
1	North, (S) flange	3 ft – 1 in.	-3.11	-32.00	928.82	28.89
2	North, (N) flange	3 ft – 1 in.	-15.66	-54.00	244.86	38.34
4	South, (S) flange	6 ft – 2 in.	32.93	-7.00	121.26	39.93
5	South, (E) web	6 ft – 2 in.	-10.44	-61.00	484.41	50.56

6	South, (N) flange	6 ft – 2 in.	-53.79	-103.00	91.47	49.21
7	South, (N) flange	4 ft – 7 in.	-27.97	-93.00	232.53	65.03

Table F.14: Model 5, calculated strain results in columns

Gauge	Column, location	Distance from removed column	Theoretical change in strain, $\Delta\varepsilon_T$	Experimental change in strain, $\Delta\varepsilon_E$	Percent difference (%)	$\Delta\varepsilon_T - \Delta\varepsilon_E$
11	(N) Beam	1 ft – 0.65 in.	368.97	136.00	63.14	232.97
12	(N) Beam	1 ft – 0.65 in.	368.97	171.00	53.65	197.97
13	(S) Beam	1 ft – 0.65 in.	302.90	252.00	16.80	50.90
14	(S) Beam	1 ft – 0.65 in.	302.90	272.00	10.20	30.90
15	(S) Beam	12 ft – 9 in	-31.68	81.00	355.69	-112.68
16	(N) Beam	12 ft – 9 in	27.83	-10.00	135.93	37.83